NASA-CR-195093

Investigation of the Effects of Manufacturing Variations and Materials on Fatigue Crack Detection Methods in Gear Teeth

Jeffrey A Wheitner and Donald R. Houser
The Ohio State University
Columbus, Ohio

January 1994

Prepared for
Lewis Research Center
Under Grant NAG3-1147

TABLE OF CONTENTS

Table of Contents v

List of Tables vii

List of Figures viii

Chapter I Introduction
1.1 Background 1
1.2 Literature Review 3
1.3 Thesis Overview 8

Chapter II Fatigue Crack Detection Methods
2.1 Introduction 10
2.2 Dye Penetrant Inspection 10
2.3 Magnetic Particle Inspection 12
2.4 Eddy Current Inspection 13
2.5 Ultrasonic Inspection 15
2.6 Radiography 17
2.7 System Stiffness Method 18
2.8 Acoustic Emission 19
2.9 Shot Peening 25
2.10 X-Ray Diffraction 28

Chapter III Equipment and Methods
3.1 Single Tooth Bending Fatigue 29
3.2 Gear 29
3.3 Fixture 31
3.4 Fatigue Testing Machine 36
3.5 Accelerometer 37
3.6 Spectrum Analyzer 37
3.7 Acoustic Emission 40
3.8 Testing Procedure 41
3.9 Kinematic Analysis 44

Chapter IV Results
4.1 Introduction 51
4.2 Nondestructive Inspection Methods 51
4.3 System Stiffness Measurements 52
4.4 Acoustic Emission 56

4.5 Residual Stress Measurements 64
4.6 Fixture Alignment 65
4.7 Tooth Stresses 68
4.8 Fatigue Life Curves 71

Chapter V Conclusions and Recommendations
5.1 Conclusions 77
5.2 Recommendations 80

References 82

Appendix A Gear Drawing SK 56249-560 84

Appendix B Lead and Profile Ckecks 86

Appendix C Surface Profile Traces 92

Appendix D Accelerometer Specifications 96

Appendix E Computer Program for Remote Operation of Wavetek 5820 Spectrum Analyzer 98

Appendix F Acoustic Emission Transducer Sensitivity 102

Appendix G Fatigue Life Data 104

LIST OF TABLES

Table 3.1 Gear Geometry and Materials 30

Table 3.2 Shot Peening Specifications 31

Table 4.1 Material Properties of Gears Tested 69

Table G.1 Fatigue Life Data for 4118A 105

Table G.2 Fatigue Life Data for 4118B 105

Table G.3 Fatigue Life Data for 4118C 106

Table G.4 Fatigue Life Data for 9310 106

Table G.6 Fatigue Life Data for 9310P 107

Table G.7 Fatigue Life Data for 8620 107

Table G.8 Fatigue Life Data for ADI 675 108

LIST OF FIGURES

Figure 2.1 Dye Penetrant Inspection 11

Figure 2.2 Magnetic Particle Inspection 12

Figure 2.3 Eddy Current Inspection Technique 14

Figure 2.4 Ultrasonic Inspection Method 16

Figure 2.5 Acoustic Emission Parameters 21

Figure 2.6 Acoustic Emission Ringdown Counts 22

Figure 2.7 Stress Distribution After Shot Peening 26

Figure 2.8 Effect of Self Stresses on the Bending Stress in a Plate 27

Figure 3.1 Numbered Test Gear 32

Figure 3.2 Gear Test Fixture 33

Figure 3.3 Beveled Anvil 36

Figure 3.4 Model of Fatigue Testing System 38

Figure 3.5 Schematic of Test Equipment 42

Figure 3.6 Acoustic Emission Transducer Location 43

Figure 3.7 Fixture Deflections 44

Figure 3.8 Fixture Model 45

Figure 3.9 Fixture Model Deflections at Gear Axis (point 1) 47

Figure 3.10 Link B (L-Arm) 48

Figure 3.11 MTS Cylinder Seal Forces 49

Figure 4.1 System Stiffness for 4118C at 170 ksi. Root Stress 54

Figure 4.2 System Stiffness for 8620 at 187 ksi. Root Stress 54

Figure 4.3 System Stiffness for 9310 at 262 ksi. Root Stress 55

Figure 4.4 System Stiffness for 9310P at 262 ksi. Root Stress 55

Figure 4.5 Acoustic Emission Count vs. Fatigue Life for 4118A 56

Figure 4.6 Acoustic Emission Count vs. Fatigue Life for 8620 57

Figure 4.7 Acoustic Emission Count vs. Fatigue Life for 9310 58

Figure 4.8 Acoustic Emission Count vs. Fatigue Life for 9310P 59

Figure 4.9 Example of Conditions for Failure on the Case 60

Figure 4.10 Example of Conditions for Failure on the Core 61

Figure 4.11 Hardness Profiles Near the Pitch Radius 61

Figure 4.12 SEM of 9310 Gear Tooth Showing Fatigue Striations 62

Figure 4.13 SEM Showing Cup and Cone Failure in 9310 Gear Tooth ... 63

Figure 4.14 Acoustic Emission and Crack Length as a Function of Fatigue Life 64

Figure 4.15 Strain Gage Readings Across Face Width (0.0004 in./in. Misalignment) 67

Figure 4.16 Strain Gage Readings Across Face Width (0.0001 in./in. Misalignment) 67

Figure 4.17 Gear Root Stresses 68

Figure 4.18 Ratio of Fatigue Propagation Life to Total Life as a Function of Total Life 71

Figure 4.19 Fatigue Life Plot for 4118 Test Gears 72

Figure 4.20 Fatigue Life Plot for 9310 Test Gears 72

Figure 4.21 Fatigue Life Plot for 8620 Test Gears 73

Figure 4.22 Fatigue Life Plot for ADI 675 Test Gears 73

Figure 4.23 SEM of ADI 675 Gear Tooth (500x) 75

Figure B.1 Profile Checks for a 4118 Gear 87

Figure B.2 Lead Checks for a 4118 Gear 87

Figure B.3 Surface Topography for a 4118 Gear 88

Figure B.4 Profile Checks for an 8620 Gear 88

Figure B.5 Lead Checks for an 8620 Gear 89
Figure B.6 Surface Topography for an 8620 Gear 89
Figure B.7 Profile Checks for a 9310 Gear 90
Figure B.8 Lead Checks for a 9310 Gear 90
Figure B.9 Surface Topography for a 9310 Gear 91
Figure C.1 Root Surface Finish Measurments for 4118.Gear..... 93
Figure C.2 Root Surface Finish Measurments for 8620.Gear 94
Figure C.3 Root Surface Finish Measurments for 9310.Gear..... 95

Chapter I

Introduction

1.1 Background

Gears may fail, or cease to be useful by several means. According to experts in the gearing field, the most common modes of failure are:

1. Fracture due to bending fatigue
2. Fracture due to impact
3. Surface wear
4. Surface pitting

Bending fatigue failures are perhaps the most serious from the viewpoint of the machine operator because when the tooth breaks, the machine becomes partially or completely inoperable due to the lack of a constant gear mesh. The customer generally takes a very dim view of gear tooth bending failures, even if the gear has operated in heavy service for several thousand hours. Gear bending failures must be avoided if the integrity of the product is to be maintained.

Gear bending fatigue life may be influenced by factors such as dimensional variations between mating gears, variations in manufacturing tolerances, wear on splines, shafts and bearings, and deflection of shafts, bearings, and housings. Bending fatigue may be simulated in the laboratory by two methods. The first is a rotating bending fatigue test in which the gear is run in mesh with another gear, simulating actual use. This test has the advantage of simulating the actual loads applied during the gear service life, but it has some disadvantages. It is time consuming, requires testing the entire

gear, and adds the risk of surface damage which could influence the bending fatigue results. The second type of test is a single-tooth bending fatigue test. This procedure applies cyclic loading near the tip of a tooth while the gear is held stationary by some type of support. This procedure can be repeated with several teeth on each gear so that many data points can be collected from each gear. This method also produces only failures due to bending fatigue.

The fatigue life of a gear tooth can be thought of as the sum of the number of cycles required to initiate a crack (Ni), plus, the number of cycles required to propagate the crack to such a length that fracture occurs (Np).

$$N = Ni + Np$$

The factors that govern crack initiation are thought to be related to localized stress or strain at a point, while propagation of a fatigue crack is a function of the crack tip parameters such as crack shape, stress state, and stress intensity factor. During a test there is no clear transition between initiation and propagation. The mechanisms of initiation and propagation are quite different and modelling them separately produces a higher degree of accuracy, but then the question that continually arises is "what is a crack?" The total life prediction in a fracture mechanics model presently hinges on the assumption of an initial crack length, and this length can significantly affect the total life prediction. The size of the initial crack is generally taken to be in the range of 0.01 in. to 0.2 in. [Fuchs, 1980].

Several researchers have used various techniques to determine the beginning of the crack propagation stage. Barhorst [1991]showed the relationship between dynamic stiffness changes and crack propagation. Acoustic emissions, which are stress waves produced by the sudden movement of stressed materials, have also been successfully

used to monitor the growth of cracks in tensile and fatigue specimens of [Dunegan, Harris, and Tetelman, 1969; Dunegan and Tetelman, 1974; Pollock, 1989]. The purpose of this research is to determine whether acoustic emissions can be used to define the beginning of crack propagation in a gear using a single-tooth bending fatigue test.

1.2 Literature Review

For many decades fatigue failures have challenged designers . Fatigue has been the subject of numerous studies in aircraft, turbo-machinery, automotive, and gearing applications. Bending fatigue is the number one cause of failure in gears and according to Lester [1984] nearly one third of all gear failures are due to tooth bending fatigue.

Single-tooth bending fatigue is a widely used method for testing gear teeth. This method eliminates the possibility of other failure modes and generally provides consistent results. One of the difficulties of fatigue tests is determining when a crack is present. Several non-destructive methods of crack detection exist.

Barton and Kusenberger [1971] suggest several methods of non-destructive testing (NDT) and discuss the limitations of each. Magnetic particle testing may be used for magnetic materials and can sometimes detect defects below the surface. The detectable defects are on the order of 0.002 in. Liquid penetrants, which can be used on any material are capable of locating surface defects as small as 0.00004 in.; however, typical resolution is closer to 0.001 in. Ultrasonic inspection can locate surface and subsurface flaws greater than 0.015 in. but is very difficult to use and is sometimes unreliable on complicated geometries such as gears. Eddy current methods may be used on metallic materials and can detect flaws as small as 0.010 in., but they are also very geometry sensitive. Radiography, or x-ray, inspection is limited to the resolution of the film, and the smallest flaws which can be detected are larger than 10% of the part

thickness. Other detection methods mentioned include strain gages, optical holography, magnetic perturbation, and radioactive gas penetrant methods.

Ermolov, Petrovanov, and Vadkovskii [1989] have tested several nondestructive testing methods for welded aluminum parts. They observed that by using visual inspection at 7-10x magnification surface defects with an opening of 0.005 mm and length of 0.01 mm could be detected when the surface was chemically etched and properly prepared. This was a very slow and tedious process. They also observed that by using dye penetrant inspection on an etched surface they could detect cracks with an opening of tenths of a micrometer, depth of 0.01 mm, and length of 0.1 mm. Eddy current and ultrasonics were also investigated but have lower sensitivities than previously described methods.

Another method of determining the presence of a crack is by monitoring the compliance or stiffness of the part. One method of determining compliance is by using a compact tension test. This method uses a notched specimen that is loaded in tension. A non cyclic load is applied and load, extension, and crack length are simultaneously monitored. The compliance of the specimen can be obtained from a plot of load versus extension. The compliance can then be directly related to the crack length. All of the available literature dealing with compliance methods used a compact tension specimen for the test.

Nicholas, Ashbough, and Weerasooriya [1984] used compliance measurements during creep and fatigue crack growth to predict crack length. A lack of one-to-one correspondence between crack length and compliance was observed for several nickel-based superalloys. It was proposed that the cause of this unusual data was due to a complex three dimensional stress state which may also have been subject to environmental conditions.

Barhorst [1991] determined the relationship between crack length and gear tooth stiffness using a single tooth bending fatigue test. This test used an accelerometer to measure dynamic stiffness as the test progressed. It was shown that by monitoring the dynamic stiffness, initiation of a fatigue crack could be detected by a small drop in dynamic stiffness.

The final method of crack detection and propagation that was reviewed is the monitoring of acoustic emissions. Pollock [1989] used acoustic emissions to correlate emission count rate with strain in two metal matrix composites. Also, emissions were monitored during tension testing of a welded joint to detect faulty joints. During this test it was observed that emissions were recorded due to sliding between the part and fixture and were eliminated when the part was clamped firmly.

Tatro [1971] points out that acoustic emission activity is most dramatic in high strength brittle materials for which supplementary information is most needed. Softer materials with higher ductility generally show less emission production. He also states that the quantity of acoustic emission, its onset as a function of stress or strain, the point at which its maximum occurs, and the broadness of the peak are all measures of material behavior.

According to researchers at the Instron Corporation, when fatigue testing a compact tension specimen, crack initiation is always accompanied by an increase in acoustic emission output. They also found that in high strength steel the emissions increase long before the crack is visible, while in lower strength steels the increase in acoustic emissions coincides with the appearance of a fatigue crack. The recording of emissions before a fatigue crack was visibly present was thought to be due to plastic deformation near the crack tip. It was also observed that during a tensile test if the load was reduced the emissions stopped and did not continue until the previous maximum load was obtained.

Green [1978] detected fatigue cracks in a compact tension specimen of high strength steel. He also detected corrosion flaking in a pressure vessel while proof testing by loading the vessel to a pressure higher than the operating pressure while observing the acoustic emission count.

Dunegan and Harris [1974] used a notched fatigue specimen to study the relationship between crack growth rate, cyclic stress intensity factor, load cycling rate, and acoustic emission activity. They found that crack growth rates of less than 10^{-6} in./cycle could be detected and that acoustic emission counts per cycle were closely related to the energy released by crack extension per cycle. Their results also showed that fatigue crack growth occurs in an accelerating and decelerating manner even though the stress intensity range remains uniform. They also determined that the emission count rate passes through a peak that is believed to be associated with a plane strain-plane stress transition. The effect of instrumentation sensitivity and frequency bandpass were also investigated, and it was found that acoustic emission techniques are suitable for a variety of cyclically loaded structures, even in the presence of high background noise.

Lenain [1979] describes a method for detecting the location of a flaw by strategically locating two or more acoustic emission transducers and measuring the time for a stress wave to arrive at the transducers. The most accurate method for determining the location requires a four channel system with three transducers placed at the verticies of an equilateral triangle and the fourth placed in the center of the triangle.

A paper by AE International described the use of two high speed mini- computers and several AE transducers to determine and locate flaws in large pressure vessels. One computer analyzes the emissions and displays them on a video screen which has been programmed to display the structure, all welds, and any attachments. The other computer performs a statistical analysis of all of the incoming signals and prints out the location, relative significance, and statistical accuracy of the sources on a hard copy

scaled layout of the structure being inspected. The number of channels required can range from 24 to over 100 depending on the size of the structure.

One method of detecting fatigue cracks called "proof testing" was investigated by Dunegan, Harris, and Tetelman [1969]. They found that when a structure that has been fatigue tested at cyclic stress, Sc, is proof tested at a higher stress, Sp., acoustic emissions will only occur at stresses above the previous maximum stress. Thus, if the structure is fatigue tested further and then proof tested at Sp, it will only show emissions if a crack is present because the material at the crack tip will only have been exposed to a maximum stress of Sc before the proof test. This method can be used to determine if a fatigue crack is present as well as if it has grown since the last proof test. This technique is used in aircraft and pressure vessel applications to warn of impending failures.

Lazarev and Rubinshtein [1989] used a microcomputer to record AE from a compact tension specimen during fatigue tests. They found that the sources of AE during loading of the specimen are: friction of the edges of a fatigue crack during its opening, plastic deformation of material at the crack tip after opening of its edges, and crack jumps. The loading fixture and loading surfaces were ground smooth and gear oil and sound insulation were used on the loading clamps to reduce the effect of noise from the drive. The spectrum of AE was analyzed and it was found that the AE pulse from a crack jump was characterized by a relatively uniform spectrum extending to 1-2 MHz, while plastic deformation and friction, which are the main portion of the AE energy, were related to the low frequency part of the spectrum. They also observed changes in the AE count rate and amplitude during tensile loading of 40 steel samples with pre-exising fatigue cracks. Elastic loading was characterized by fine, random, small amplitude AE surges. As plastic deformation began to take place, the count rate monotonically increased due to plastic deformation at the crack tip. After a time the count rate began to monotonically decrease because of exhaustion of material in which plastic deformation

due to localized yielding was taking place. Very soon after the count rate began to decrease, the amplitude of the AE greatly increased. This was due to subcritical crack extension as confirmed by fractography of the fracture surface. This work confirms that plastic strains at the crack tip are characterized by continuous AE with a large number of signals of small amplitude, and AE count rate provides the best information in this case. Crack extension and jumps are characterized by single AE signals of high amplitude and monitoring AE amplitude provides the best information.

Bowles [1989] investigated AE from rivet holes in the wing spar of an airplane during simulated loading. He found that the total AE detected near a crack is not representative of the cracking activity. It is not sufficient to monitor total activity occurring in the region of the load cycle where AE due to a crack growth could occur. This data must be compared to the level of AE during the entire load cycle. This research did show significant increases in AE activity during the peak loads as compared with the AE activity throughout the rest of the load cycle for crack sizes greater than 0.3-0.6 mm deep.

Friesel [1989] used AE to distinguish between fretting failures and crack propagation. He used a computer, two digital recorders, and a tape recorder to collect and analyze the data. He calibrated the setup by inputting an impulse which he created by breaking a 4 mm long piece of 0.03 mm pencil lead. After statistical analysis of the data he determined that he could accurately distinguish between fretting or crack growth over 95% of the time by analyzing emissions. The five most important features used in classification were signal rise time, amplitude, energy, autocorrelation, and power spectral density.

1.3 Thesis Overview

This thesis is divided into five chapters. Chapter II describes possible non-destructive testing methods for detecting and measuring fatigue cracks and results of

these tests are discussed. It also describes the theory and use of acoustic emissions and x-ray diffraction.

Chapter III contains a description of the gears and test fixture used throughout the testing. The theory behind single tooth bending fatigue tests and the procedures used in completing the experimental work are also described. Finally, an analysis of the testing system is shown.

Chapter IV presents the experimental results of the single tooth bending fatigue tests and a discussion of these findings. Chapter V contains conclusions, and recommendations for further study.

Chapter II

Fatigue Crack Detection Methods

2.1 Introduction

Several nondestructive methods exist for locating surface and subsurface cracks. The methods that are discussed in this work are dye penetrant inspection, magnetic particle inspection, eddy current, ultrasonic inspection, radiography, a stiffness method, and acoustic emission. The principles, advantages, and limitations of each process will be discussed in the following sections.

Shot peening, a method of introducing residual stresses into the surface of a part, and x-ray diffraction, a method of measuring these residual stresses, are also discussed in this chapter.

2.2 Dye Penetrant Inspection

The dye penetrant method of inspection uses a brightly colored dye to reveal surface flaws. The method consists of at least five steps, shown in Fig. 2. The first step is to apply the liquid penetrant to the area on the part where the flaw is located. The dye then enters the flaw by capillary action and is allowed to penetrate for a few minutes. Excess dye is removed from the surface by washing with either water or a solvent depending on what type of penetrant is being used. At this point the flaw can sometimes be detected by examining the part carefully.

The next step is to apply a developer which forms a film over the surface. The developer acts as a blotter to accelerate the natural seepage of the penetrant out of the flaw

and to spread it out to enhance the penetrant indication. After the part is sufficiently developed, the final step is inspection. The surface of the part is examined for any traces of penetrant bleedback which would indicate some type of surface flaw. If a visible dye is used as the penetrant, the part is inspected under white light. When fluorescent penetrant is used, a dark inspection environment is needed, and a black (ultraviolet) light is used for inspection. The penetrant will fluoresce brightly under black light indicating surface flaws.

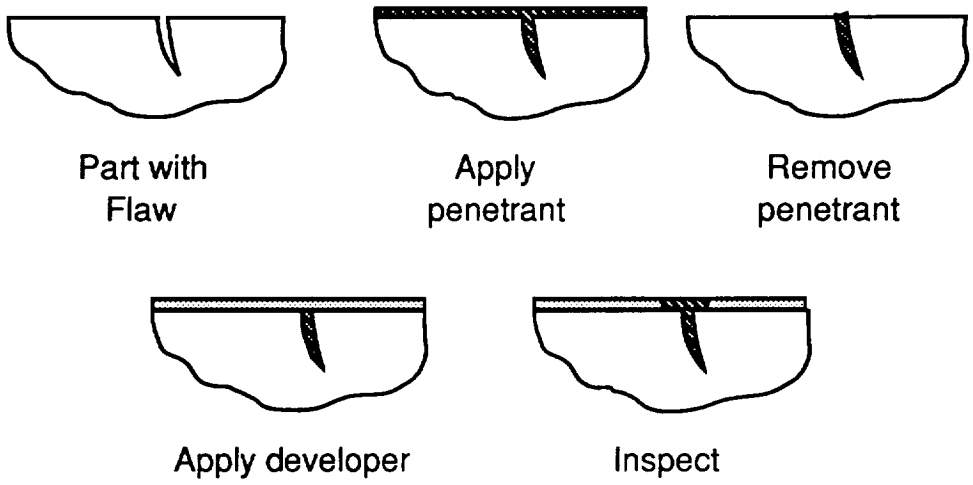

Figure 2.1 Dye Penetrant Inspection

Some of the advantages of dye pentrant inspection methods include: they are easy to use, they are relatively inexpensive, and they are portable and can be used at the test site. The main disadvantage of dye penetrants is that they only detect flaws open to the surface. During a fatigue test, when the crack is very small, there are very large forces holding the crack closed when the load is removed. This phenomenon is known a crack closure. If dye penetrants are to be used to detect fatigue cracks, the load must be applied during the entire inspection process to ensure that the crack is open to the surface.

2.3 Magnetic Particle Inspection

Magnetic particle inspection, better known as Magnaflux™, is a method of detecting surface and sub-surface flaws in ferromagnetic (magnetizable) materials. It depends on the fact that when a material is magnetized, discontinuities that lie transverse to the magnetic field direction will cause a leakage field at and above the surface of the part. This leakage field is detected by spreading a layer of fine ferromagnetic particles over the surface. These particles are attracted to and held by the leakage field. These particles form an outline around the defect and generally indicate its location, size, and shape. The magnetic particles may be applied over the surface as either a dry powder or in a carrier such as water or oil.

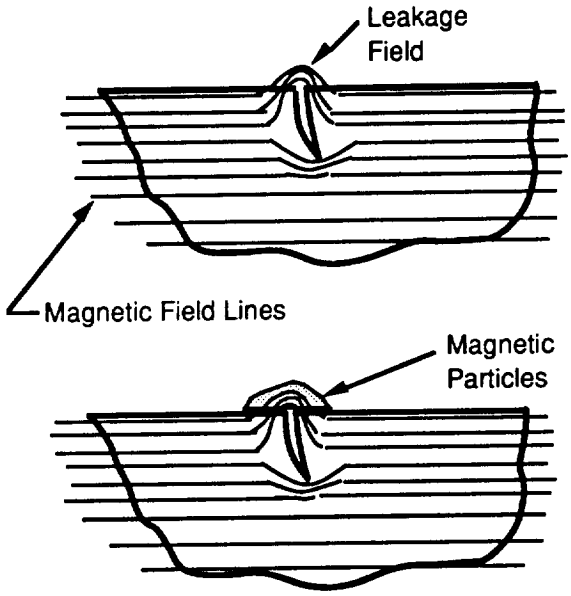

Figure 2.2 Magnetic Particle Inspection

The magnetic particle method is a sensitive method for detecting small, shallow cracks in ferromagnetic materials. Discontinuities that do not actually break through the surface may also be detected. If a discontinuity is fine, sharp, and close to the surface, a

clear indication will be produced. If the flaw is deeper, a weaker indication will be produced. The deeper the flaw, the larger it must be to give a good indication when using this method.

There are certain limitations to using magnetic particle inspection. A few of them are indicated here. The method can only be used on ferromagnetic materials which include iron, steel, nickel and cobalt alloys. Nonferromagnetic materials, which cannot be inspected using magnetic particle methods, include aluminum, copper, magnesium, titanium alloys, lead, and some austenitic stainless steels. For best results the magnetization direction must be normal to the principal plane of the discontinuity which sometimes requires multiple magnetizations. Demagnetization is often required following inspection.

Thin coatings including paint or nonmagnetic plating can significantly reduce sensitivity of the inspection. Also large currents are sometimes required for very large parts and local heating of parts may be significant. Finally, even though the method is relatively simple, experience and skill are often required to judge the significance of an indication.

2.4 Eddy Current Inspection

Eddy current inspection is based on the principle of magnetic induction. The parts are inspected by passing an energized coil over the part and observing the changes in electrical properties of the coil such as resistance, and inductance, as in Fig. 2.3. The probe coil causes a magnetic field to be generated inside the test part, and this magnetic field causes small currents called eddy currents to be generated inside the test part. These eddy currents cause a magnetic field opposite to the field generated by the probe coil, thus reducing the inductance and increasing the apparent resistance of the probe coil.

The inductance and resistance will remain constant as long as no defects are encountered. When the probe moves over a discontinuity, the eddy current field is disrupted, and the inductance and resistance of the coil change. By measuring the changes in inductance and resistance, the size, shape, and location of the defect can be determined.

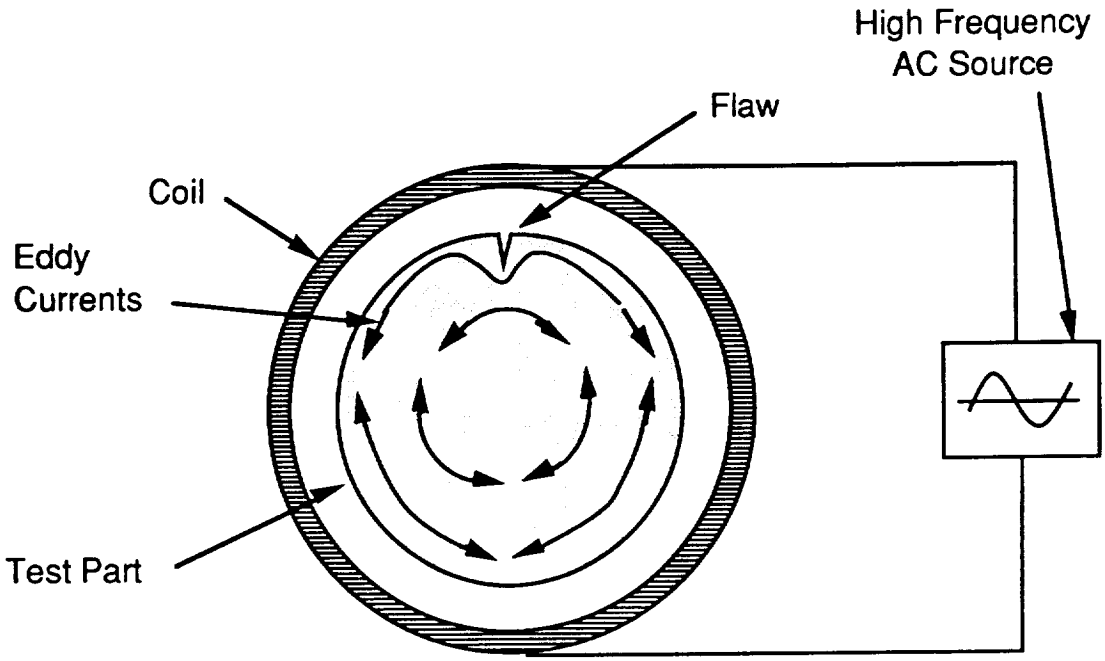

Figure 2.3 Eddy Current Inspection Technique

The eddy current method is a very versatile inspection method that can be used on any electrically conducting material. Because the principle of magnetic inductance is used, direct contact between the probe and the part is not required. This method may also be used to measure properties such as grain size, heat treatment condition, and hardness. Eddy currents can also be used to detect cracks, inclusions, voids, and differences in composition or microstructure.

One of the disadvantages of using eddy current inspection is that, like magnetic particle inspection, it is only useful for locating defects at, or just below the surface. Another disadvantage is that the method requires skilled operators to perform the inspection and interpret the results. The other difficulty with the eddy current method is that some variables in the material may cause instrument signals that mask defects or are mistakenly identified as defects.

2.5 Ultrasonic Inspection

Ultrasonic inspection is one of the most widely used nondestructive inspection methods. It is accomplished by introducing a beam of very high frequency sound waves into a material and measuring the reflected or transmitted energy. When the sound waves encounter a flaw, some of the energy is scattered and is not reflected or transmitted to the sensing transducer.

There are typically three parameters that may be measured: attenuation of reflected or transmitted sound waves, time of transit of sound waves from the point of entry to the point of exit, or features in the spectral response of either the reflected or transmitted waves. The most common parameter used is the transit time. If the speed of sound in the test material is known, the distance to the flaw can be calculated by measuring the time of transit.

The basic equipment needed for ultrasonic testing is a signal generator, a transducer that emits a series of ultrasonic waves, a couplant (similar to dish soap) which will transfer energy from the transducer into the test part, a transducer (can be the same as the transducer emitting ultrasonic waves) that will receive the reflected or transmitted waves and convert them to a voltage output, an amplifier, a display such as a CRT to record output, and a timer to trigger and control all of the elements of the system.

An oscilloscope is typically used to display the results of the inspection. When using a single transducer, if a pulse is introduced into the test specimen and there is no flaw; two spikes will appear on the screen. The first is the initial pulse entering the specimen, and the second is the reflection of the wave off of the opposite side of the part. If the surfaces are smooth, nearly 100% of the energy is reflected from a solid/gas interface. If a flaw is present, a third pulse will be observed on the screen indicating the relative location of the flaw.

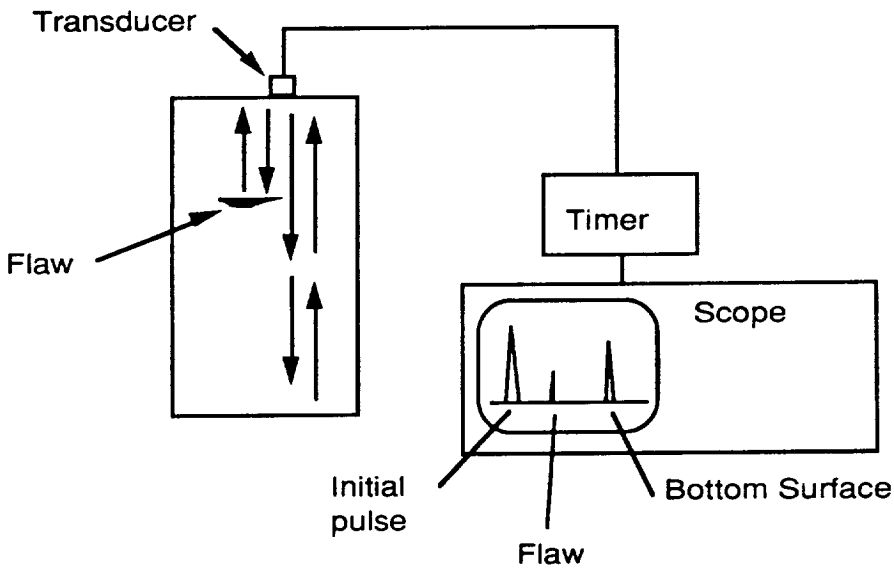

Figure 2.4 Ultrasonic Inspection Method

The main advantage of ultrasonic inspection is superior penetrating power that allows detection of flaws deep in the part. High sensitivity can also be achieved to detect extremely small flaws. Compared to other inspection methods, greater accuracy is possible for determining location, size, orientation, shape, and nature of internal defects. Another significant advantage in some cases is that access to only one surface is necessary.

One of the limitations of ultrasonic testing is that experienced technicians are needed to interpret the results. Another disadvantage is that discontinuities that occur just below the surface may not be detectable. Other limitations are: parts that are rough, irregularly shaped, very thin, or not homogeneous may be difficult to inspect, and finally, couplant is needed to insure good transfer of the ultrasonic waves between the transducer and the part.

2.6 Radiography

Radiography, otherwise known as x-ray inspection, refers to the absorption of penetrating radiation by the test part. There are two methods of inspecting a part using either x-rays or gamma-rays. The first and most widely known is the film method. This method involves exposing the test part to a radiation source and recording on radiographic film the image of the radiation that is not absorbed. Another technique involves real-time imaging in which the unabsorbed radiation is converted to an electronic signal and displayed on a viewing screen or computer monitor. When using real-time radiography, the part can be rotated so that it may be inspected from different directions.

Radiation is absorbed to differing degrees by the test piece depending on thickness, density, and variations in composition. When a flaw is present, more or less radiation is absorbed so the amount of radiation penetrating the part and reaching the film will differ near the flaw. There are several disadvantages to radiography method including very high cost and the danger of exposure to harmful radiation.

Radiography can only detect flaws which have a significant length in the direction parallel to the x-ray beam. This makes several exposures at different angles necessary for complete inspection. Features that consist of a 1% or greater difference in absorption compared with surrounding areas can sometimes be detected with very sensitive equipment. Another limitation of radiography is that irregular part shapes often lead to

confusing and difficult to interpret results. Radiography does not provide sufficient accuracy to determine the initiation of fatigue cracks, due to their small size and the irregular shape of gears, so this method was not used in this research.

2.7 System Stiffness Method

The stiffness of a spring is a measure of the force developed in the spring per unit displacement. Compliance is the reciprocal if stiffness. Compliance is usually measured by using a compact tension specimen. This is a tensile specimen in which a notch is cut to provide a large stress concentration so that a crack will initiate at the notch tip. The specimen is loaded in tension and the load, deflection, and crack length are measured, and a plot of load versus displacement is constructed. The compliance of the specimen can be determined from the slope of the load-displacement curve.

In this research, as in that of Barhorst [1991], a slightly different method was used. Instead of measuring the displacement, the second derivative of displacement with respect to time, or acceleration (a) was measured and plotted against load. The ratio of load to acceleration (F/a) is called inertance. Because the testing was completed at a constant frequency, the inertance can be multiplied by the square of the testing frequency (ω^2) to obtain system stiffness.

During fatigue testing, the system stiffness and life of the gear teeth were monitored for a cyclic load with constant maximum amplitude. An accelerometer was screw mounted to the test fixture to monitor acceleration of the fixture. The load being applied and the resulting acceleration of the test fixture were input to a spectrum analyzer and the frequency responnse (F/a) at the testing frequency was recorded by a computer. When a crack began to propagate, the acceleration for a given load increased causing the ratio of force to acceleration to decrease. Thus, the system stiffness of the gear and fixture decreased. The correlation between stiffness decrease and crack length was then

determined so that the crack length could be estimated from the reduction in dynamic stiffness.

2.8 Acoustic Emissions

Acoustic emissions (AE) are small amplitude transient elastic stress waves resulting from a sudden release of energy during deformation and failure processes in stressed materials. They are used to give early warning of failure or to monitor plastic deformation and fracture of materials. AE can be compared to measuring seismic activity in the earth in order to predict earthquakes, with AE measurement being on a much smaller scale.

The classic sources of AE are crack growth and plastic deformation. Sudden movement at the source produces a stress wave which radiate outward into the structure and excites a piezoelectric transducer. As the stress in the material is increased, many more emissions are produced.

The source of AE energy is the elastic stress field in a material, and without stress, no emissions occur. Inspection must therefore be carried out using controlled loading of the structure in the form of a proof load before service, controlled variation of load while the part is in service, fatigue tests, creep tests or a complex loading program.

Acoustic emission inspection differs from other nondestructive testing methods in two respects. First, the signal originates in the material itself rather than from an external source. The second difference is that AE detects movement while other nondestructive methods detect geometrical discontinuities. There is often no single nondestructive testing method that will provide all of the information necessary and two methods are often combined. Because AE is so different from most other methods, it works very well in combination with them.

One of the major advantages of AE is that the whole volume of the part can be inspected in a single loading cycle. It is not necessary to scan the surface in search of local defects. A suitable number of sensors are simply attached to the surface at a distance of between 4 and 20 feet apart and the structure is loaded. Global AE inspection is typically used to identify areas with problems and then other nondestructive methods are used to determine exactly the nature and size of the defect. Acoustic emission testing is more material sensitive and less geometry sensitive than other nondestructive testing methods. Some of the disadvantages of AE are that it requires stress and it is very sensitive to noise.

Some of the sources of AE are plastic deformation (dislocation movement, grain boundary slip, twinning, etc.), phase transformations (martensitic), crack initiation and growth, and friction. The typical frequency range of AE is 20 to 1200 kHz and the equipment is highly sensitive to any kind of movement in this frequency range. Many techniques have been developed for discriminating between failure processes and noise [Pollock, 1989].

Acoustic emission sensors are typically piezoelectric crystals that convert movement into an electrical voltage. The crystal is housed in an enclosure and a wear plate is attached. The stress waves in the material excite the crystal and a voltage is passed to the preamplifier. The sensors are usually resonant type transducers which have a natural frequency between 100 kHz and 1MHz. The sensor is connected to the test material with a fluid couplant and secured with tape, adhesive, or a magnetic hold-down device. When the stress waves reach the sensor, it rings at the natural frequency. This causes the emission signal to be altered such that it contains properties of both the sensor and the event causing the signal. This is not a problem since statistical properties of the signal are usually all that are necessary for inspection. It has been shown that the exact

natural frequency of the sensor is not important as long as it is in the frequency range of AE.[Pollock, 1989]

The preamplifier typically provides a gain of about 100 (40 dB) and contains a high-pass or bandpass filter to eliminate mechanical and acoustical background noise. The most commonly used bandpass range is 100 to 300 kHz which contains the most common transducer frequency, 150 kHz. The preamp produces electrical noise and determines the sensitivity of the AE equipment. The smallest signal that can be detected at the sensor output is about 1 μV which corresponds to a surface displacement of $1x10^{-6}$ μin.[Pollock, 1989]

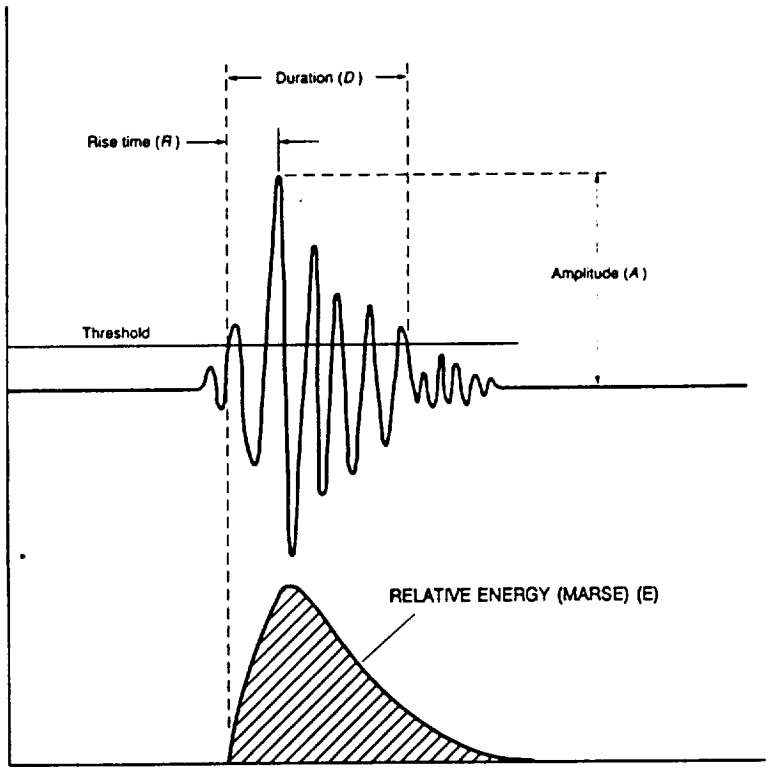

Figure 2.5 Acoustic Emission Parameters
(Courtesy of Physical Acoustics Corporation)

A typical acoustic emission signal is shown in Fig. 2.5. The 5 most common AE signal parameters measured are counts (N), amplitude (A), duration (D), rise time (R),

and measured area under the rectified signal (MARSE). Amplitude is the highest peak voltage attained by the AE event. Acoustic emission amplitudes are directly related to the magnitude of the source and vary over an extremely wide range from microvolts to volts.

The AE measuring device usually has an adjustable threshold value that the incoming signal is compared with to determine the significance of the event. Counts or ringdown counts are the number of times the AE signal crosses the threshold value as shown in Fig 2.6. Counts depend on the magnitude of the source event but also depend heavily on the oscillatory nature of the specimen and the sensor. Adding damping material to the specimen will sometimes reduce the number of recorded counts for a single AE event by reducing the oscillations of the specimen.

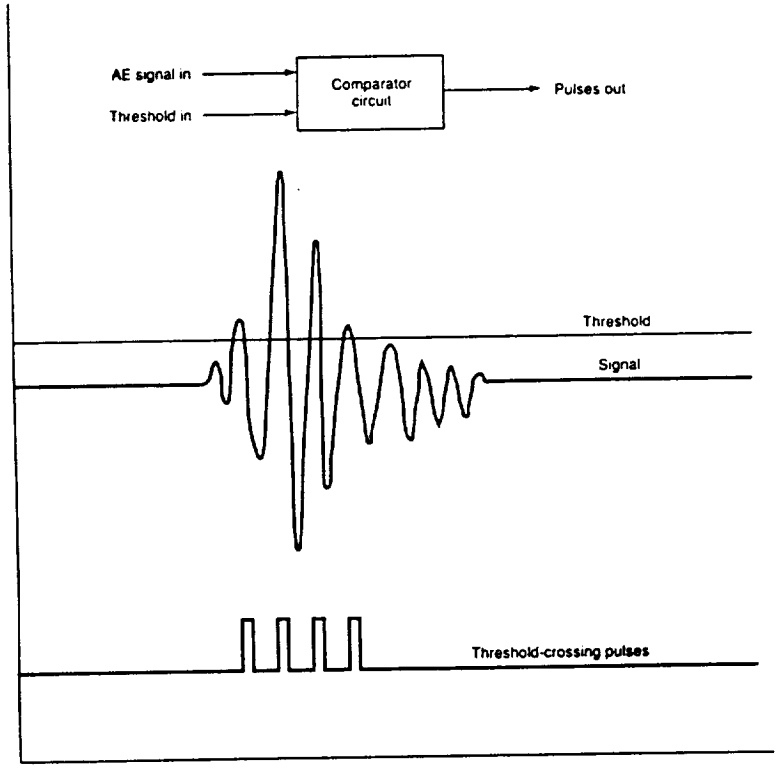

Figure 2.6 Acoustic Emission Ringdown Counts
(Courtesy of Physical Acoustics Corporation)

Duration is the elapsed time from the first threshold crossing to the last. This parameter depends on source magnitude, structural acoustics, and reverberation, similar to counts, and is used for classification of defect types. The rise time is the elapsed time from the first threshold crossing to the signal peak. This parameter is affected by the wave propagation processes between the source and the sensor and can be used for defect classification.

MARSE, sometimes known as energy counts, E, is the measured area under the rectified signal envelope. This parameter has gained acceptance as a replacement for counts because it is sensitive to signal duration and amplitude. MARSE is also less dependent on threshold setting and operating frequency.

Noise is one of the most significant problems in AE testing. Some examples of noise that affects AE measurement are electrical and electromagnetic noise from ground loops, power switching circuits, radio transmitters, and electrical storms. Acoustic noise from fluid flow through valves and pumps, friction from movement of structures on their supports, and impact processes also affect AE signals. Noise problems may be controlled in several manners. First, the noise may be stopped at the source. Second, it may be possible to reduce the noise by using impedence mismatch barriers or damping materials at strategic points on the structure. When using cyclic loading, the AE circuit may be electronically switched on or off during the noisy parts of the cycle. Differential sensors are also a possibility for use in noisy environments.

Acoustic emission is produced by stress induced deformation and is therefore highly dependent on the stress history of the structure. It is also dependent on the type of deformation and the material producing the emission. Most materials respond instantly to applied stress, emitting and then stabilizing quickly. Other materials take some time to settle down after a load has been applied. In other cases constant loading may cause continuous damage and the material may never stabilize.

Materials are usually tested using an increasing load. The first load application will typically produce many more emissions than subsequent loadings. For instantaneously plastic materials such as metals, subsequent loadings will produce no emissions until the previous maximum load is exceeded. This behavior is called the Kaiser effect, and Dunegan and Tetelman [1974] showed that for materials that obey the Kaiser Effect, emission on a repeat loading indicates that damage occurred between the first loading and the repeat. The AE that occurs at loads below the previous maximum or when the load is held constant is very important. It has been found that structurally significant defects will exhibit these behaviors while emission related to stabilization of the structure such as relief of residual stress will not occur on subsequent loadings [Pollock, 1989]. This becomes very important in fatigue testing because the structure should not emit after the first cycle under a constant cyclic load until a crack that is structurally significant is produced.

Acoustic emission from crack growth is one of the most important uses of AE. Because of stress concentrations in their vicinity, cracks and other defects will emit during rising load while unflawed material elsewhere is silent. It is necessary to distinguish between AE produced by the activity of the plastic zone at the crack tip and the AE produced from crack movement or propagation. Growth of the plastic zone is characterized by many emissions of low amplitude. These emissions are a result of fracture of precipitates and inclusions such as manganese sulfide stringers in steels, and the triaxial stress field that exists at the crack tip.

Acoustic emission due to crack front propagation depend on the nature of the crack growth process. "Microscopically rapid mechanisms such as brittle intergranular fracture and transgranular cleavage are readily detectable, even when the crack is growing one grain at a time at subcritical stress levels" [Pollock, 1989]. Slow and continuous crack growth such as microvoid coalescence (ductile tearing) is not detectable in itself,

but may be detected by the associated plastic deformation occuring near the crack tip due to high stress concentrations.

Acoustic emission is a very valuable tool for detecting cracks in the early stages of growth. AE can also be used to study crack growth and warn of an impending failure. Because of the Kaiser effect, a part will not produce AE until a significantly large crack is initiated, and AE may be used to determine where to stop a fatigue test and determine the initial crack size at the start of emission. This crack size could be used in a fracture mechanics prediction model for fatigue failures.

2.9 Shot Peening

Shot Peening is a method used to induce compressive stresses into the surface of a part to help increase the fatigue life of the part. Shot peening consists of treating the part with controlled high speed impact of many balls called shot. Peening produces compressive residual stresses near the surface which are offset by residual tensile stresses deeper in the part.

Residual stresses or self-stresses are stresses that exist in a part when no external load is present. Shot peening produces residual stresses near the surface of parts by plastically stretching a relatively shallow layer of material near the surface. The surface material is made longer, wider, and thinner than it was before peening. This expansion of the skin is restrained by the bulk of the interior of the part and causes high compressive stresses near the surface, balanced by smaller tensile stresses in the interior. A typical stress distribution in a shot peened plate is shown in Fig. 2.7.

The peak value of compressive stress depends mainly on the material of the peened part and restraints imposed on the part during peening. If a part is peened without restraints, the value of the maximum compressive stress P is around half the yield stress of the material and usually somewhat more [Fuchs, 1986]. The residual

compressive stresses can be increased by applying tension to the part surface during peening and can theoretically be raised to the yield stress. The compressive stress at the surface is always somewhat less than the maximum compressive stress that occurs below the surface.

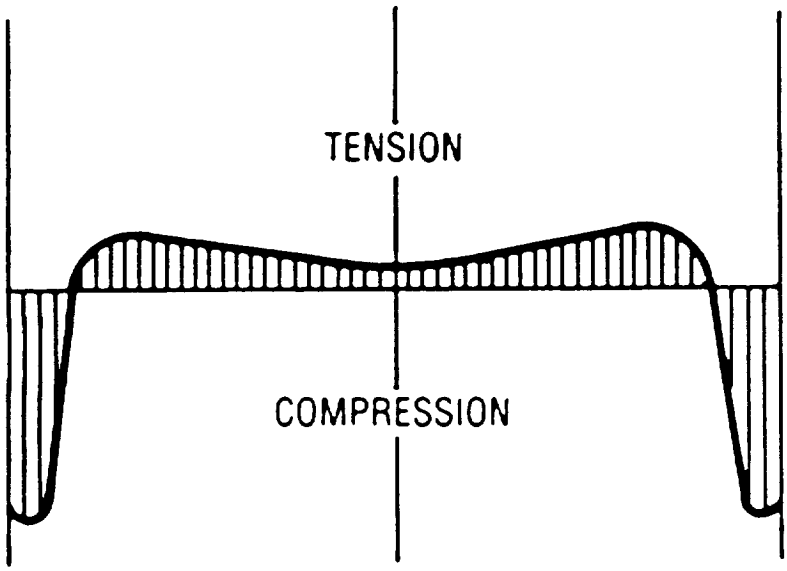

Figure 2.7 Stress Distribution After Shot Peening
(Courtesy of Metal Improvement Co., Inc.)

Changing peening parameters, such as shot velocity and size, will mainly change the width of the peak (P) and the depth (D) to which the compressive residuals extend. The peak value will only be slightly altered. The depth of the compressive stresses is roughly equal to the diameter of the peening dimples and is also proportional to the peening intensity [Fuchs, 1986].

The shot used is typically a hard steel, glass, or ceramic. The peening intensity is checked by small thin plates called Almen test strips. These strips are placed in the shot peening machine and exposed to the same intensity shot which will be used on the part.

The shot peening places compressive stresses in one side of the strip causing a curvature of the test strip. The curvature of the test strip is measured and used as a measure of the shot peening intensity.

For bending and torsion, peening provides significant improvements in fatigue life because stresses decrease toward the center of the part where small tensile stresses are present. The compressive residual stress has two effects on the fatigue life of a part. It increases the resistance of the material to formation of fatigue cracks and it also slows the growth of cracks when they are present. The effect of self stresses on the bending stress in a plate is shown below in Fig. 2.8.

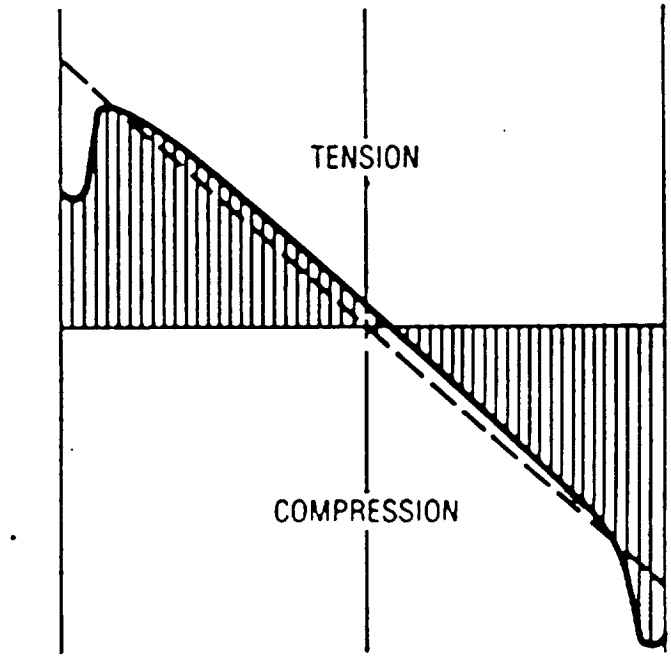

Figure 2.8 Effect of Self Stresses on the Bending Stress in a Plate

When a material containing residual stresses is loaded to a stress above the yield point, the residual stresses will diminish until the sum of all stresses is equal to the yield stress. Hence, high compressive stresses should be avoided in materials that have been

shot peened because if total compressive the stress reaches the yield stress some of the residuals will be removed. Thus, shot peening does not significantly increase the fatigue life in a reversed bending situation but it can lead to significant improvements in the zero to peak type fatigue loading experienced by gear teeth.

2.10 X-Ray Diffraction

X-Ray diffraction is a method of determining residual stresses in the surface of a part. The strain in the crystal lattice is measured, and the stresses producing this strain are calculated assuming a linear elastic distortion of the crystal lattice. To determine the stresses, the strain in the crystal lattice must be measured for at least two precisely known orientations relative to the sample surface.

Diffraction occurs at an angle 2θ defined by Bragg's Law: $n\lambda=2d \sin \theta$, where n is an integer denoting the order of diffraction, λ is the wavelength of the x-ray, d is the lattice spacing of crystal planes, and θ is the diffraction angle. For a monochromatic x-ray, the wavelength is known very precisely, and any change in lattice spacing results in a corresponding change in the diffraction angle. If the sample is rotated some angle, the relative spacing between the lattice planes will change and the diffraction angle will change. At least two different angles are needed to obtain the lattice strains and calculate stresses.

The presence of stresses in a sample results in a Poisson contraction reducing the lattice spacing and changing the diffraction angle. Because only elastic strains change the lattice spacing, only elastic strains are measured by x-ray diffraction. This method is relatively accurate but very expensive and time consuming.

Chapter III

Equipment and Methods

3.1 Single Tooth Bending Fatigue

The single tooth bending fatigue test is a test in which a gear is supported by some means, either by resting a tooth on a support, or by fixing the mounting shaft, and the test tooth is cyclically loaded. The object of this test is to isolate the test gear and cause failure of the test tooth by fatigue only. This test can be used to evaluate the effects of gear metallurgy, dimensions, surface finish, residual stresses, etc. of the test gear.

The single tooth bending fatigue fixture used in this research was developed by SAE because of the wide variation of testing specimens and procedures used in the gearing industry. The SAE fixture and test gear design were used exclusively throughout this research. This chapter provides a description of the test gears, test fixture, fatigue testing machine, a discussion of the testing procedure, and an analysis of the fixture.

3.2 Gear

The test gear is a six diametral pitch spur gear with 34 teeth, 20° pressure angle, and an outer diameter of 6.000 in. See Table 1 for a complete description of the test gear. Several materials were used for the test gears including carburized 4118 alloy steel, carburized 8620 alloy steel, carburized 9310 alloy steel, carburized and shot peened 9310 alloy steel, and shot peened Austenitized Ductile Iron (ADI 675). The test gears were manufactured by several companies to specifications shown on Dwg. SK56249-560 in Appendix A.

Table 3.1 Gear Geometry and Materials

Number of teeth	34	**Materials**	**Surface Finish**
Diametral Pitch	6	9310 Steel, #9310	Ra = 0.21 μin.
Pressure Angle	20°	Shot Peened, #9310P	Ra = 0.36 μin.
Base Circle Diameter	5.3249 in.	4118 Steel, #4118A	Ra = 0.80 μin
Root Diameter	5.187 in.	4118 Steel, #4118B	Ra = 1.05 μin
Circular Tooth Thickness	0.2618 in.	4118 Steel, #4118C	Ra = 1.59 μin
Addendum	0.166 in.	8620 Steel, #8620	Ra = 1.33 μin
Dedendum	0.240 in.	ADI 675, #ADI	NA
Whole Depth	0.406 in.		
Minimum Fillet Radius	0.0768 in.		
Diameter Over Pins	6.069-6.067 in.		
Pin Diameter	0.2880 in.		

The Carburized 9310 gears were all manufactured and heat treated together. Four of these gears were shot peened to specifications shown in Table 3.2. These gears are referred to in this work as group #9310 and 9310P respectively. Nine of the 4118 gears were manufactured by one company using three different cutting speeds, feeds, and tools to give three different root surface finishes. These gears were then heat treated together to give similar case depths and properties. These gears are referred to as group #4118A, 4118B, and 4118C. A different company donated 4 carburized 8620 test gears, group #8620. One ADI 675 test gear referred to as #ADI675 was donated by a third party and tested for comparison. The 9310 gears were not crowned; however, all others were. Sample profile and lead checks for each gear group tested are shown in Appendix B.

Surface profilometer traces used to determine surface roughness, Ra, are also shown in Appendix C.

Table 3.2 Shot Peening Specifications

Specification	Shot Size	Intensity	Coverage
MIL-S-13165	MI-330-H	12-16A	200%

Before testing a gear, one tooth must be removed to provide clearance for the lower support anvil. As shown in Fig. 3.1, the tooth to be tested is always three teeth away from the tooth supported by the lower anvil . After a tooth has been broken off, the tooth adjacent to the space becomes the support tooth for the next test. For example, in Fig. 3.1, if tooth #1 is removed by grinding, then tooth #2 will be the first support tooth and tooth # 5 will be the first tooth tested and broken. After tooth #5 is removed, tooth #6 will become the support tooth, and tooth #9 will be fatigue tested. This pattern continues around the gear until 16 teeth have been tested. In order to reduce errors in the testing procedure, the gear and fixture design is such that support teeth are never tested.

3.3 Fixture

Due to the large variations in gear testing procedures and specimen design throughout the gear industry, a standardized test fixture and testing technique was developed by the Gear Metallurgy Committee, Division 33, of the SAE Iron and Steel Technical Committee [Buenneke, Slane, Dunham, Semenek, Shea, and Tripp, 1982]. Variations in testing procedures cause difficulty in determining the relative importance of metallurgical factors on the fatigue life of hardened gears. To reduce the variation and increase reproducibility, the Gear Metallurgy Committee chose a single tooth bending

fatigue (STBF) technique, and a standard sized gear. It was tested by four companies--Caterpillar Tractor Co., Clark Equipment Co., Dana Corp., and International Harvester in a round robin testing program using identically designed fixtures and gears. The SAE testing technique was chosen for this research in order to obtain results to compare with test results of others.

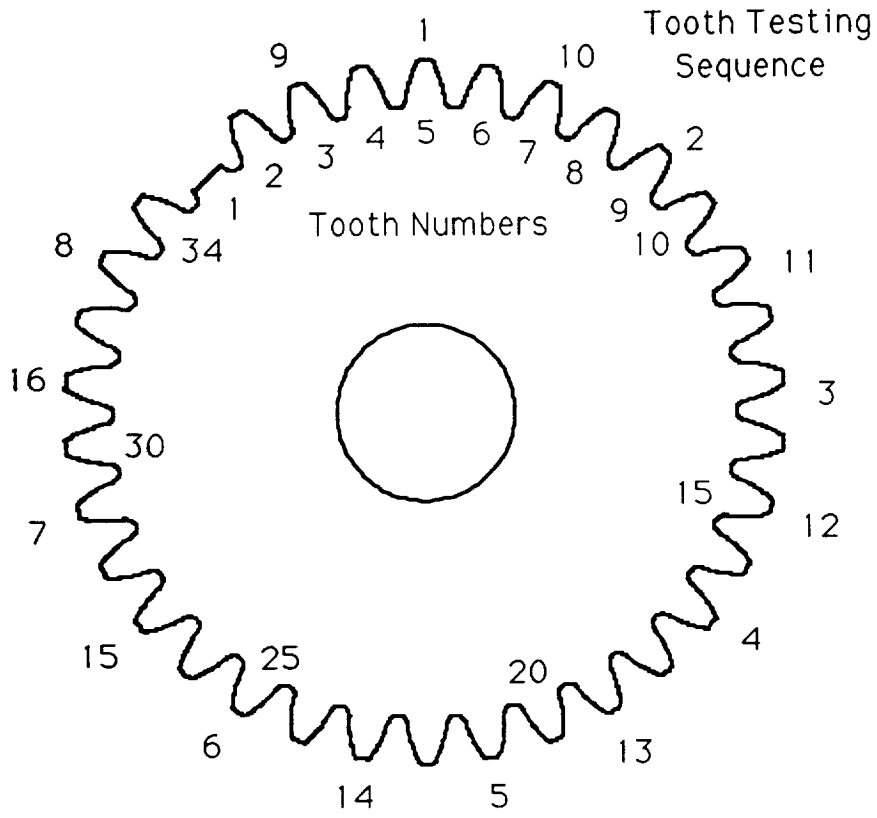

Figure 3.1 Numbered Test Gear

The SAE test fixture, shown in Fig. 3.2, is adaptable to a variety of driving mechanisms and support platens, and it can be positioned horizontally or vertically. The compressive force is applied by the testing machine through a spherical ball bearing to a

spherical seat in the upper anvil. The replaceable upper anvil insert, which is not crowned, has been designed to load the tooth being tested near the tip. The replaceable lower anvil insert, which is also not crowned, is designed to resist the load applied through the upper anvil. It contacts the support tooth near the root to insure that the tip loaded tooth always fails. According to Buenneke and colleagues [1982], "This approach provides less load to fracture and positive control of the loading point on the tooth to provide less data scatter."

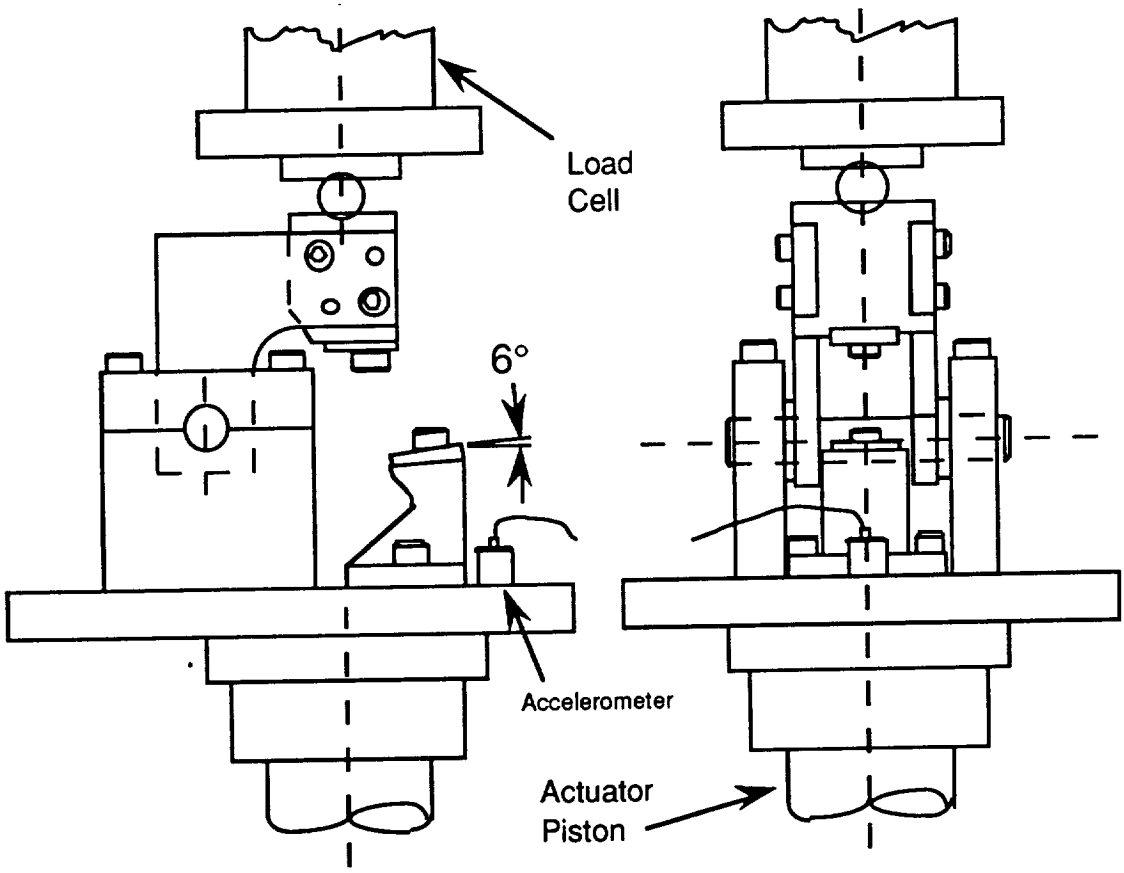

Figure 3.2 Gear Test Fixture

The main advantage of this test fixture is that the base, load anvil, support anvil, and gear are all inherently aligned because they are all mounted to a common shaft. The gear is mounted on the shaft and supported by needle bearings at both ends. It is

restricted from rotating by the lower anvil. When testing the first tooth of a gear, the tooth adjacent to the supported tooth must be ground off for clearance of the support anvil. The load anvil is also mounted on the common shaft and supported by needle bearings allowing it to rotate about the gear axis and contact the tooth to be tested near its tip. The load is applied through a large ball bearing to reduce misalignment and ensure a line of force straight between the upper and lower anvils, and tangent to the base circle of the gear. This eliminates any unnecessary torques on the gear and fixture which may be generated by the fixture.

There are a few problems with the SAE fixture that should be taken into consideration. The first is that the gear is mounted rigidly on bearings. This has the advantage of positively locating the load application point during each test with very little setup time. However, when the load is applied, the tooth deflects some amount. The pressure between the tooth and upper anvil insert is so large that friction forces allow little or no relative motion between the tooth and insert. This causes a binding effect in the gear and induces compressive forces in the tooth being tested. It also causes a bearing reaction force on the support shaft due to the couple produced by the deflection and rotation of the gear.

One solution to reduce the bearing forces is to replace the needle bearings in the gear with rubber spacers. These spacers will be rigid enough to support the gear, but will allow some motion when the tooth is deflected, reducing the unwanted compressive stresses in the gear tooth.

The second difficulty with the SAE fixture is the lack of any method to align the anvils. Due to the design of the fixture, the anvils should be inherently aligned, but due to wear on the inserts and chipping of the inserts when the tooth fractures, some misalignment occurs. The only solution to this problem is to turn the inserts over or make new inserts.

Insert misalignment poses a serious problem when un-crowned gears are tested. If one side of the inserts are worn or chipped and misalignment occurs, this will cause edge loading of the tooth and incorrect results will be produced. There is no quick fix for this problem. The load anvils need to be redesigned to allow rotational motion to provide a good contact pattern across the tooth. One method used by Caterpillar to check the contact pattern is to put a piece of pressure sensitive paper between the tooth and anvil insert and load the fixture. The pressure sensitive paper is preimpregnated with a dye and changes color when a pressure is applied. The greater the pressure, the darker the paper becomes. This allows the contact pattern to be adjusted for any testing load.

The fixture was fabricated by Advanced Machining Technology, Columbus, Ohio, for the Gear Dynamics and Gear Noise Research Laboratory at the Ohio State University. The fixture used for this research was slightly modified from the original SAE fixture. The original fixture had an upper and lower anvil that were parallel. In the revised version, the lower anvil was fabricated at a 6° angle as shown in Fig. 3.2. This was done to increase the contact area of the lower anvil. The effect of this modification was to cause eccentric loading and moments when the tooth deflected. Also, this modification caused the support tooth to be loaded further from the root, increasing the stresses applied in the root of the tooth. This caused one of the gears to fail at the support tooth instead of the upper, tip loaded, test tooth.

It was originally proposed that this angled anvil was also causing large bearing loads on the support shaft when the tooth deflected, which caused large transverse motion of the fixture. To test this proposition and eliminate some of the unwanted transverse motion, the lower anvil insert was replaced with an insert containing a 6° bevel ground into it to simulate the original fixture, as shown in Figure 3.3. This makes the anvils once again parallel and the line of force between the anvils tangent to the base circle of the gear to eliminate eccentric loading of the gear teeth and unwanted moments.

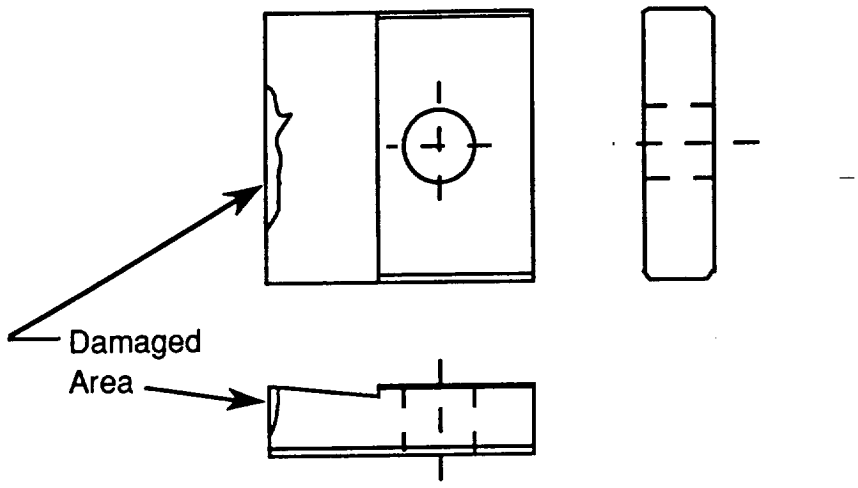

Figure 3.3 Beveled Anvil

This new anvil contacted the support tooth very near the root and the contact was only along the outer edge. This edge contact caused very high contact stresses in the insert and after testing 4 teeth, the anvil insert began cracking along the edge as shown in Fig 3.3. The beveled anvil insert became unusable and was replaced by the original insert. The beveled anvil insert did not reduce the horizontal deflection and a kinematic analysis was performed as shown in Sec. 3.9. The original flat insert provided a flat contact surface for the support tooth and was used for all subsequent testing.

3.4 Fatigue Testing Machine

The SAE test fixture was mounted on an MTS Systems Corporation Model 810 fatigue testing machine using a 55 kip hydraulic actuator. The lower base plate of the fixture was bolted to the lower platen of the MTS machine which is attached to the actuator. The upper platen of the machine contains the load cell. A small steel plate with a spherical seat machined in one side was placed on the ball bearing. The upper surface of the small plate was ground smooth, and coated with M-6 density multi-purpose

grease, and allowed to slide on the load cell mounting plate. No relative motion between the plate and the load cell was actually observed during testing but this setup allows the spherical assembly to self-align when the load is applied.

The MTS machine was controlled by an MTS 442 controller through which a force signal from the load cell was output. The controller was set at a gain of 3 and stability setting of 4 throughout the testing.

3.5 Accelerometer

A PCB model #302B03 piezoelectric accelerometer with a sensitivity of 299.9 mV/g was screw mounted to the base of the SAE fixture as shown in Fig 3.2. Complete specifications can be found in Appendix D. The accelerometer was used to measure the vertical motion of the fixture that was used for determining the stiffness of the system.

The accelerometer output was amplified by a Kistler model #504E4 dual mode amplifier using a medium time constant amplification. The gear was tested at 10 Hz, but the acceleration signal was filled with high frequency noise.

A Krohn-Hite model #3200 adjustable low-pass filter was used to eliminate all noise above 100 Hz. Without the filter, the higher frequencies contaminated the accelerometer signal and caused the spectrum analyzer to auto-scale the signal in such a way that the 10 Hz peak was barely distinguishable. When the filter was added, the 10 Hz peak was very distinct.

3.6 Spectrum Analyzer

The load signal from the MTS 442 controller was input to channel B of a Wavetek model #5820 two-channel spectrum analyzer. The accelerometer signal was input to channel A of the spectrum analyzer. The spectrum analyzer was used to calculate a transfer function of force divided by acceleration, $F/a(i\omega)$, called inertance.

This transfer function can be related to the stiffness of the gear tooth during the fatigue test. For example, the stiffness (k) of a spring is a measure of the force developed for a given displacement of the spring, F/x=k. Inertance (F/a) on the other hand is a measure of the force required to produce a given acceleration. The inertance of the entire fixture is measured during the fatigue tests and a method of obtaining the gear tooth stiffness from the inertance is described below.

The data obtained by using the system stiffness method produced a value for the stiffness of the total system. An analysis of the test fixture and gear was completed to determine the actual gear tooth stiffness from the total system stiffness. An analysis was completed using the model shown below in Fig. 3.4. It was discovered that because if the location of most of the fixture mass in relation to the tooth being tested, the dynamic effects of the mass were negligible and a static analysis can be used.

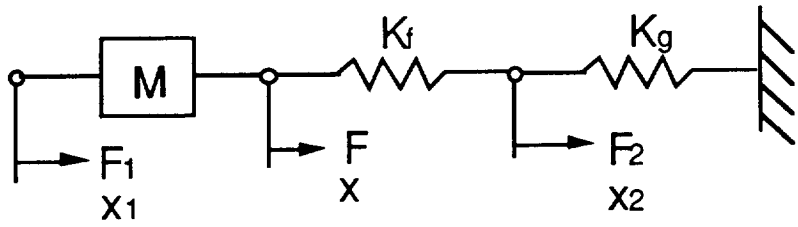

F_1 - Force Applied to Fixture by Actuator
F_2 - Force Applied to Gear by Fixture
x_1 - Deflection of Fixture
x_2 - Deflection of Gear Tooth
K_f - Fixture Stiffness
K_g - Gear Tooth Stiffness
M - Mass of the Fixture

Figure 3.4 Model of Fatigue Testing System

Assuming that the base of the fixture is rigid, the deflection on the left side of the mass is the same as the deflection on the right side, $x=x_1$. Also, because the forces on both sides of a spring are the same, $F=F_2$. The stiffness of the gear tooth can be determined from the stiffness of the entire fixture.

$$F_2 = K_f (x-x_2) = K_f (x_1-x_2) \quad (3.1)$$

$$K_g x_2 = F_2 = K_f (x_1-x_2) \quad (3.2)$$

$$K_g = K_f ((x_1-x_2)/x_2) \quad (3.3)$$

This analysis shows that the dynamic effects of the fixture mass have no effect on the fixture stiffness. Since the stiffness of the fixture is constant for all gears, and is not effected by the testing frequency, it can be measured statically. For the static test, the fixture is loaded to some force and the displacement of the fixture and gear tooth are measured. For static loading, the mass may be neglected and the following relationships hold.

$$F_1 = K_f (x_1-x_2) \quad (3.4)$$

$$K_f = F_1/(x_1-x_2) \quad (3.5)$$

The values of F_1, x_1, and x_2 can be measured, and the fixture stiffness may be calculated. The gear stiffness may be calculated another way that allows the stiffness measurements recorded by the computer to be used. Because the testing frequency is constant, the displacement of the fixture (x_1) may be calculated from the acceleration of the fixture by multiplying the acceleration by ω^2. If the transfer function is being measured, $F_1/\ddot{x}$ is known. From this, the stiffness of the gear tooth can be determined as follows.

$$Kg = \frac{F_1}{x_2} \tag{3.6}$$

$$F_1 = Kf(x_1 - x_2) \tag{3.7}$$

$$x_2 = -\frac{F_1}{Kf} + x_1 \tag{3.8}$$

$$Kg = \frac{F_1}{x_1 - \frac{F_1}{Kf}} \tag{3.9}$$

$$Kg = \frac{1}{\left(\frac{F_1}{x_1}\right)^{-1} - \left(\frac{1}{Kf}\right)} \tag{3.10}$$

$$\frac{F_1}{x_1} = \frac{F_1}{\ddot{x}_1} * 400\pi^2 \tag{3.11}$$

The transfer function magnitude was saved for further analysis on floppy disk using a Compaq 80286 computer. During the test, the computer was connected directly to the spectrum analyzer via the General Purpose Interface Board (GPIB) connector. A computer program to set up the spectrum analyzer and operate the analyzer in remote mode was written in TBASIC . The program is given in Appendix E.

3.7 Acoustic Emission

Acoustic emissions from the gear were monitored during the fatigue testing with a Physical Acoustics model #NANO30 acoustic emission sensor resonant at 300 kHz. The transducer sensitivity is shown in Appendix F. The emissions were amplified using a Physical Acoustics model #1220 preamplifier set at 40 dB gain.

The emissions from the gear were monitored by a Physical Acoustics model #1200A crack detector. This instrument was able to display either the total emission counts or the count rate on a digital display. The emission counts were recorded on a

Gould model #110 strip chart recorder at speeds of 10 cm/hr. For greater resolution, speeds of 50 cm/hr were sometimes used.

Mechanical noise from the hydraulic valves on the MTS machine and the bearing friction of the fixture sometimes caused noisy signals from the acoustic emissions equipment so a damping material was attached to the gear. This material was similar to a tar and had a self stick backing. It was cut into strips about 1 in wide and 3 in long and two strips were placed in each side of the gear. This lowered the background noise by approximately 3 dB but had no adverse effect on crack detection.

3.8 Testing Procedure

A schematic of the test setup is shown in Fig. 3.5. This system setup was used throughout the testing. The first step in the testing process was to power up all electronic equipment. and assemble the SAE fixture. The fixture and the gear tooth to be tested were wiped clean with a rag and the surfaces of the boss that were in contact with the fixture were coated with a thin film of M-6 density multi-purpose grease. The gear was lined up and the shaft was inserted. At this time, a thin coat of grease was applied to the two gear teeth in contact with the fixture anvils.

The next step was to attach the acoustic emission sensor to the gear. The old adhesive was removed from the sensor using 200 grit sandpaper, being careful not to damage the ceramic wear plate on the sensor. The sensor was attached to the gear just below the root of the tooth being tested with superglue as shown in Fig 3.6. Next, the ball bearing and sockets were wiped with a rag and cleaned with 200 grit sandpaper until all corrosion was removed. These parts were greased carefully so that all surfaces in contact were thoroughly covered to eliminate wear and fretting corrosion.

The MTS controller interlocks were adjusted to shut off the hydraulic system if the load increased to over 20,000 lb. or decreased to below 500 lb. The upper interlock

setting was used for safety so that the fixture would not be overloaded. The lower interlock setting was used so that when the tooth fractured completely off, the machine would stop. This allowed automation of the system and it did not require that someone monitor it at all times.

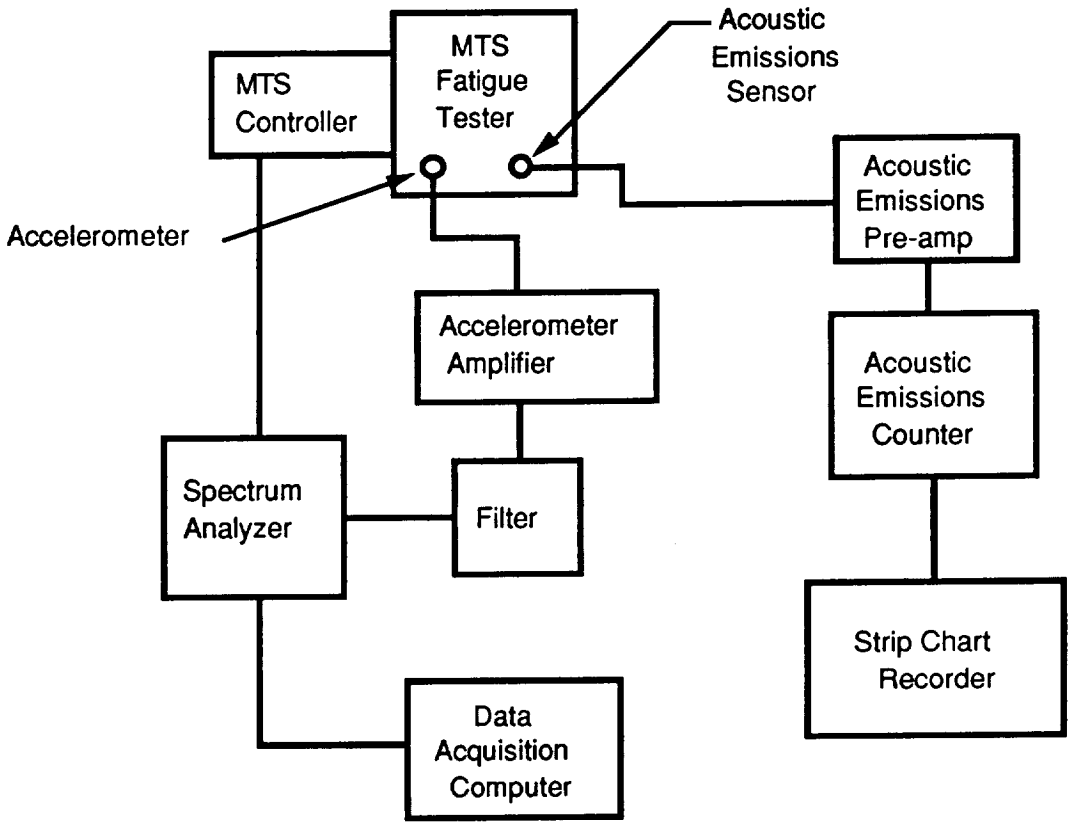

Figure 3.5 Schematic of Test Equipment

The next step was to turn on the MTS tester and run the test at a load at about 50% lower than the testing load to allow the spectrum analyzer to take several averages of the signals and stabilize. Next, the computer program was run to set up the spectrum analyzer and prepare it for taking data. The load was increased to the testing load and the data collection was begun. The MTS controller was periodically adjusted for the first fifteen minutes of testing to adjust for drift due to the increase in the hydraulic fluid

temperature. The load typically decreased about 300 lb during warm-up if the controller was not readjusted. Once the temperature reached a steady state condition, the load stayed constant and no adjustment was needed.

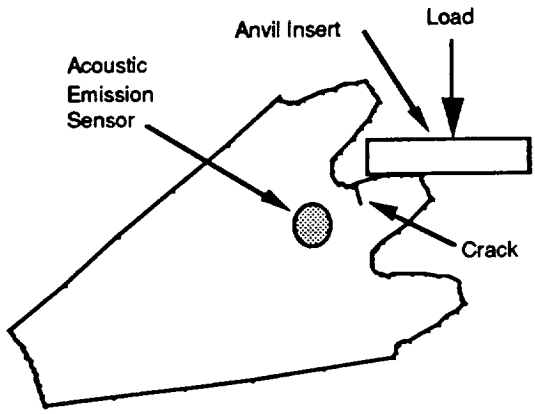

Figure 3.6 Acoustic Emission Transducer Location

Once data collection was begun, the acoustic emission equipment was adjusted. The gain was turned up until constant emissions were recorded from the mechanical background noise and then the gain was set 3 dB below this point and the counter was reset. The gain setting was usually 9 dB on the 1200A crack detector depending on the geometry and material of the gear. The 4118 gears sometimes caused excessive background noise and were monitored at a gain setting of 6 dB. The strip chart was then adjusted to the desired speed, typically 10 to 50 cm/hr. The system was then left alone and checked hourly to examine the MTS load for drift, check the strip chart recorder for emission activity, and inspect the gear for any cracks.

The computer program continuously read the transfer function magnitude and compared it with the initial value. If it dropped below 99% of the initial value, the program began recording the transfer function magnitude and the number of cycles that

had occurred. Once the gear tooth fractured and the machine stopped, the transfer function dropped to zero, and the computer recorded the data to the hard disk. After fracture, the gear was removed, cleaned and rotated to test the next tooth.

The SAE Gear Metallurgy Committee recommends that the tests be run with a load ratio of 10%. The load ratio (R) is the ratio of the minimum load to the maximum load $R= (L_{min}/L_{max})*100\%$. All of the testing in this research was done using a load ratio of 10% and a testing frequency of 10 Hz. When referring to testing loads in this document, only maximum loads will be stated.

3.9 Kinematic Analysis

The 9310 gears were initially tested at 16,000 lb. During this testing, a lateral deflection of the fixture of 0.010 in. was observed for tooth deflections of 0.010 in. as shown in Fig 3.7. It was unclear what was causing the transverse motion so a full kinematic analysis of the system was performed.

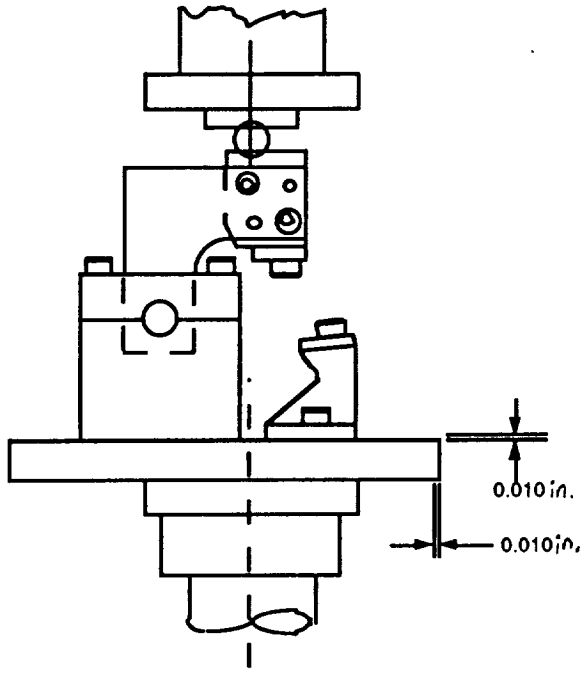

Figure 3.7 Fixture Deflections

The model used for the analysis is shown in Fig. 3.8. CADAM, a computer aided design program, was used to aid in the analysis. The base of the fixture was bolted to the actuator of the MTS tester making this a rigid connection; therefore, the actuator

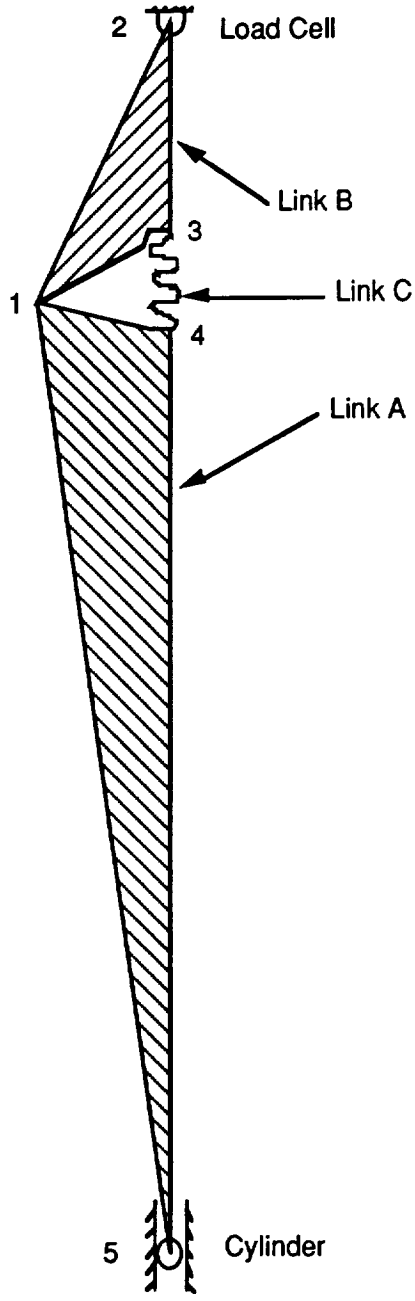

Figure 3.8 Fixture Model

piston, fixture base, and lower anvil were considered link A in the model. The upper anvil and ball bearing are link B and the gear is link C. All three links were connected at a pivot at the center of the gear axis, point 1. The lower end of link A, modelling the actuator piston inside its cylinder, was constrained to move only vertically. Link B was constrained to only rotate about the center of the ball bearing, point 2, in contact with the upper platen of the MTS machine. In this analysis, the fixture and the two anvils are assumed rigid, and because of this, all deflection is assumed to occur in the test tooth.

This model was used to model the action of the test fixture, gear, and the MTS testing machine. In order to model the motion of the fixture during a test, the lower end of link A was deflected 0.010 in. vertically upward, simulating the actuator motion of the testing machine. The resulting motion of the model was then analyzed using CADAM. Since link A and B are assumed rigid, the motion of link A was calculated and plotted, and then the motion of link B was determined and plotted. Due to the vertical motion of link A relative to link B, the decrease in distance between the anvil inserts, the upper gear tooth undergoes a deflection of 0.010 in. This deflection was modeled as a rotation of the tooth about the point of intersection of the tooth center line and the root diameter of the gear, and the gear tooth rotated clockwise 1.94°.

The deflection of the gear tooth cause rotations of links A and B. Because of these rotations, the pivot point, which is coincident with the gear axis centerline, translates up and to the left. Due to the deflections described above, link A rotates counterclockwise about point 5, its base. This causes the gear axis, point 1, to translate 0.0144 in. to the left and 0.0078 in. up., for a total deflection of 0.0164 in. These deflections are shown in Fig. 3.9.

The 0.010 in. deflection of the gear tooth corresponds to a 16,000 lb. load as observed on the load cell of the MTS machine. In the model, it was assumed that the 16,000 lb. load was transmitted to the gear normal to the anvils during the entire cycle.

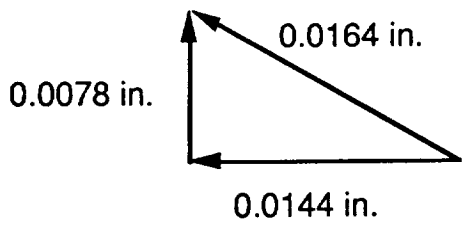

Figure 3.9 Fixture Model Deflections at the Gear Axis (Point 1)

In order to determine why the fixture was deflecting horizontally, link B, shown in Fig. 3.10, was analyzed to determine the bearing forces at the gear pivot which would translate as bearing forces on the actuator piston seal. Because the mechanism is in static equilibrium, the sum of all forces is identically zero. Equating forces in the x-direction to zero we obtain:

$$\Sigma F_x = 0 = F_{1x} + F_{2x} + F_{3x} \tag{3.12}$$

Equating forces in the y direction to zero gives:

$$\Sigma F_y = 0 = F_{1y} + F_{2y} + F_{3y} \tag{3.13}$$

From the previous assumption it is given that F_2 = 16,000 lb. Due to the deflection and rotation of the tooth, the top part of the fixture rotates clockwise about point 2. The angle of rotation of the fixture can be calculated so that the x and y components of the bearing force can be obtained as follows:

$$\theta = \sin^{-1}\left(\frac{0.0144}{4.970}\right) = 0.166^{\circ}$$

F_2 = 16,000 lb.

$F_{2x} = F_2 \sin(0.166°) = 46.4$ lb.

$F_{2y} = F_2 \cos(0.166°) = 15{,}999.9$ lb.

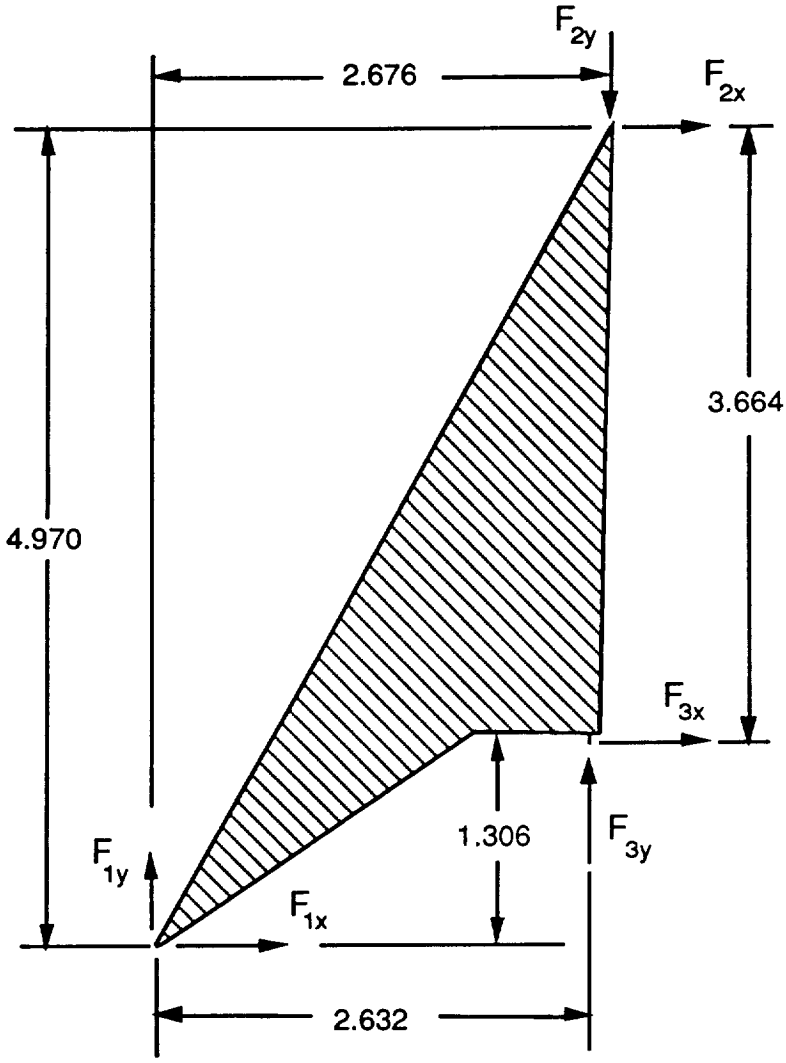

Figure 3.10 Link B (L-arm)

Because the mechanism is in static equilibrium, the sum of moments about any point is zero. Equating moments about point 1 gives:

$$M_1 = 0 \qquad (3.14)$$

$$0 = F_{2y}(2.632) - F_{3y}(2.676) - F_{3x}(4.970) - F_{2x}(1.306)$$

$$F_{3x}=[15{,}999.9(2.632)-16{,}000(2.676)-46.4(1.306)]/4.970$$

$$F_{3x} = -153.9 \text{ lb.}$$

$$F_{1x} = - F_{2x} - F_{3x} \qquad (3.15)$$

$$= 46.4 - 153.9$$

$$= - 107.5 \text{ lb.}$$

Thus, the transverse bearing force at the gear axis is 107.5 lb. to the left. This force causes a side load on the actuator piston seals. Figure 3.11 shows the actuator piston AB and the horizontal reaction loads that occur during testing. The system is in equilibrium so the sum of moments about any point is zero. Summing moments about point A gives the piston seal reaction force.

$$M_A = Fb(17.05) - Fs(6.50) = 0$$

$$Fs = Fb(17.05)/(6.50) = 107.5(17.05)/(6.5)$$

$$Fs = 282 \text{ lb.}$$

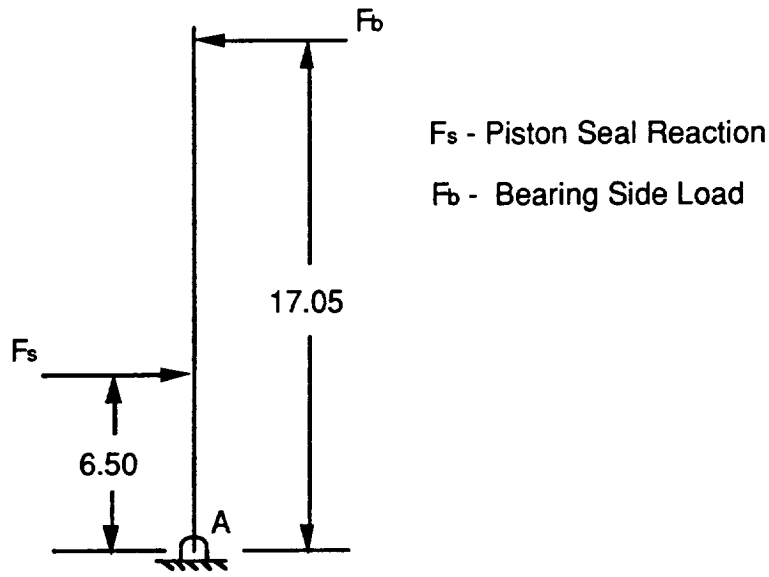

Figure 3.11 MTS Cylinder Seal Forces

According to MTS specifications, the actual side load is much lower than the 9000 lb. allowable side load. It was concluded that the MTS machine actuator piston seals were sufficiently compliant to allow lateral deflections to occur. According to engineers at the Materials Research Lab Inc., typical lateral deflections on their testing machine are approximately 0.010 -0.020 in and have negligible effects on the experiment. Because the side loads obtained from the SAE fixture loaded to 16,000 lb were less than 300 lb. and the maximum allowable side load according to MTS is 9000 lb., it was concluded that no damage to the machine was occurring, and the horizontal motion had no effect on the gear fatigue testing process.

Chapter IV

Results

4.1 Introduction

This chapter contains the results of fatigue testing gears of four different materials. First, the results of several non-destructive inspection methods are discussed including dye penetrant, magnetic particle, eddy current, compliance, and acoustic emission methods. Next, fixture alignment methods and results are discussed for crowned and uncrowned gears.

Finally, during the investigation of crack detection methods, fatigue life curves for all of the materials tested were generated. These are presented and compared. Also two different fatigue failure characteristics will be discussed.

4.2 Nondestructive Inspection Methods

Several nondestructive methods were used in this research to determine the point at which a fatigue crack initiated in the root of a gear tooth. A 9310 gear was cyclically loaded until a fatigue crack had initiated. This crack was not visible when the load was removed, but when the maximum testing load was applied, the crack extended across the entire face width and was 0.032 in. deep.

A visible dye penetrant was used to inspect the flawed gear tooth and no indications were observed. Because the load was removed, the crack closed up so tightly that the dye could not penetrate the crack. It was concluded that if dye penetrants are used, the gear should be loaded during the entire inspection process.

Ultrasonic testing was also used to inspect the damaged gear. The ultrasonic method also showed no relevant indications due to the very tight crack closure.

The eddy current and magnetic particle inspection methods were also used without success to inspect the flawed gear. It was determined that the crack closes so tightly that the electrical conductivity near the cracked region is not significantly altered, and tests which use the electrical properties of the material show no indications of flaws in this region.

One possible method of detecting the flaw is to complete these tests with the gear tooth under load. Due to the limited access to the gear when it is in the fixture and the safety hazards associated with the high testing loads required, none of these tests were carried out with the tooth under load.

4.3 System Stiffness Measurements

One nondestructive testing method used successfully to monitor fatigue cracks was the system stiffness method. The stiffness of the system was measured during the testing by monitoring the force applied to the system and the resulting acceleration. It was determiuned that a drop in the system stiffness, corresponded with initiation of a fatigue crack.

The stiffness of the system was measured for all teeth that were tested. This was done using a spectrum analyzer as explained in Ch. 3. The stiffness change during the fatigue testing was recorded using a computer and typical results are shown below.
The first plot, Fig. 4.1, is a plot of the system stiffness of a 4118 steel gear. This plot shows the typical shape of the system stiffness plot for all of the 4118 gears. All of the plots have been normalized to an initial stiffness of 100 to aid in comparison between different teeth and materials.

One trend that is observed in the data is that as the load is increased, the system stiffness at failure increases. This can be explained by thinking about the area of the final fracture surface. As the load is increased, a larger area is needed to cause similar stresses. Thus, at higher loads, the final fracture surface is larger, and therefore, the stiffness is greater.

Another very important trend that is followed by all of the gears tested is that the life to fatigue crack initiation is the greater part of the total life. In the plots shown, the initial value of the system stiffness is normalized to 100 at the beginning of testing when the gears have not been previously loaded. At that time there are no significantly large cracks that will reduce the stiffness. As the test continues, the stiffness begins to decrease when a fatigue crack initiates and propagates to some critical length.

Figure 4.1 shows that the fatigue crack propagation life (126,000 to 142,000 cycles) of 16,000 cycles is only 11.2% of the total fatigue life for the tooth. This trend is continued in all of the materials tested. From Fig. 4.4 we see that the fatigue initiation life of the shot peened 9310 gear is approximately 70,000 cycles while the fatigue crack propagation life is only 2700 cycles, which is only 3.7% of the total fatigue life.

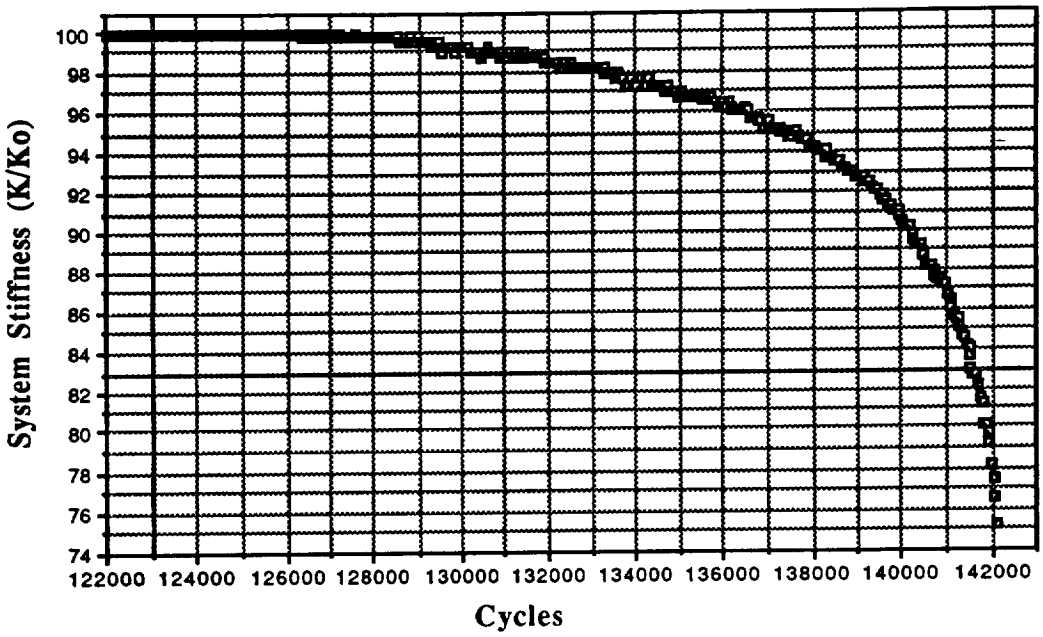

Figure 4.1 System Stiffness for 4118C at 170 ksi. Root Stress

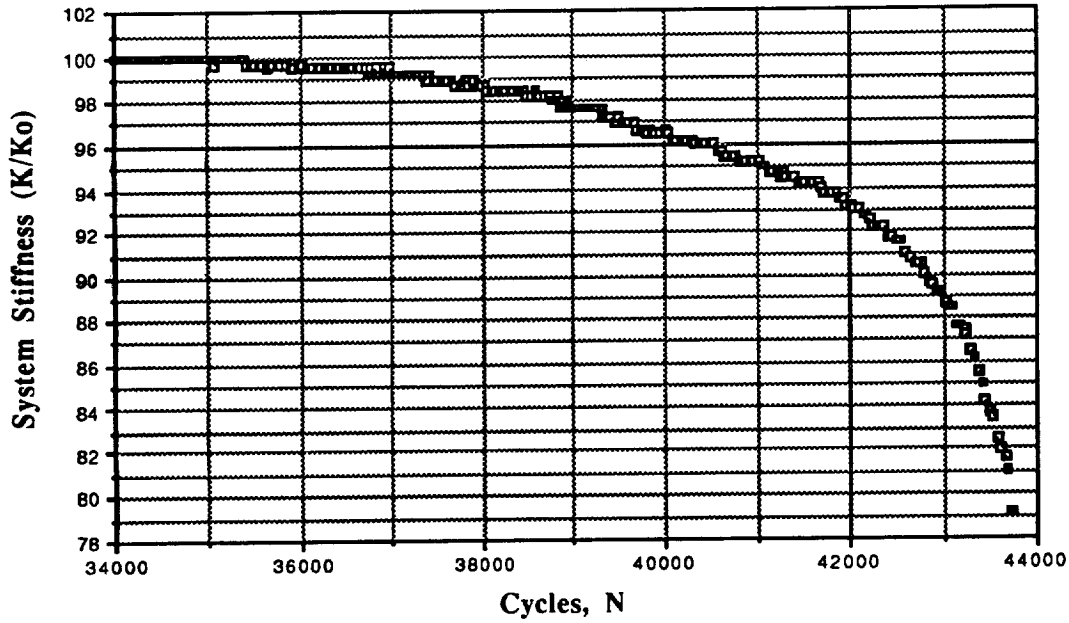

Figure 4.2 System Stiffness for 8620 at 187 ksi. Root Stress

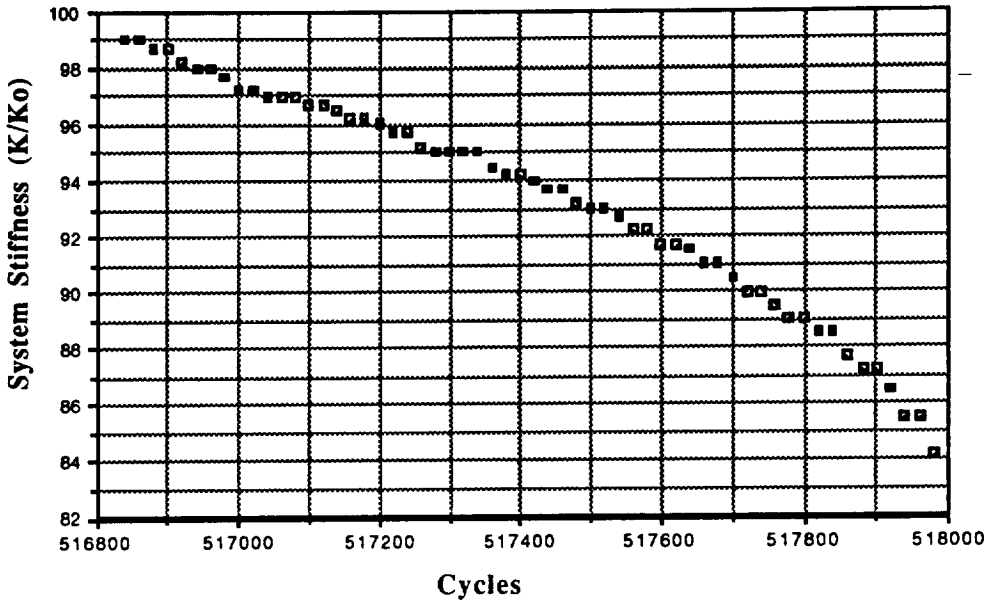

Figure 4.3 System Stiffness for 9310 at 262 ksi. Root Stress

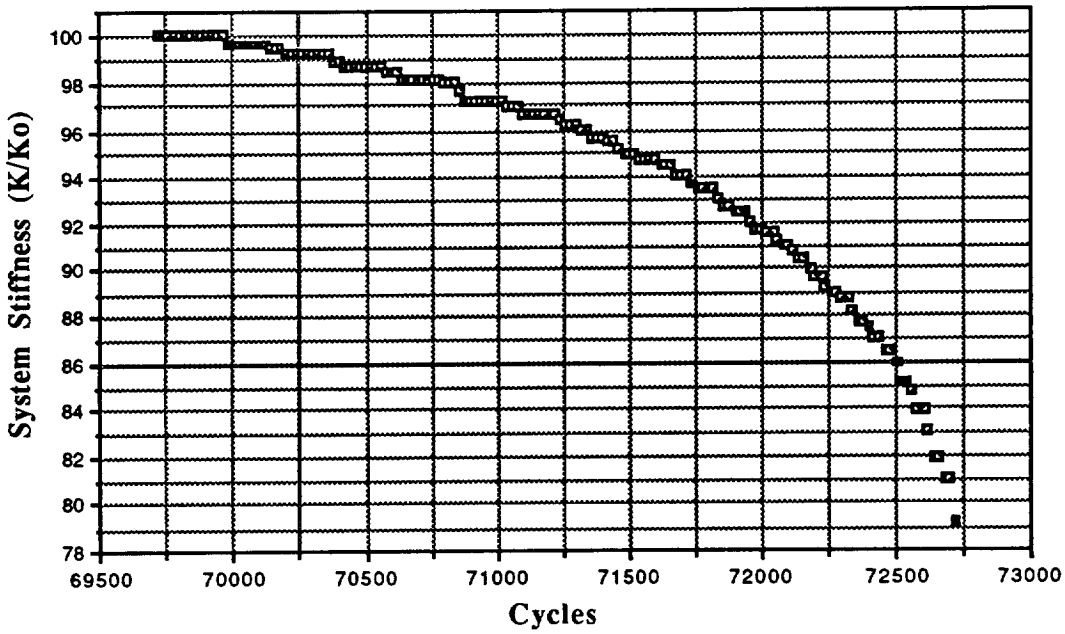

Figure 4.4 System Stiffness for 9310P at 262 ksi. Root Stress

4.4 Acoustic Emission

During testing, an acoustic emission transducer was attached to the gear to detect when a fatigue crack initiated. This method worked very well for the 4118 and 8620 gears but not so well for the 9310 gears. When the fatigue crack began to propagate in the 4118 gears, the acoustic emissions began to climb slowly, and as the crack propagated, the emission rate remained relatively constant. Near failure, when the part was deforming very rapidly, the acoustic emission rate increased very rapidly. Typical acoustic emission count vs. life plots for the crowned 4118 and 8620 gears are shown in Fig. 4.5 and 4.6.

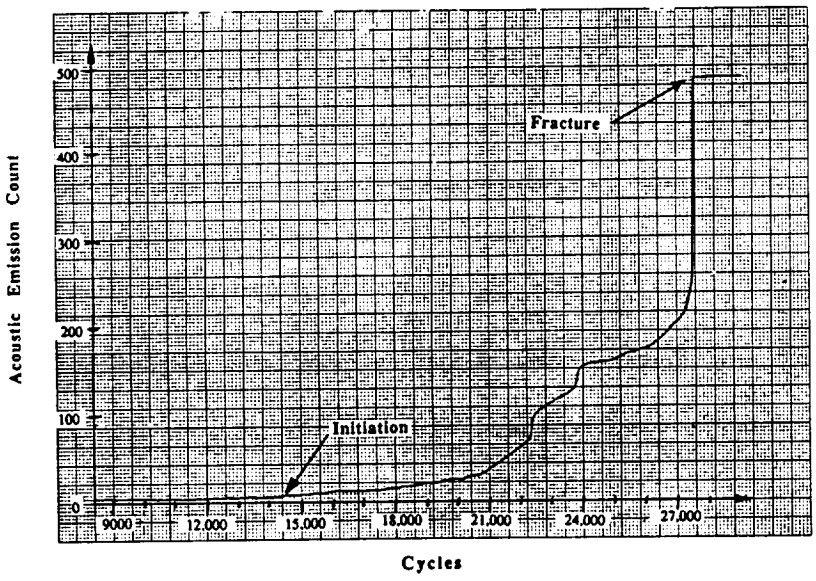

Figure 4.5 Acoustic Emission Count vs. Fatigue Life for 4118A Gear Tooth

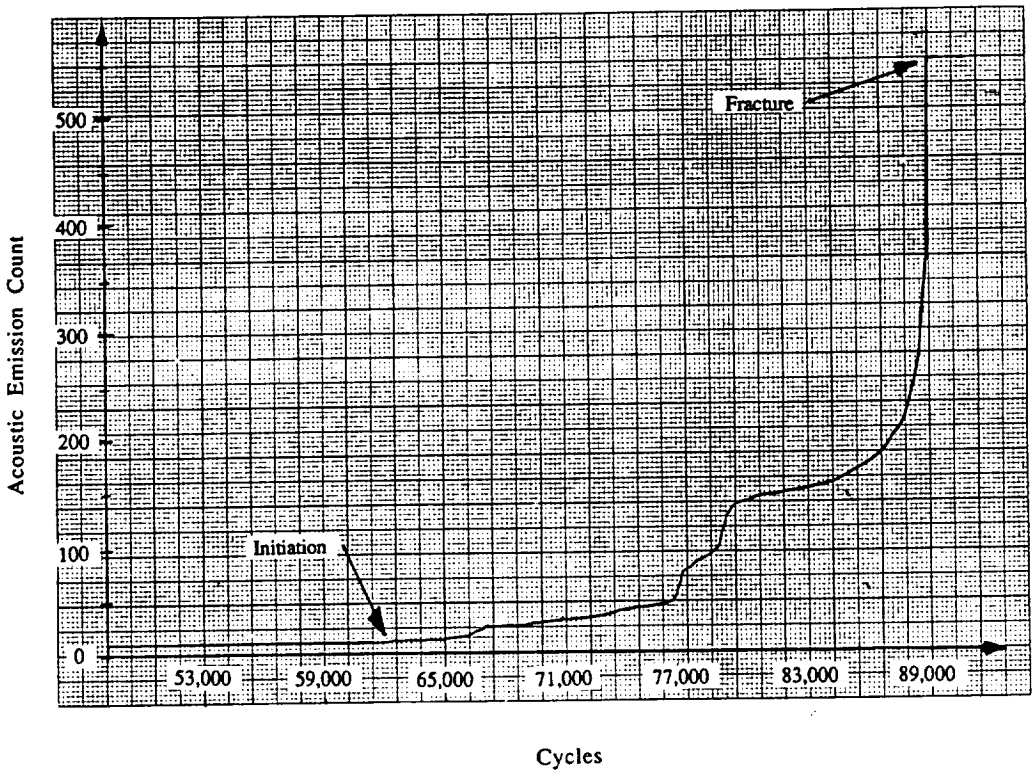

Figure 4.6 Acoustic Emission Count vs. Fatigue Life 8620 Gear Tooth

As can be seen from Fig. 4.5, the emission count begins to increase at around 12,000 cycles. This appears to be when a discontinuity reaches a critical length and begins to propagate. The emissions continue at nearly a constant rate, producing a slope that is nearly constant. The crack reaches another critical state and the emission count rate increases causing an increase in the slope of the counts-life curve. This slope remains constant until the tooth is near fracture at which time the count rate and total counts increase dramatically until fracture.

The initially slow count rate could be a result of the gears being crowned. The crack begins in the middle, and propagates outward to the edges of the teeth. The crack

is not visible until it reaches the edges of the tooth. Once the crack is across the entire thickness and through the case layer, the count rate remains fairly constant during propagation. As the crack reaches the fracture length, excessive plastic deformation occurs at the crack tip during each loading cycle which accounts for the very large count rate prior to failure.

In the 9310 gears, the crack initiation mode was very different. As the gear reached a critical point, the gear instantaneously cracked across the thickness. When this happened, the gear let out an audible pop that sounded like the snapping of one's fingers. After this snap, the gear was inspected, and a crack was found that traversed across the entire face width. At the same time this pop was heard, the acoustic emissions rose very rapidly as shown in Fig. 4.7 and 4.8. After this abrupt jump in emissions the count rate decreases, and the curve flattens out during propagation . As the gear nears failure, the emission rate once again increases very rapidly until failure.

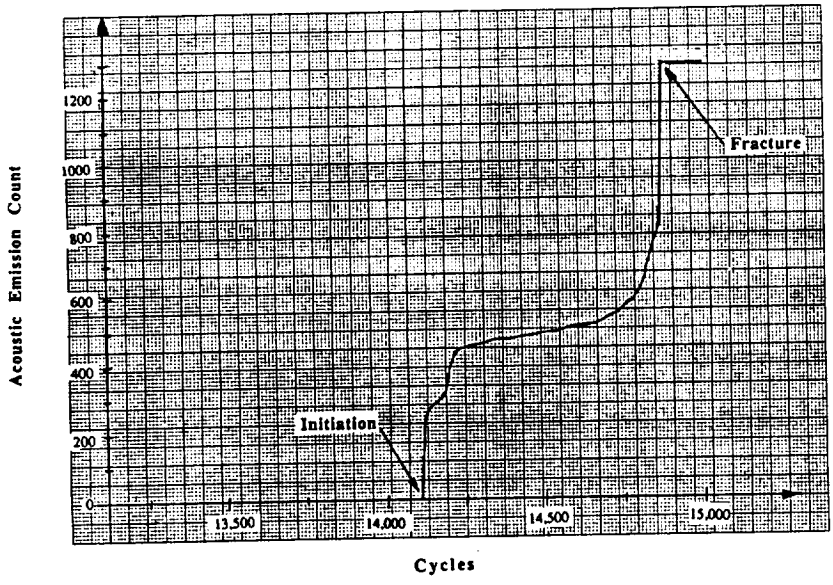

Figure 4.7 Acoustic Emission Count vs. Fatigue Life for a 9310 Gear Tooth

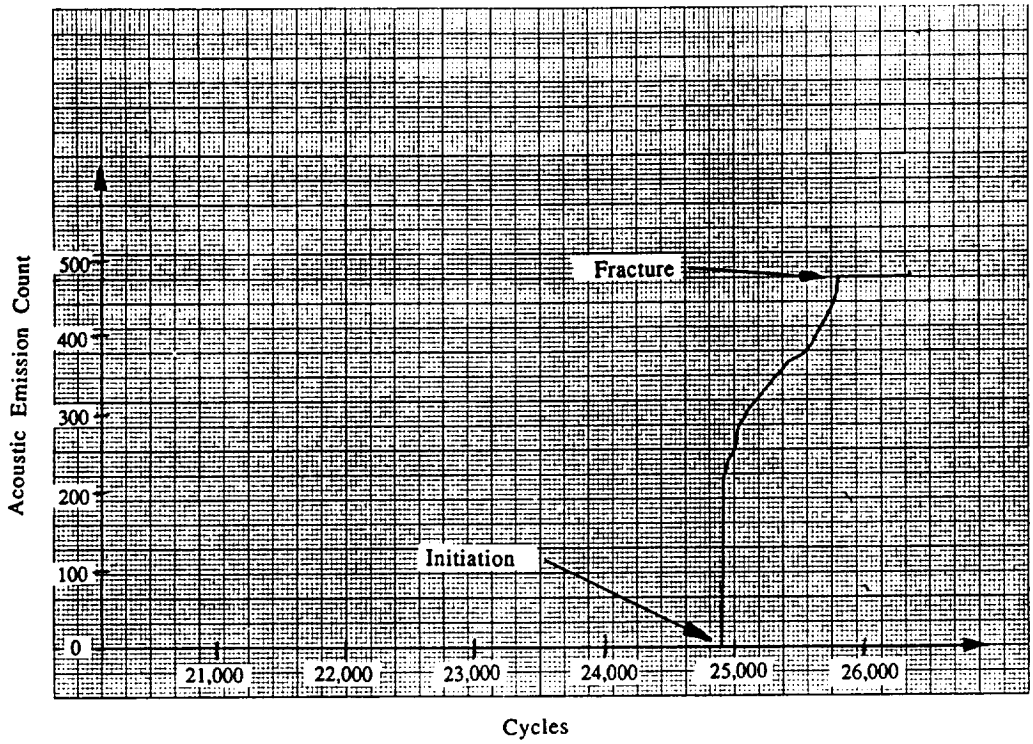

Figure 4.8 Acoustic Emission counts vs. Fatigue Life for a 9310P Gear Tooth

It is proposed that in the 9310 gears, a small discontinuity is growing below the surface near the case-core transition. After the crack reaches a critical value this sudden burst that occurs is the crack propagating rapidly to the surface. This failure is consistent with failures that occur below the surface of carburized steel in which the endurance limit of the core is much lower than the endurance limit of the case. The endurance limit is directly proportional to the hardness of the material in steels.

Figure 4.9 shows that if the endurance limit of the case and core are sufficiently similar or if the bending stress gradient is large, failure will occur in the case layer at the maximum stress location, which is at the surface in bending. This is the scenario that would be expected in most gear teeth since the teeth are exposed to very high loads, the tooth thickness is small, and bending stress gradient is very large.

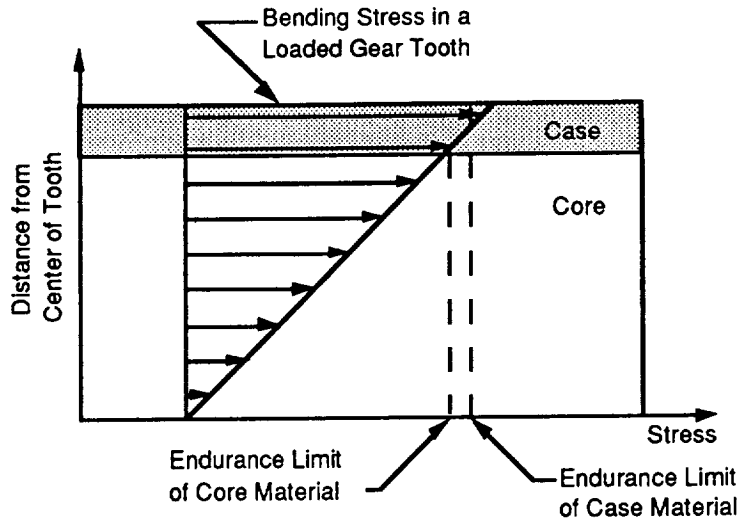

Figure 4.9 Example of Conditions for Failure in the Case

The opposite situation occurs when the case and core have very different endurance limits as seen in Fig 4.10. This situation could occur when the core has a much lower hardness than the case layer. This appears to be the case in the 9310 gears, because after fracture, there is a very large shear lip along the final failure surface. There is also a very distinct cup and cone type failure along this edge, suggesting that the core is much softer and much more ductile than the case layer. The hardness profile for the 9310 gears at a location 2/3 of the tooth hight from the tip, roughly the pitch line, are shown in Fig 4.11. These plots confirm the fact that the case layer is much harder than the core.

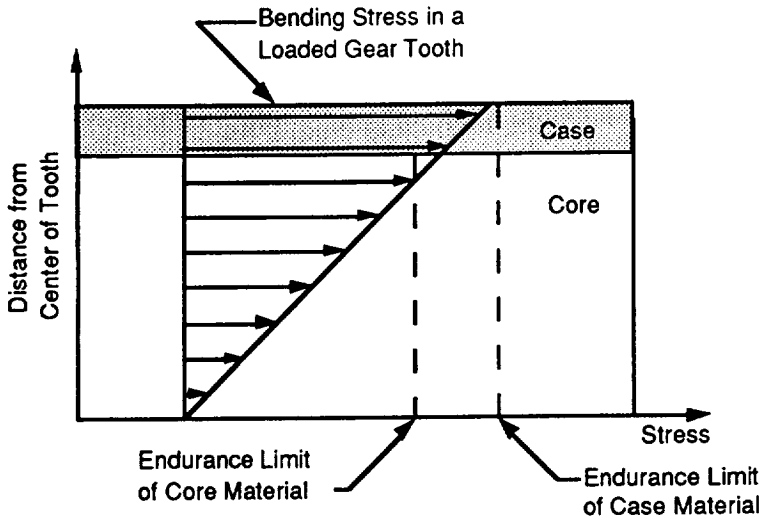

Figure 4.10 Example of Conditions for Failure in the Core

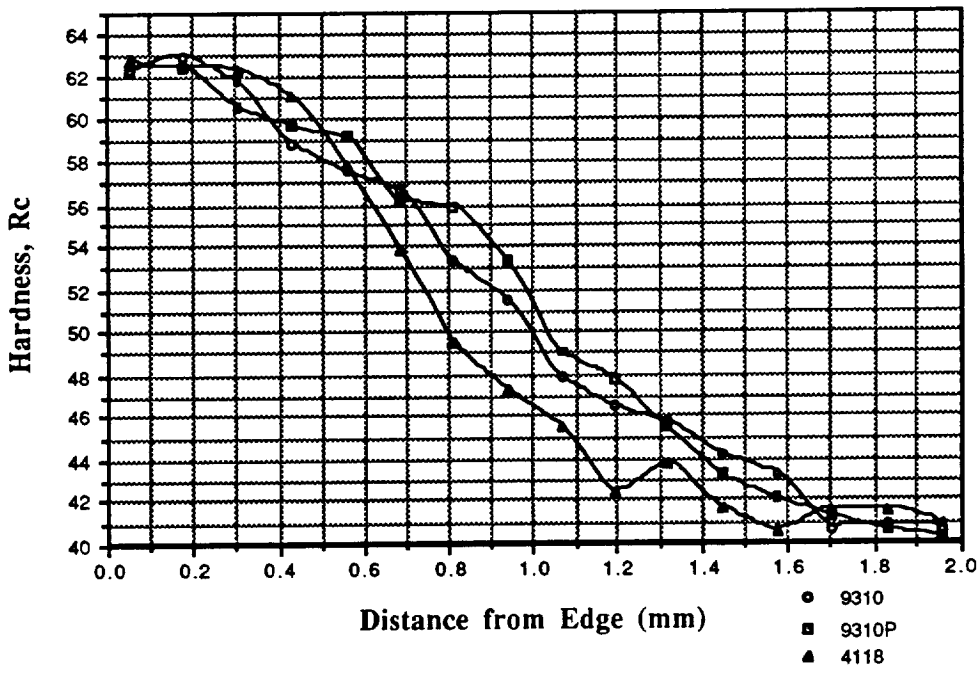

Figure 4.11 Hardness Profiles Near the Pitch Radius

Scanning Electron Micrographs (SEM) of two broken teeth from the 9310 gears reveal that the fatigue fracture area is very small, typically less than 1 mm, and transition from fatigue to rapid crack growth is very distinct. Two SEMs are shown below. The fatigue striations on the surface which have been worn down as the crack opens and closes are shown in Fig 4.12, and cup and cone type failure can be detected in Fig. 4.13.

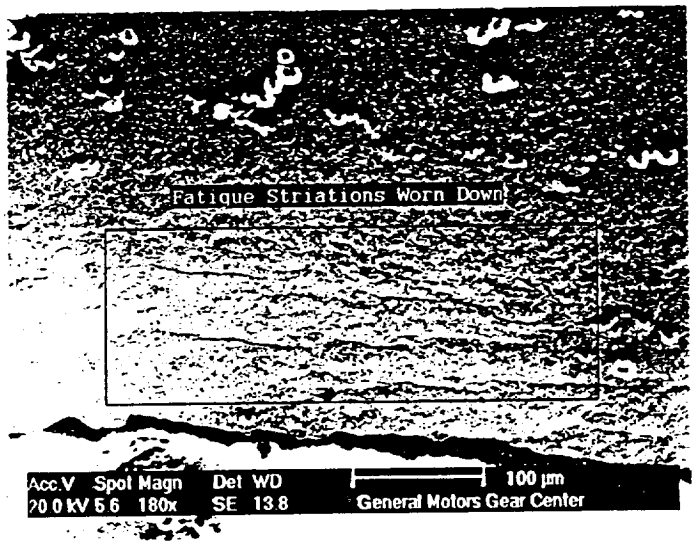

No etch 180x magnification

Figure 4.12 SEM of 9310 Gear Tooth Showing Fatigue Striations

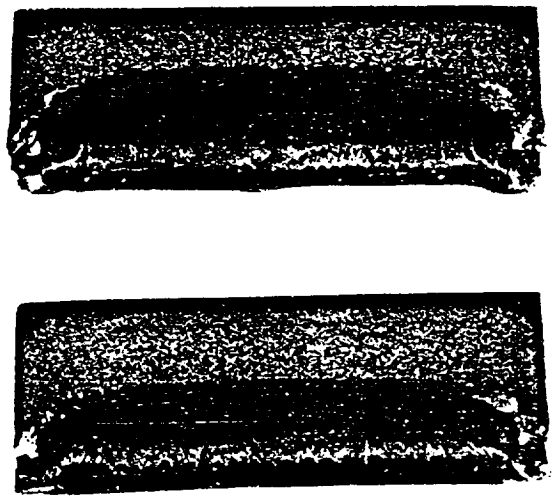

No etch 3x magnification

Figure 4.13 SEM Showing Cup and Cone Failure in 9310 Gear Tooth

Acoustic emission works very well for predicting the onset of a fatigue crack in the 8620 steels. Figure 4.14 shows a plot of the acoustic emission counts and through-the-thickness crack depth as measured along the side of the tooth. The acoustic emissions begin roughly 4000 cycles before a crack is visible, thus giving ample warning that a crack has reached a critical length and is beginning to propagate.

The crack was examined using a 10x magnifying lens and the depth was measured along the side of the tooth with a scale. This probably is not a very exact measure of the area of the crack front, because the crack front is most likely circular shaped and deeper in the center, rather than staight across. The material at the crack tip in the center of the face width is under conditions nearly consistent with plane strain which

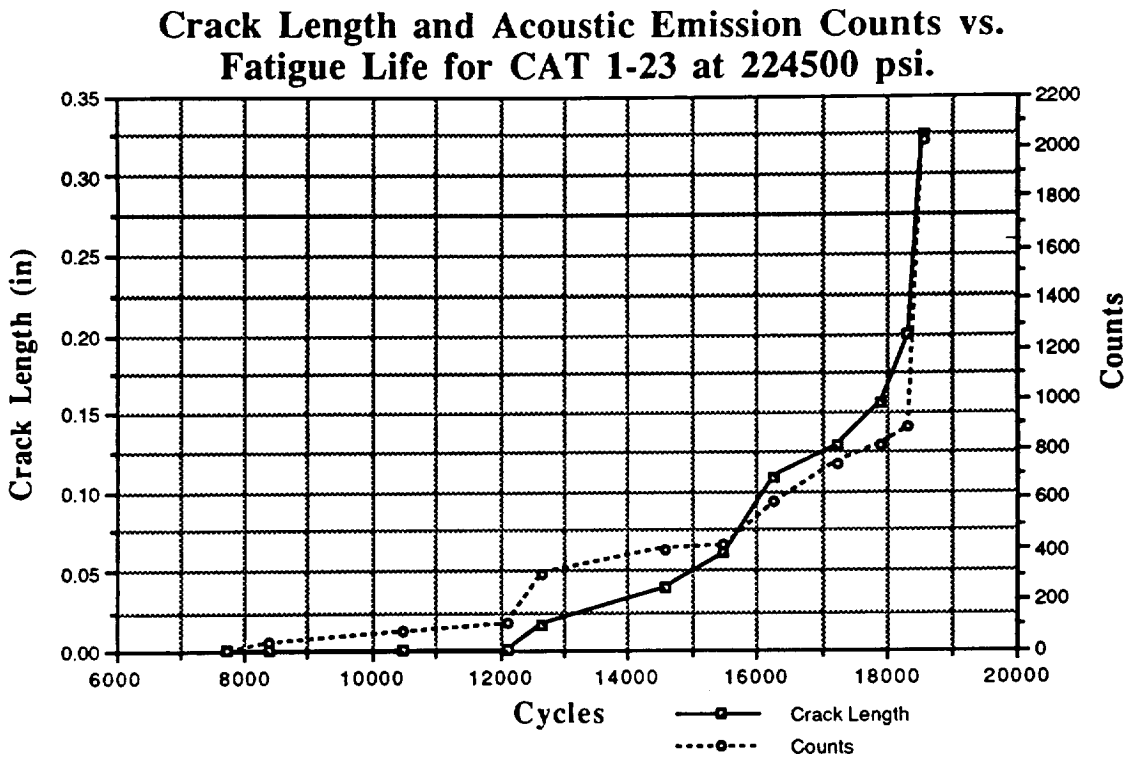

Figure 4.14 Acoustic Emissions and Crack Length as a Function of Fatigue Life

causes a more rapid crack growth rate than the condition of plane stress at the edges of the tooth.

4.5 Residual Stress Measurements

All of the gears obviously have very high residual stresses at the surface because they are being fatigue tested well above the ultimate strength of the material. These surface residual stresses are due to carburization. In the carburization process, the gear is heated to very high temperatures and surrounded by gas containing carbon. Some of the carbon atoms are forced into the surface of the steel. These excess carbon atoms are packed very tightly at the surface. As the part cools, the density of the steel is lower below the surface, and the core contracts more than the surface layer. This causes small

tensile forces in the core of the material and very large compressive forces in the thin case layer. This additional carbon in the case layer also greatly increases the hardness at the surface. The ultimate and fatigue strength are directly related to the hardness of the material so the fatigue strength of the case layer is also increased by the carburizing process.

The root surface residual stresses for two of the gears were checked by x-ray diffraction. The first gear checked was the unpeened 9310 gear. It had surface residual stresses as high as 94 ksi and an average residual stress from two different roots of 83.4 ksi. The shot peened gear had an average residual stress of 114.4 ksi. This shows that the shot peened gear has residual stresses about 30 ksi greater than the unpeened gear. These higher residual stresses should increase the fatigue life of the shot peened gear, but the results of this experiment reveal that the shot peened gear was much less resistant to fatigue than the unpeened gears.

One explanation for this behavior is that the shot peening process may have created microcracks at the surface which caused stress concentration areas and acted as initiation sites for fatigue cracks. The surface finish of materials has been shown to have a significant impact on the high-cycle fatigue life of machine parts; however, it has very little effect on the low-cycle fatigue or static strength of the part.. The fatigue lives of the peened and unpeened gears showed similar behavior in low cycle fatigue tests, suggesting that the surface may have been damaged by the peening process. More data is needed to determine the exact cause of the failures and the relative importance of the peening parameters on the bending fatigue resistance of carburized gear teeth.

4.6 Fixture Alignment

Initially, three strain gages were applied to a 9310 gear to use as a standard for checking alignment of the fixture. The results of the strain gage check are shown in Fig.

4.15. This figure shows the gage readings for increasing loads from 500 to 9000 lbs. As can be seen from the figure, the loads on the left are slightly higher than those on the right. Because the 9310 gears were not crowned, this misalignment caused higher loads on the left side of the gear teeth. The first eight teeth tested showed fatigue failures initiating at the left edge when the failure surface was viewed under a 20x stereo microscope. Pressure sensitive paper was also placed between the upper anvil of the fixture and the gear tooth and this showed that the contact was heavier on the left side of the tooth.

The base of the fixture was then stone ground smooth and set on a Starrett grade B granite surface plate. A dial indicator was used to measure the alignment of the shaft. It was determined that the shaft had a misalignment of 0.0004 in/in which caused the heavy loading on the left side. Stainless steel shims of different thicknesses were placed under the left bearing block until the misalignment was reduced to less than 0.0001 in/in. At this point the strain gaged gear was again loaded and the results are shown in Fig. 4.16.

Figure 4.16 shows that the load is now even across the tooth. The values of strain at the two edges are nearly identical at all loads. The strain in the middle of the tooth is slightly higher due to plane strain conditions in the center of the tooth and plane stress conditions at the edges. The remainder of the testing was carried out with the shims in place.

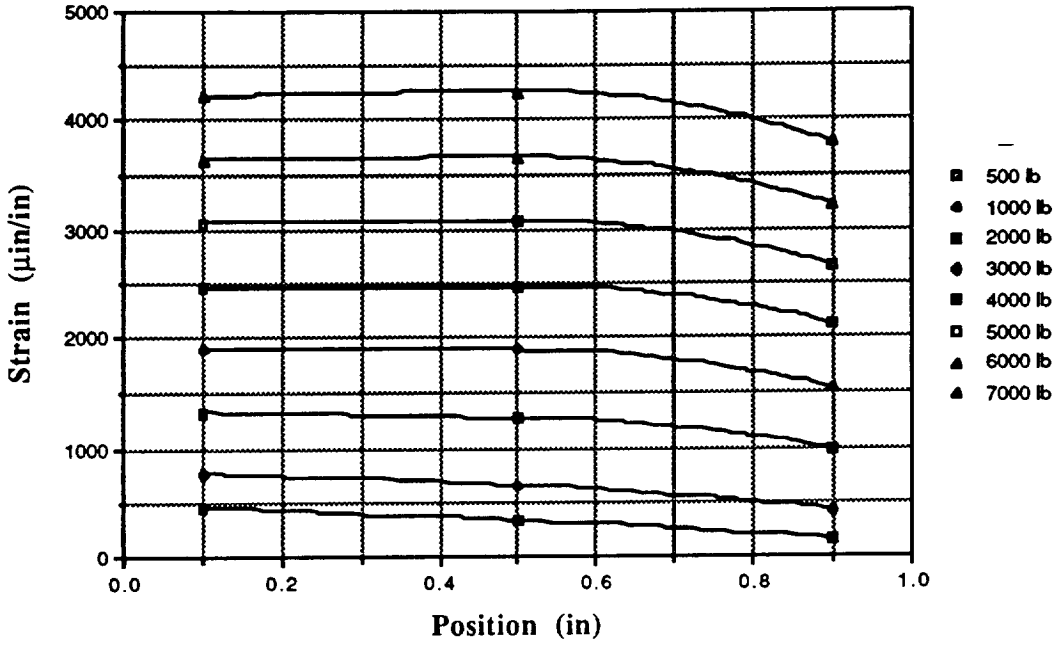

Figure 4.15 Strain Gage Readings Across Face Width (0.0004 in/in Misalignment)

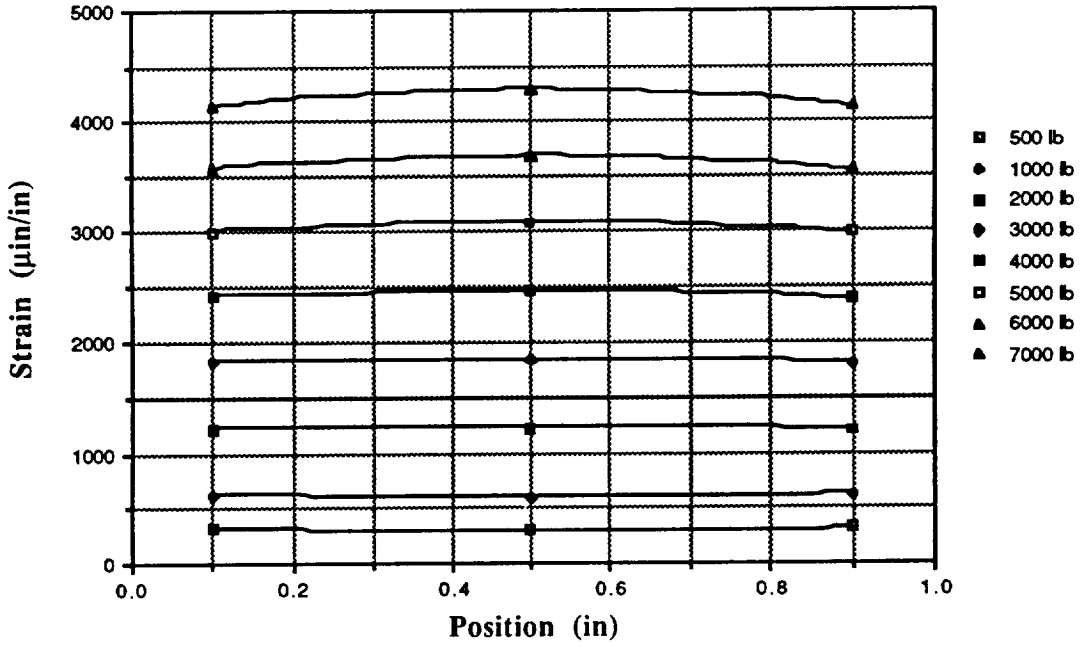

Figure 4.16 Strain Gage Readings Across Face Width (0.0001 in/in Misalignment)

Further testing and microscopic examination of 6 teeth revealed that the cracks were initiating in the center of the teeth after the alignment was adjusted. This suggests that the fixture was aligned properly and no further alignment was needed. The fixture was checked periodically using this strain gaged gear and it was found that even with some wear on the anvils, the fixture alignment was satisfactory.

4.7 Tooth Stresses

The stresses in the teeth were calculated using two methods. The first is by assuming a state of plane strain and multiplying the measured strains at the center of the tooth by the modulus of elasticity for steel ($30x10^6$ psi). The second method for calculating the gear tooth stresses was by using a boundary element method in the program GEARBEM available at Ohio State University. The results of these two calculations are shown below in Fig. 4.17.

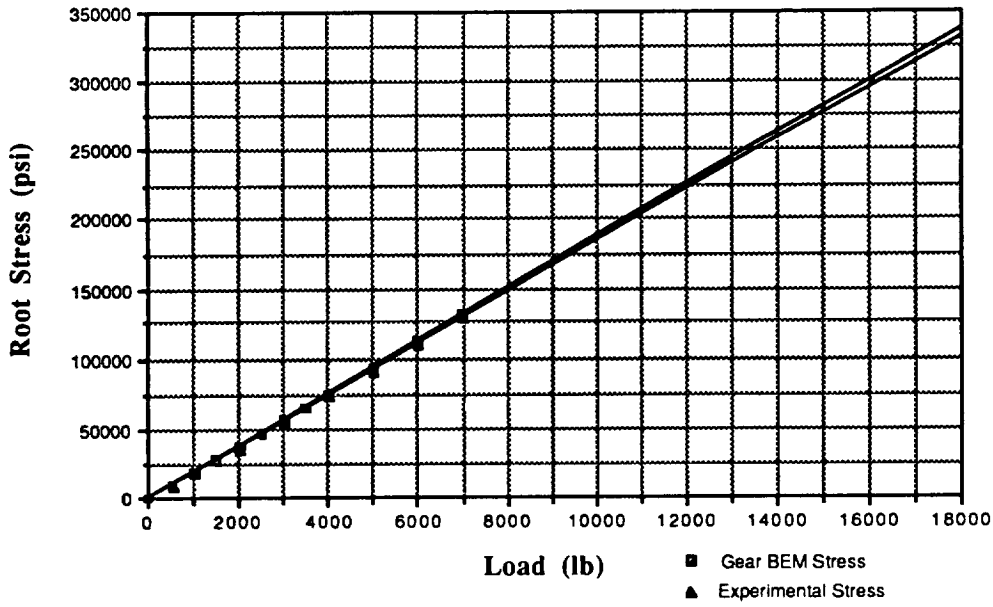

Figure 4.17 Gear Root Stresses

The two methods agree very well. At a 7,000 lb load the stresses agree to within 2%. Since both methods assume a linear stress-strain relationship, the curves can be extrapolated to the maximum testing load of 18,000 lb. which corresponds to a root stress of 335,000 psi. This root stress, which is cyclically applied is well above the ultimate strength of 9310 steel. This implies that some very large residual stresses must be present to allow fatigue testing at such high loads. The properties of the materials used in this research are given in Table 3. All values are approximate and were obtained from the manufacturers of the gears.

Table 4.1 Material Properties of Tested Materials

Material	Surface Hardness	Core Hardness	Yield Strength	Ultimate Strength
9310 Steel	Rc 60-63	Rc 33-41	260 ksi	290 ksi
8620 Steel	Rc 58-62	Rc 28-40	230 ksi	270 ksi
4118 Steel	Rc 60-62	Rc 32-42	230 ksi	270 ksi
ADI 675	NA	NA	109 ksi	124 ksi

Tables A.1 and A.7 in the Appendix show the testing stress, life to crack initiation (Ni), fatigue propagation lives (Np), total life to failure (Nf), and ratio of initiation to total life of all of the test gears. The fatigue crack initiation life, Ni, was determined by the point at which the stiffness of the fixture decreased by 1% if the initial value. The data shows that the fatigue crack propagation lives of 4118 steel are always much greater than those in 9310 steel. At lower loads, at which the total fatigue life was near 1 million cycles, the 4118 gears had one tooth with a crack propagation life of 43,600 cycles with propagation lives near 20,000 cycles being common. The unpeened

9310 gears, on the other hand, had crack propagation lives which never exceeded 1500 cycles. Shot peening seems to have improved the crack propagation life because some shot peened gears had crack propagation lives exceeding 4500 cycles. This is due to the higher residual compressive stresses in the shot peened gear which help to retard the crack growth. The total fatigue lives of the shot peened gears were much shorter at a given load than those that were not shot peened, indicating that the shot peening procedure may have damaged the surface of the gears.

Figure 4.18 shows the ratio of fatigue crack propagation life to the total life for all of the gears as obtained from Table G.1 and G.7 in Appendix G. The 4118, 8620, and the 9310 gears show the same trend. At high loads, and lower fatigue lives, the fatigue crack propagation life becomes a significant portion of the total life. In some 4118 gears at very high loads, the fatigue crack propagation life was around 40% of the total life. However, as the lives increased into the realm of actual gearing applications, the fatigue propagation life becomes a much lower portion of the total fatigue life. As the 1 million cycle range is approached, the fatigue crack propagation life becomes only about the last 10% of the total life.

For the 9310 gears, the crack propagation life was seldom greater than 10% of the total life even at very high loads. These gears also followed the trend that as the total life increases, the propagation life became an even smaller portion of the total life. Based on the sensitivity of the instrumentation used, these results imply that for high cycle fatigue failures commonly found in gearing, the life to initiate a fatigue crack is much greater than the propagation life.

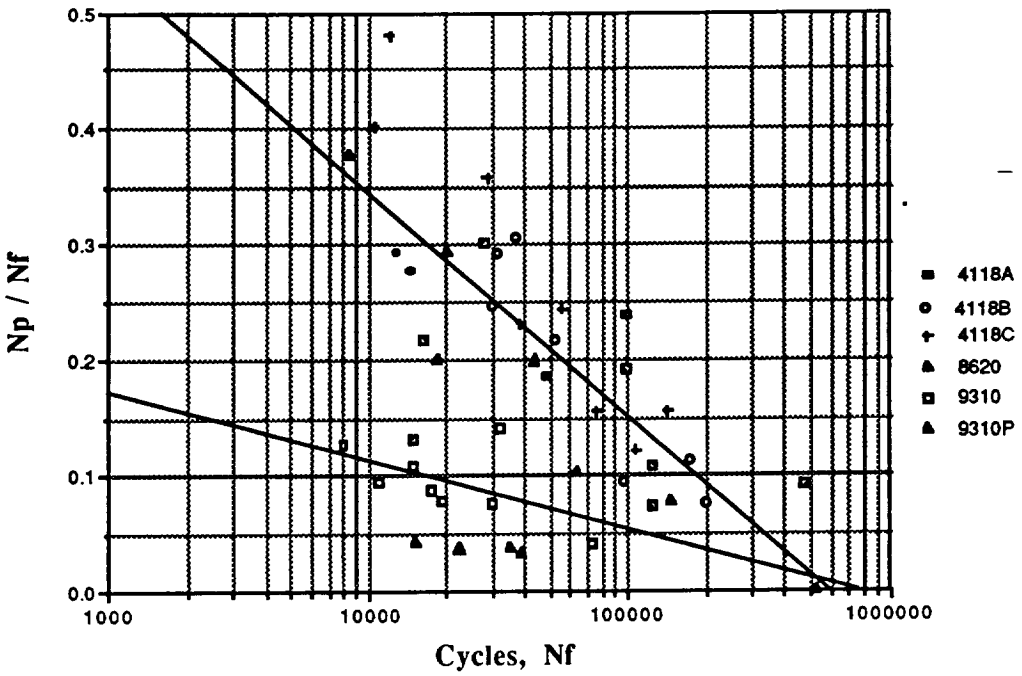

Figure 4.18 Ratio of Fatigue Propagation Life to Total Life as a Function of Total Life

4.8 Fatigue Life Curves

The gears that were tested during this research include several unpeened 9310 steel gears, two shot peened 9310 steel gears, several 4118 steel gears of three different root surface finishes, two 8620 steel gears, and an austenitized ductile iron (ADI 675B) test gear. The resulting fatigue life plots are shown in Fig. 4.19-4.22. Due to lack of testing time, it was decided to use 10^6 cycles as a runout . This is not far off from the run-out of $2x10^6$ used by some industry sponsors. This runout value allowed more time for testing in the finite life region to establish a basic shape for this portion of the curve.

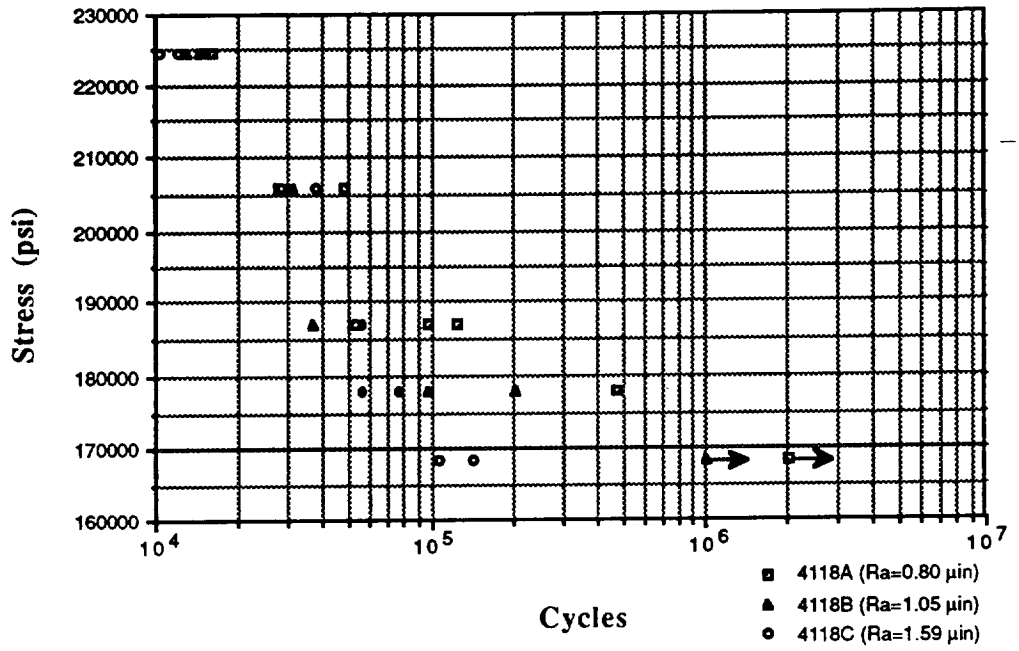

Figure 4.19 Fatigue Life Plot for 4118 Test Gears

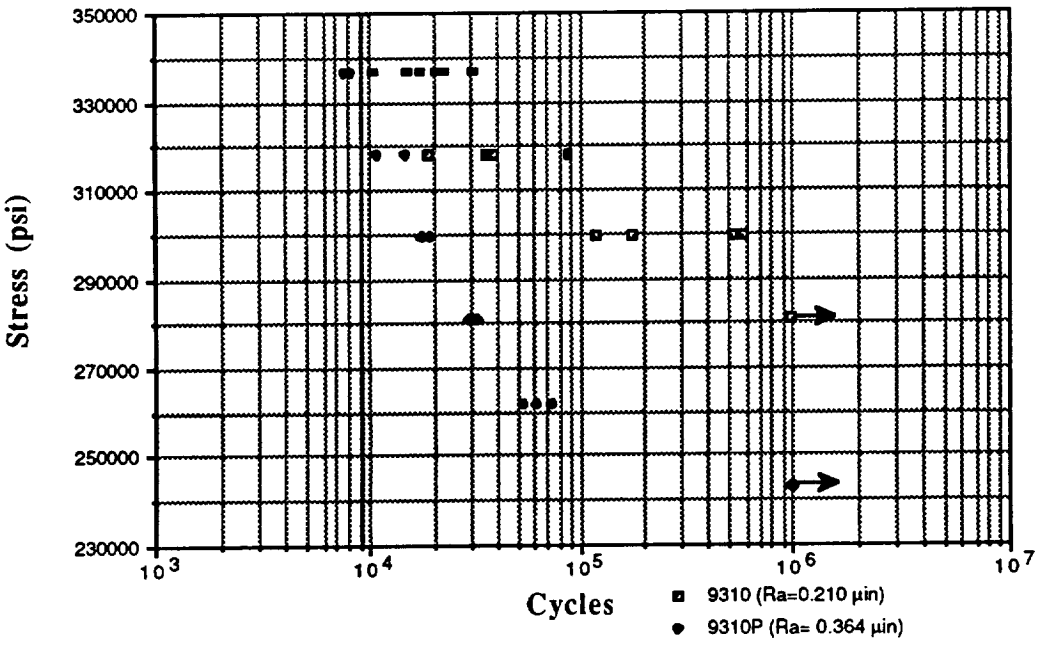

Figure 4.20 Fatigue Life Plot for 9310 Test Gears

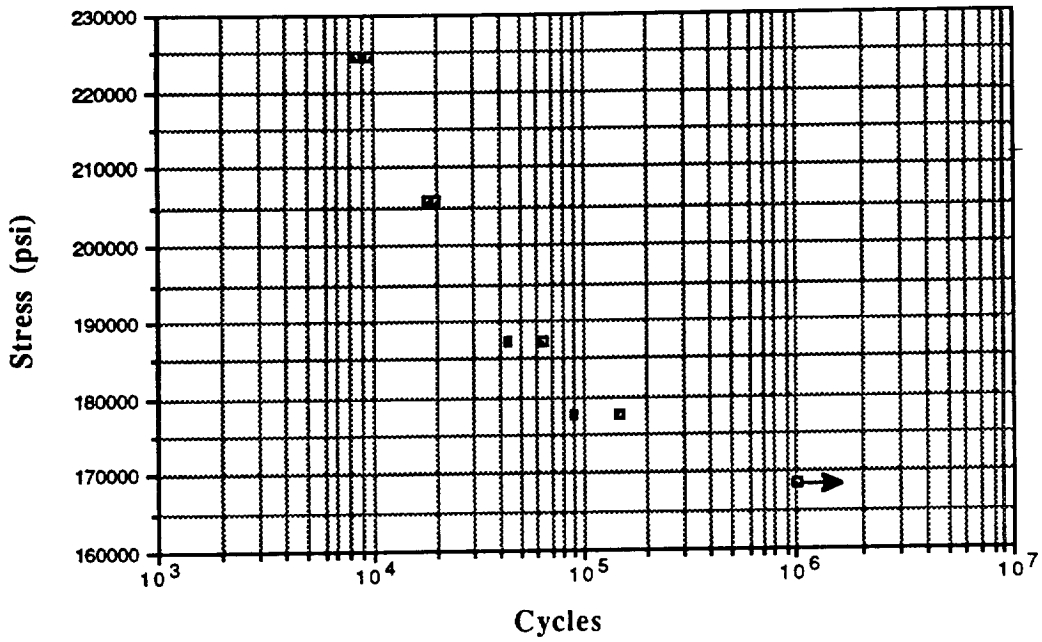

Figure 4.21 Fatigue Life Plot for 8620 Test Gears

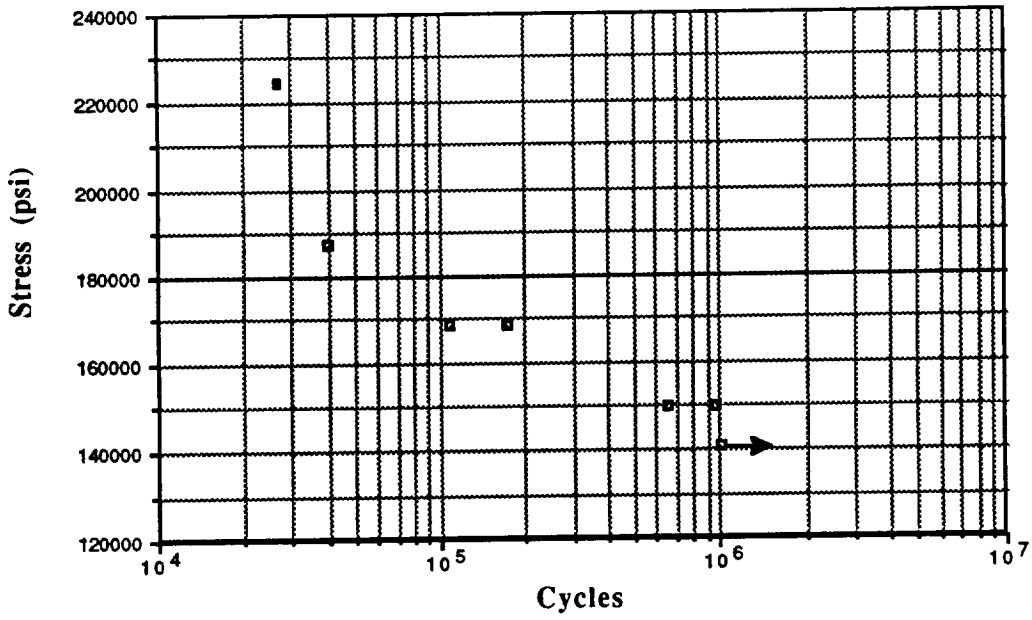

Figure 4.22 Fatigue Life plot for ADI 675 Test Gear

From Fig. 4.19-4.22, it can be seen that all of the 4118 and 8620 gears have similar fatigue strengths, while the 9310 steel gears have much higher fatigue strengths. The ADI gear has fatigue properties similar to the 8620 gears at high loads but appears to have lower fatigue resistance in the higher cycle portions of the curve near 10^6 cycles.

From Fig. 4.19 it can be seen that all of the 4118 gears have similar fatigue strengths at the very high loads, independent of the surface finish. This is to be expected since low cycle fatigue properties are related to the notch sensitivity of the material. The notch sensitivity of a material is defined as the maximum stress in a notched specimen divided by the stresses in a part without a notch loaded similarly. Steels have a relatively low notch sensitivity to defects smaller than 0.001 in. due to localized yielding which eliminates stress concentrations at very sharp discontinuities. Thus, fatigue strength for low cycle fatigue is close to the ultimate strength of the material.

The high cycle fatigue properties of materials are quite different than the low cycle properties. The small discontinuities caused by machining provide the the perfect spot for fatigue crack initiation. When the material is stressed below the yield strength, the area at the tip of a discontinuity experiences a higher stress than the surrounding material due to stress concentrations. This higher cyclic stress combined with continuous exposure to the atmosphere, which may oxidize the surface material, provides the perfect conditions for the initiation of a fatigue crack. Once the crack has initiated, the stress concentration at the tip of the crack becomes very large and the crack propagates rapidly.

Inspection of Fig. 4.20 reveals that in the realm of high cycle fatigue, the fatigue life is directly proportional to the size of the discontinuities on the surface (surface roughness, Ra). The high cycle fatigue properties of the gears with different surface finishes are similar near fatigue lives of 10,000 cycles, but begin to diverge as the fatigue lives increase.

The 4118 gears, with surface roughness values (Ra) of 0.80 and 1.05 μin., 4118A and 4118B respectively, have greater fatigue resistance at the lower testing loads than gear 4118C with a surface roughness of 1.59 μin. This is evident when the fatigue lives are compared at 177 ksi. Groups 4118A and 4118B have run-outs at 10^6 cycles at this stress, while group 4118C fails at approximately 13,000 cycles. From this small sample of data is appears that surface roughness (Ra) values above 1.1 μin. begin to significantly affect the fatigue life of 4118 steel gear teeth.

Upon examination of Fig 4.21, it is seen that the fatigue life of the 8620 gears, which have a surface roughness of 1.33 μin have fatigue properties comparable to those of 4118A and 4118B.

The ADI gear had fatigue lives comparable to the 8620 gears for fatigue stresses in the range of 170 to 220 ksi but as the load is lowered, and the high cycle fatigue effects are most prevalent, the ADI gear falls short of the 8620 in fatigue resistance. This can be explained by looking at the picture from the scanning electron microscope (SEM).

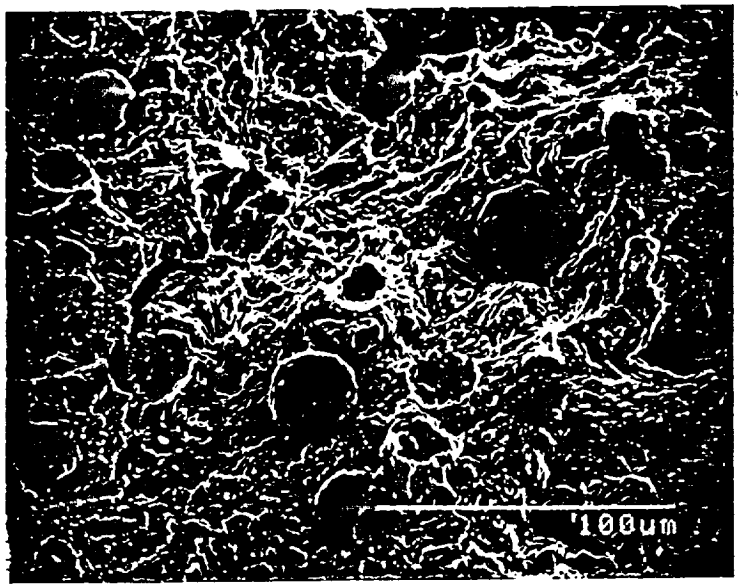

Figure 4.23 Scanning Electron Micrograph of ADI Gear Tooth (500x)

The SEM revealed that a crack initiated at the surface and propagated through the iron matrix between graphite nodules. ADI is filled with spherical graphite nodules that act as stress raisers to help initiate and propagate fatigue cracks.

Figure 4.20 shows the fatigue life of several 9310 steel gears that were manufactured exactly alike and heat treated in the same batch. Four of the gears was then shot peened. Rather peculiar results were obtained in this research. The fatigue life of the shot peened gears was significantly lower than that of the unpeened gears. The fatigue strength at root stresses of roughly 280 ksi. was reduced from a run-out at 10^6 cycles in the 9310 group to a failure at $3x10^4$ cycles in the shot peened gears.

One possible cause for the reduction in fatigue life is that the gears were over peened or peened at to high an intensity and the shot peening process created small microcracks on the surface of the part. These microcracks act as fatigue crack initiation sites, thus reducing the fatigue life of the part.

Chapter V

Conclusions and Recommendations

5.1 Conclusions

The SAE single tooth bending fatigue fixture used in this research in conjunction with a hydraulic fatigue testing machine produced very consistent results. The fixture uses a common shaft to mount the gear, stationary support anvil, and the oscillating testing anvil. This configuration allows very good reproducibility of the tests with little data scatter.

One problem with the fixture is the lack of any method of aligning the anvils across the face width of the gear teeth. This causes a built in misalignment in the fixture if the machining tolerances are not strictly enforced. This misalignment causes edge loading on the tooth face when uncrowned gears are tested, and incorrect fatigue data results.

The fixture was aligned by placing shims under the bearing blocks. Using a strain gaged gear for a standard, it was determined that the misalignment was eliminated.

Several gear materials and surface finish conditions were investigated. The gear materials tested were 4118 steel, 8620 steel, 9310 steel, shot peened 9310 steel, and austenitized ductile iron 675, and the 8620 gears were manufactured to three different root surface finishes.

Fatigue life curves for all gears were plotted. It was determined that the fully ground 9310 gears, which had the best surface finish, also had the best fatigue resistance to a zero to maximum fatigue loading cycle.

All of the 9310 gears were manufactured from the same heat of steel and carburized together. After heat treating, four of these gears were shot peened. The results of this process were quite peculiar. The shot peened gears showed much lower fatigue resistance than the unpeened gears.

It was proposed that the gears may have been over-peened or peened at too great an intensity, and this may have caused microcracks on or near the surface. These results require further investigation to determine the exact cause of the reduction in life due to shot peening.

Several nondestructive methods were used in this research to determine the point at which a fatigue crack initiated in the root of a gear tooth. A 9310 gear was cyclically loaded until a fatigue crack had initiated. This crack was not visible when the load was removed, but when the maximum testing load was applied, the crack extended across the entire face width and was 0.031 in deep.

A visible dye penetrant was used to inspect the flawed gear tooth and no indications were observed. When the load was removed, the crack closed up so tightly that the dye could not penetrate the crack. it was concluded that if dye penetrants are used, the gear should be loaded during the entire inspection process.

Ultrasonic testing was also used to inspect the damaged gear. The ultrasonic method also showed no relevant indications due to the very tight crack closure. The eddy current, and magnetic particle inspection methods were also used to inspect the flawed gear without success. It was determined that the crack closes so tightly that the electrical conductivity near the cracked region is not significantly altered, and tests which use the electrical properties of the material show no indications of flaws in this region.

One possible method of detecting the flaw is to complete these tests with the gear tooth under load. Due to the limited access to the gear when it is in the fixture and the

safety hazards associated with the high testing loads required, none of these tests were carried out with the tooth under load.

One method which was used with great success was a stiffness method. This method consisted of measuring the force applied to the testing fixture and the resulting acceleration of the system. These two signals were input to a spectrum analyzer and the system stiffness was monitored. It was determined that a drop in the system stiffness corresponded with the initiation of a fatigue crack. The stiffness changes for different materials were investigated.

From the system stiffness data, it was discovered that the fatigue life corresponding to fatigue crack propagation was only about 10% of the total fatigue life in the high cycle fatigue range typical of gearing designs. As the total life of the part increases, the portion of the life corresponding to fatigue crack propagation decreases. This data suggests that for high cycle fatigue more attention should be focused on initiation rather than propagation.

One other method that was used to determine fatigue crack initiation was acoustic emission (AE). This involved mounting a sensor on the gear to be tested and monitoring the area where a fatigue crack was expected. High frequency stress waves, or AE, produced by the gear during deformation signified the initiation of a fatigue crack. This method worked well at predicting the initiation of fatigue cracks in all materials tested, and acoustic emissions correlated very well with the growth of fatigue cracks.

When testing the crowned 8620 gears, the acoustic emissions began several thousand cycles before the fatigue crack could be detected visually. The emission rate was constant at the beginning of initiation, rose gradually to higher value and remained constant at this higher rate during fatigue crack growth. The emission rate then rose very sharply near final fracture. The AE counts correlated very well with the crack length.

For the 9310 gears, there were no emissions during testing until a point when the tooth suddenly cracked making an audible sound like snapping ones finger. At this time, the AE count rose abruptly, and a crack in the root of the gear was present. It was typically 0.02-0.04 in deep and extended across the entire face width. This phenomena occurred in all 9310 gears tested.

It is proposed that the failure is initiating beneath the surface at the case-core interface and the snap that is heard is the crack rapidly propagating through the case material to the surface. More testing is needed to determine the exact initiation mechanism and failure mode.

Acoustic emissions seems to be a very good method of determining when a crack is initiating in the root of a gear tooth. The only real difficulty with the method is that it is very sensitive to mechanical noise such as fluid flow through valves, and bearing friction noise. This noise can be reduced by attaching damping material to the gear surface. This reduces the oscillations of the gear and reduced the AE counts related to the noise. Damping material also allows the AE instrument gain to be increased by 3 dB, increasing the sensitivity, without the AE signal being contaminated by mechanical noise.

5.2 Recommendations

The first recommendation is that the effect of load position on the test tooth be investigated. If the loading location turns out to not be a critical factor, a rubber or plastic spacer could be used in place of the needle bearings inside the gear to allow some deflection and eliminate the binding effect when the gear tooth deflects. Second, a complete metallurgical study should be undertaken to determine the cause of the reduction in fatigue strength in the shot peened 9310 test gears. Third, more data should be taken in the high cycle fatigue fatigue range near 1 million cycles to obtain an estimate of the

fatigue endurance limits of the materials being tested and to study the fatigue life curves near the transition from finite to infinite life.

Acoustic emissions should be used to determine the point at which to stop a test and investigate the size of the initial fatigue crack. If the initial crack size could be determined, a fracture mechanics method could be used to very accurately predict fatigue crack propagation. Some other methods of locating and measuring fatigue cracks such as AC field methods and acetate tape methods could also be investigated.

REFERENCES

Acoustic Emission in Metals, Instron Corporation, (I-C-7-2), Canton, Massachusetts.

Barhorst, F.A., Master's Thesis, The Ohio State University, Department of Mechanical Engineering, 1991.

Barton, J.R. and Kusenberger, F.N., "Fatigue Damage Detection," Metal Fatigue Damage-Mechanism, Detection, Avoidance, and Repair, ASTM STP 495, American Society for Testing and Materials, pp. 123-227, 1971.

Buenneke, R.W., Slane, M.B., Dunham, C.R., Semenek, M.P., Shea, M.M., & Tripp, J.E., "Gear Single Tooth Bending Fatigue Test," SAE Technical Paper Series, No. 821042, International Off-Highway Meeting and Exposition, Milwaukee, Wisconsin, September, 1982.

Bowles, S.J., "Acoustic Emission Load-Cycle Dependence Applied to Monitoring Fatigue Crack Growth Under Complex Loading Conditions," NDT International, Vol. 22, No. 1, pp. 7-13, February 1989.

Dunegan, H.L. and Harris, D.O., "Gear Failure-Tooth Bending Fatigue," SAE Technical Paper Series, pp. 1-7, September 1985.

Dunegan, H.L., Harris, D.O., and Tetelman, A.S., "Prediction of Fatigue Lifetime by Combined Fracture Mechanics and Acoustic Emission Techniques, Procedings of the Airforce Conference on Fatigue and Fracture of Aircraft Structures and Materials, AFFDL TR 70-144, December 1969.

Dunegan, H.L. and Tetelman, A.S., "Acoustic Emission," Research Development, Vol. 22, No. 5, pp. 20-24, February 1974.

Ermolov, M.I., Petrovanov, N.E., and Vadkovskii, N.N., "Comparative Tests of Methods of Surface Inspection, The Soviet Journal of Nondestructive Testing, Vol. 25, No. 11, pp. 839-844, July 1990.

Friesel, M.A., "Application of Signal Analysis to Acoustic Emission from a Cyclically Loaded Aluminum Joint Specimen," Materials Evaluation, Vol. 47, No. 7, pp. 842-848, July 1989.

Fuchs, H.O., Shot Peening, Paramus, New Jersey, 1986.

Fuchs, H.O., Optimum Peening Intensities, Paramus, New Jersey, 1987.

Fuchs, H.O., Ed., Shot Peening Stress Profiles, Paramus, New Jersey, 1987.

Fuchs, H.O. and Daly, J.J., Mechanical Production of Self Stresses, Paramus, New Jersey, 1987.

Fuchs, H.O. and Stephens, R.I., Metal Fatigue in Engineering, John Wiley and Sons, New York, p. 16, 1980.

Green, A.T., "Acoustic Emission Testing," Test, pp. 8-17, October/November 1978.

Lazerev, A.M. and Rubinshtein, V.D., "Examination of Acoustic Emission in Fracture Toughness Testing of Specimens," The Soviet Journal of Nondestructive Testing, Vol. 24, No. 12, pp. 837-842, August 1989.

Lenain, J.C., "General Principles of Acoustic Emission," DE 78-5, Dunegan/Endevco, San Juan Capistrano, California, 1979.

Lester, A.E., "Gear Failure-Tooth Bending Fatigue," SAE Technical Paper Series, International Off Highway and Powerplant Congress and Exposition, Wisconsin, pp. 1-7, September 1985.

Nicolas, T., Ashbaugh, N.E., and Weerasooriya, T., "On the Use of Compliance for Determining Crack Length in the Inelastic Range," Fracture Mechanics:Fifteeenth Symposium, ASTM STP 833, R.J. Sanford, Ed., American Society for Testing and Materials, pp. 682-698, 1984.

Pollock, A.A., Acoustic Emission Inspection, TR 103-96, Physical Acoustics Corporation, December 1989.

Shot Peening Applications, Metal Improvement Company, Inc., 7th Ed.

Tatro, C.A., "Experimental Considerations for Acoustic Emissions Testing," Materials Research and Standards, MTRSA, Vol. 11, No. 3, p. 17, March 1971.

"Whispered Warnings of Silent Danger," AE International, Richland, Washington.

Appendix A

Gear Drawing SK 56249-560

1. All diameters on a common centerline to be concentric to each other within .010 diameter unless otherwise noted.
2. Break all sharp edges not specified to a radius or chamfer of .010-.020. Visual inspection of this dimension is satisfactory.
3. Maximum machined surface roughness to be 125 RMS unless otherwise noted.
4. Billet or bar shall have a minimum mechanical reduction of 3 to 1 from the ingot.
5. Fluorescent magnetic particle inspect per Appendix 1.
6. Finish on teeth flanks and fillets 20 RMS maximum.
7. Mark part number and serial number with a vibro etch. Do not impression stamp.
8. Lead tolerance applies to full face width minus edge breaks. Crowning or end relief to be avoided.
9. Shot peen after final grind per Appendix 2, Class B.
10. Material: 9310 Steel VIM/VAR.
11. The fillet shall be a smooth curvature with no steps or grooves.
12. The tooth profiles and fillets shall be finish machined by form grinding with no undercut.
13. Heat Treatment:
    - A: Carburize. Appendix 3.
    - B: Carburized case hardness Rockwell C 60-63.
    - C: Effective case depth at Rockwell C50 before grinding .045"-.055".
    - D: Effective case depth at Rockwell C50 after grinding .037".055".
    - E: Core hardness Rockwell C 33-41.
14. AGMA Quality 12 for lead deviation.
    AGMA Quality 9 for profile deviation.
    Check 6 teeth ground circumference for consistency in gear accuracy.

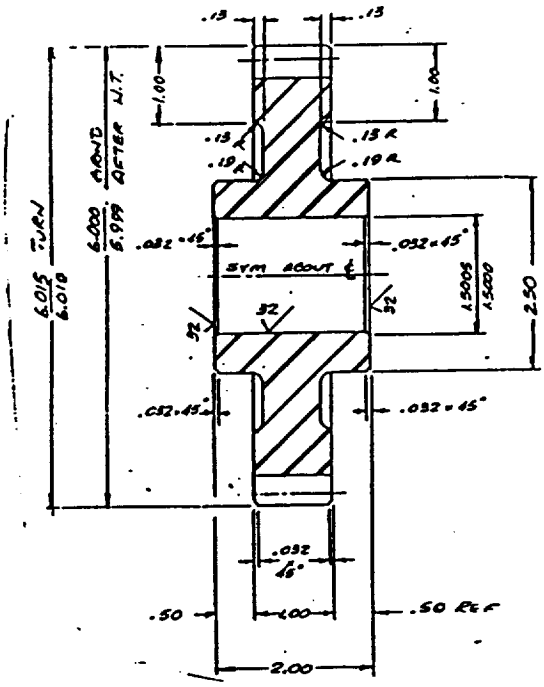

SPUR GEAR DATA

NUMBER OF TEETH	36
DIAMETRAL PITCH	6
PRESSURE ANGLE	20
BASE CIRCLE DIA	5.3719 2.6245
ROOT DIA.	6.1890 2.5935
CIRCLE TOOTH THK AT	6.6669 2.8373
THEO	0.2618
PIN MEASUREMENT OVER	0.2810
DIA PINS	6.069 - 6.063
ADD	.166
DED	.210
WHOLE DEPTH	.406
MIN FILLET RADIUS	0.0768

UNLESS OTHERWISE SPECIFIED

.DM TOLERANCES

ONE PLACE (X)	± .060
TWO PLACE (XX)	± .030
THREE PLACE (XXX)	± .010

SIZE	CAGE CODE	DWG NO	REV
A	99207	SK56249-560	—

SPUR GEAR FOR SINGLE TOOTH BENDING FATIGUE

SCALE NONE

SHEET 1

GT-9301-F

.05 1.00

Appendix B

Lead and Profile Checks

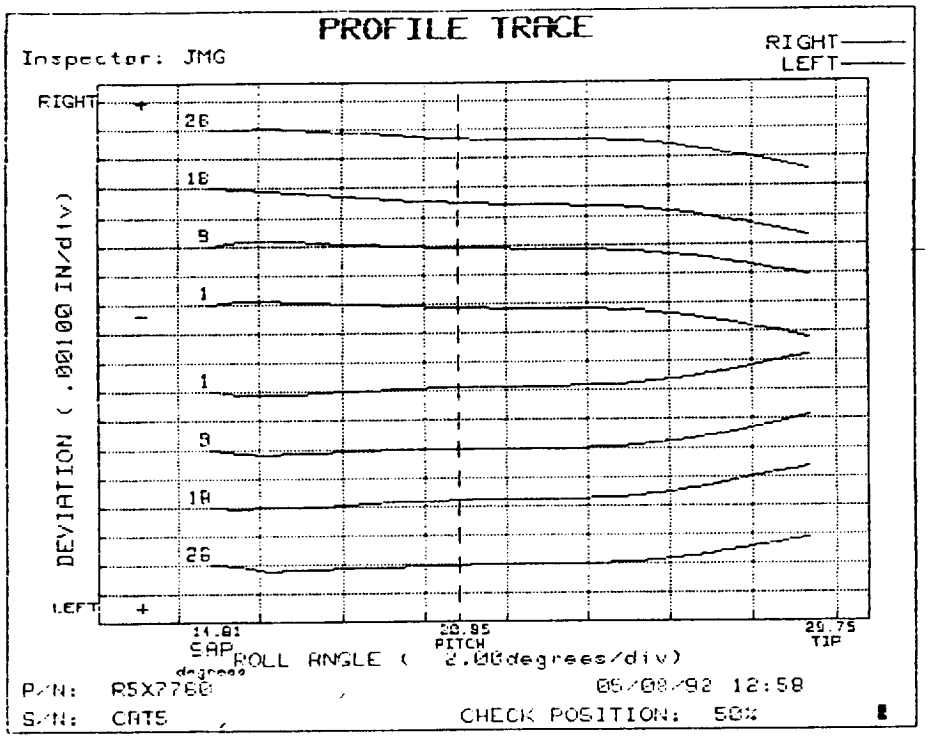

Figure B.1 Profile Checks for a 4118 Test Gear

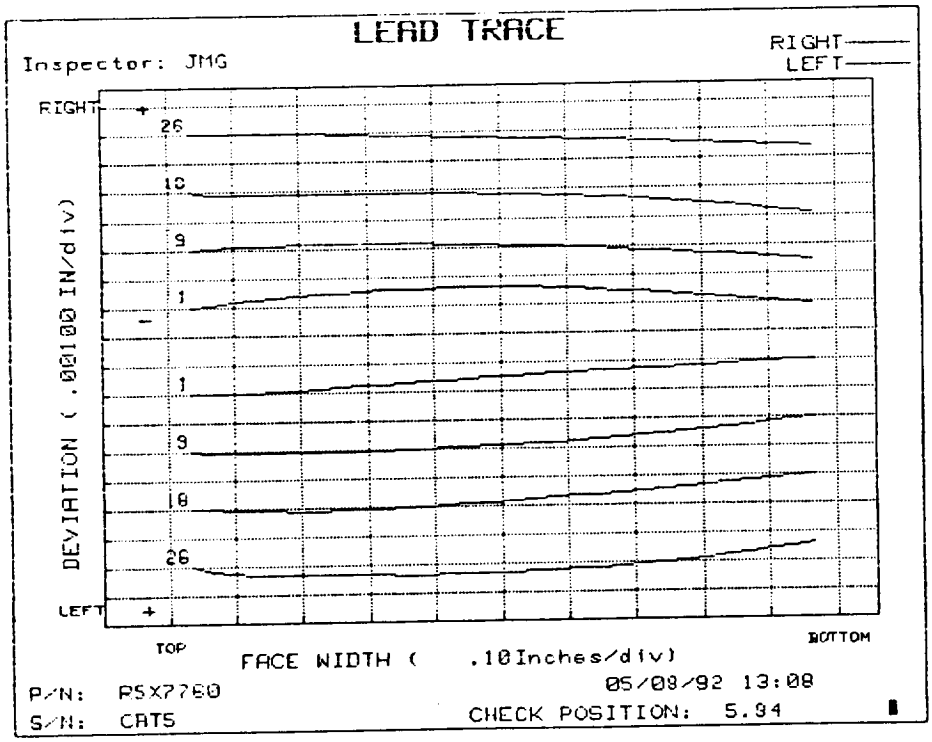

Figure B.2 Lead checks for a 4118 Test Gear

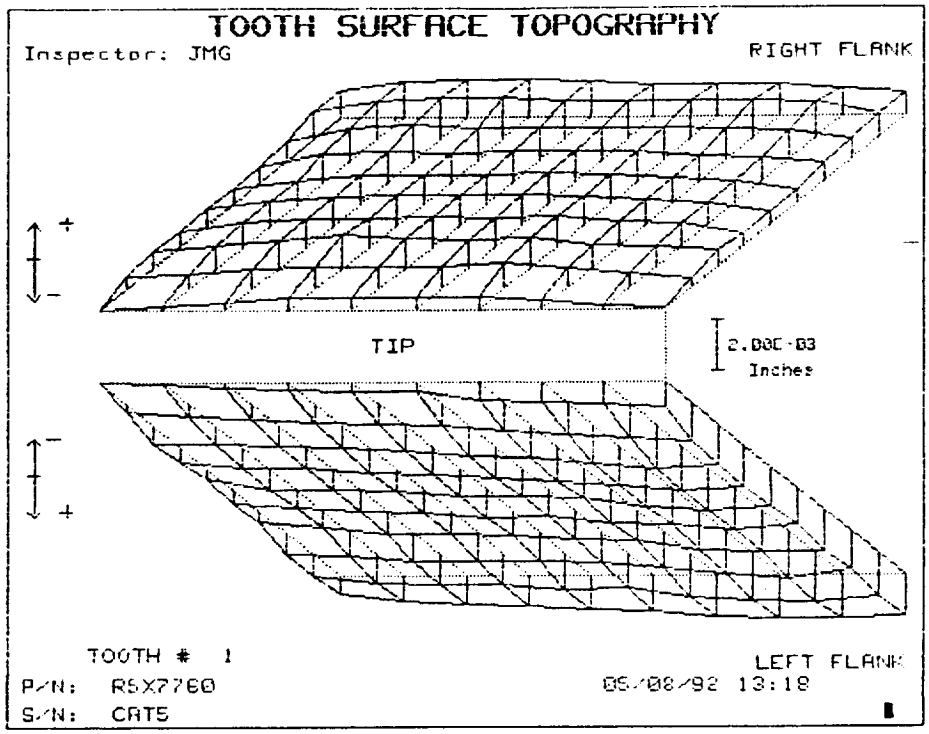

Figure B.3 Surface Topography of a 4118 Test Gear

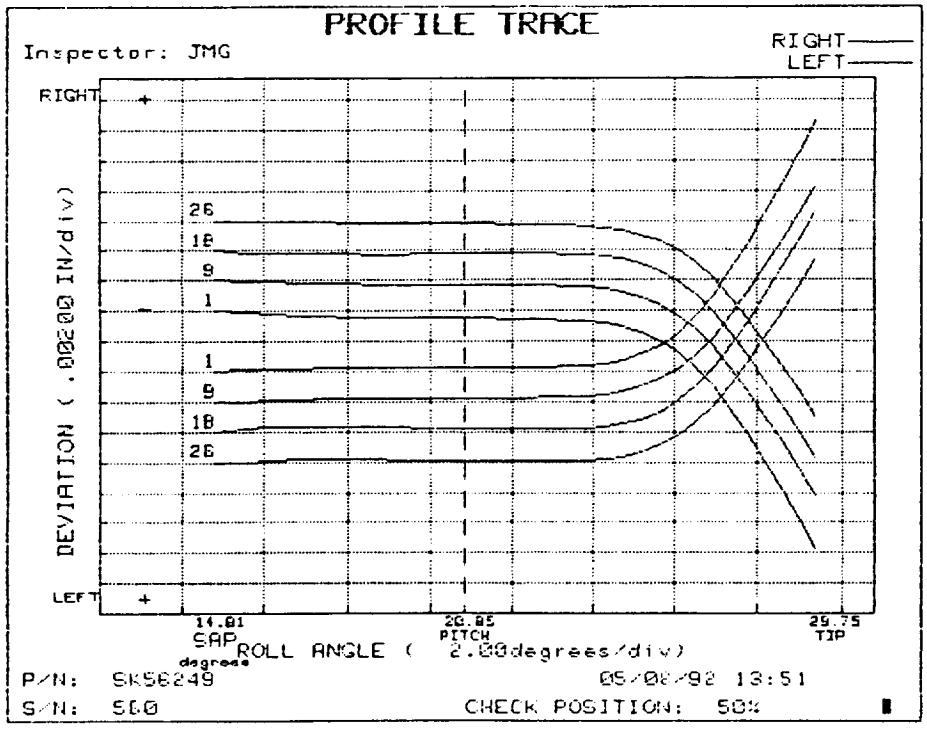

Figure B.4 Profile Checks for an 8620 Test Gear

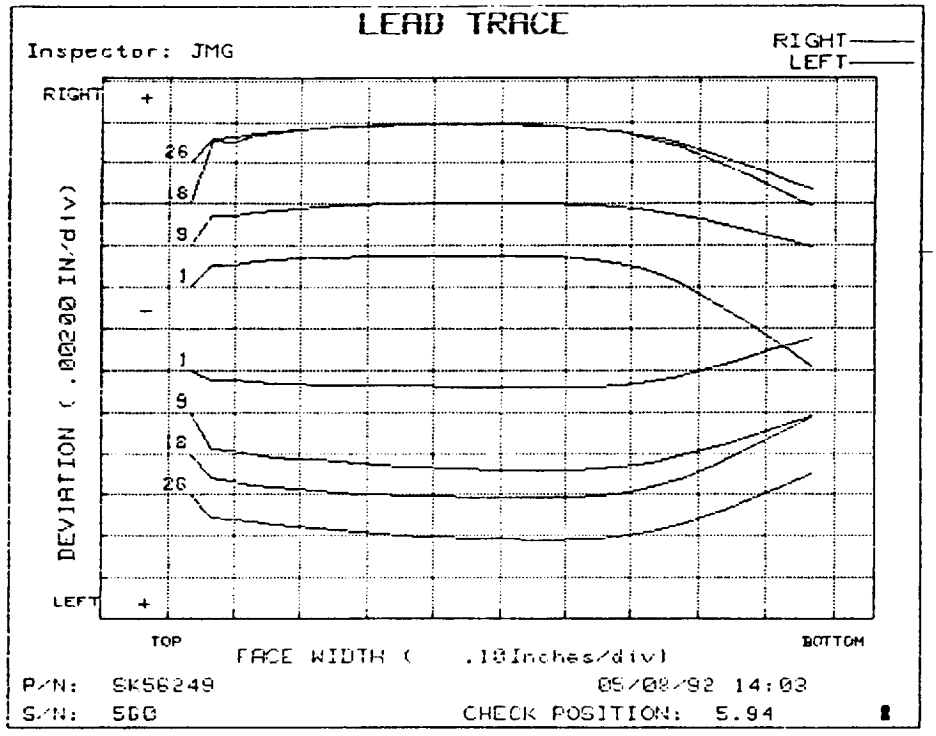

Figure B.5 Lead Checks for an 8620 Test Gear

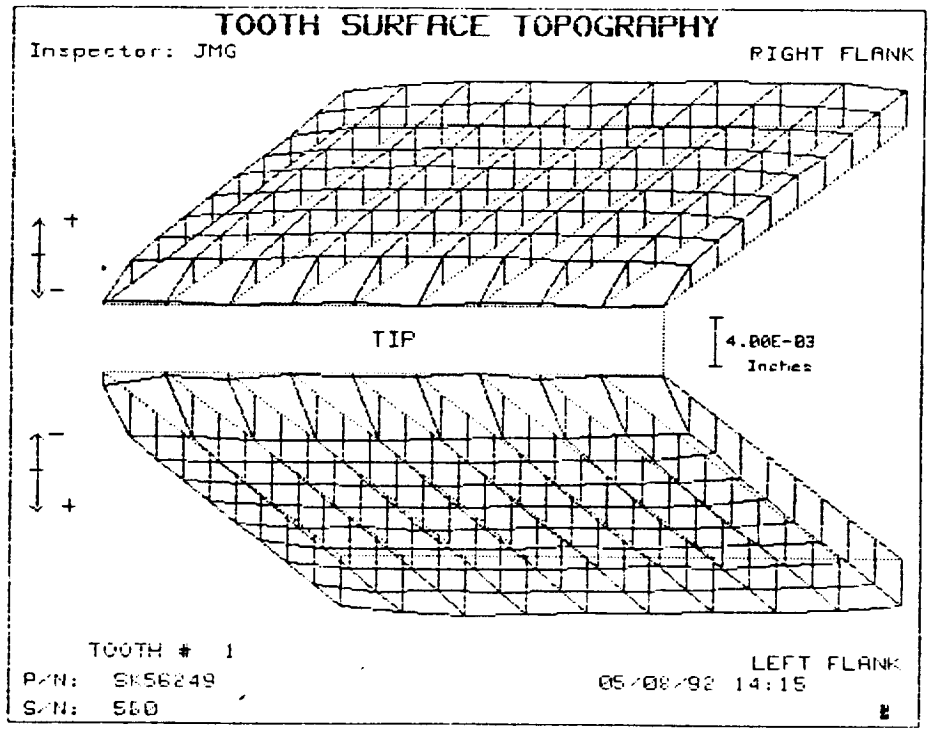

Figure B.6 Surface Topography of an 8620 Test Gear

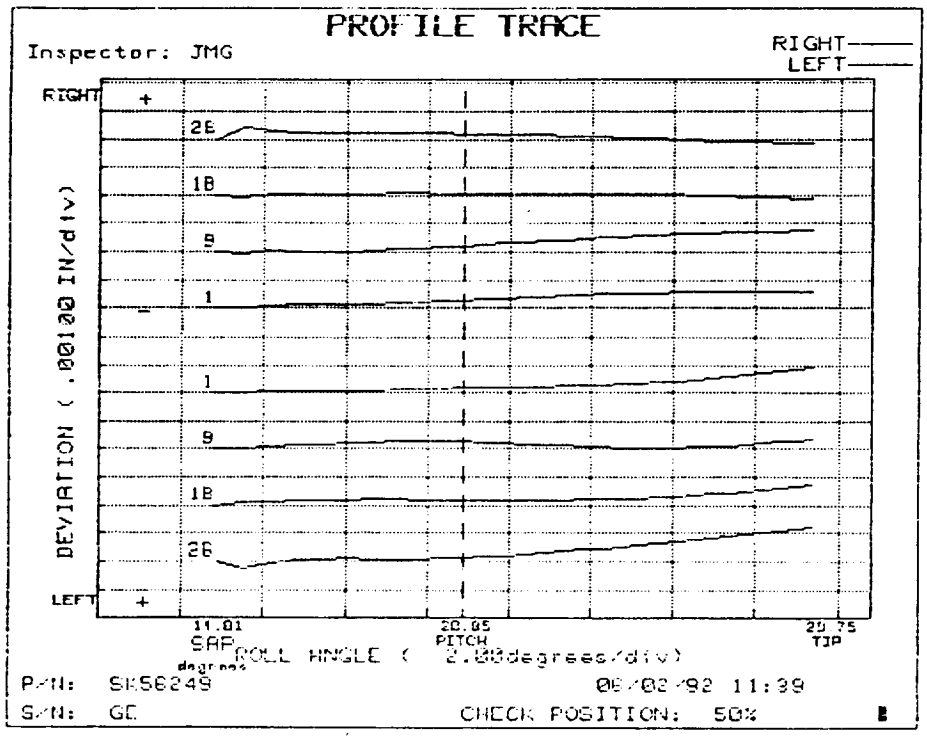

Figure B.7 Profile Checks for a 9310 Test Gear

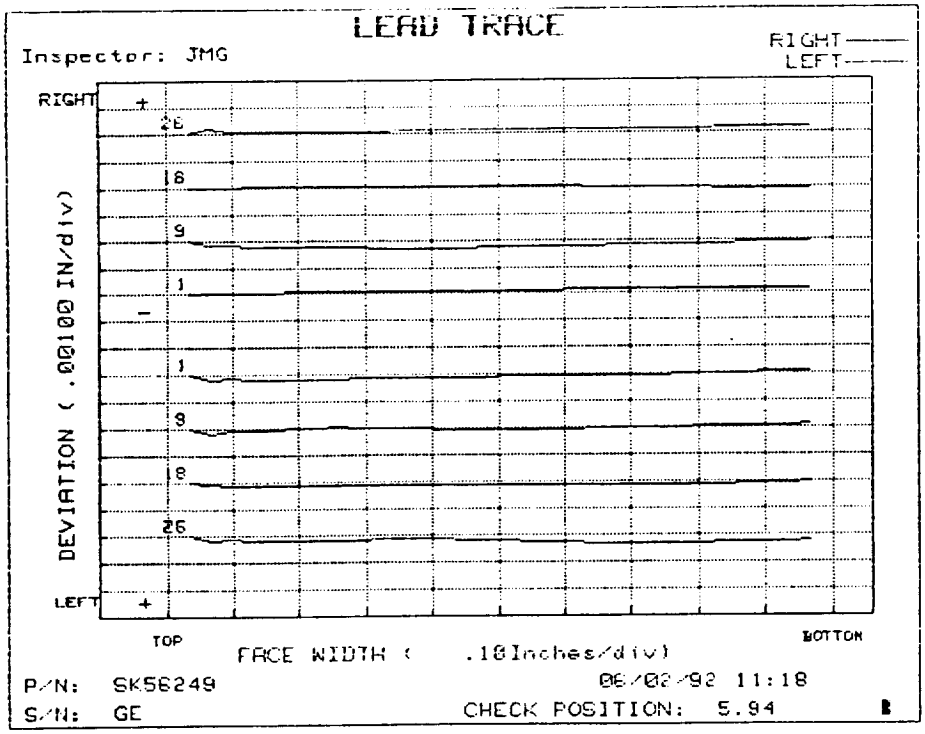

Figure B.8 Lead Checks for a 9310 Test Gear

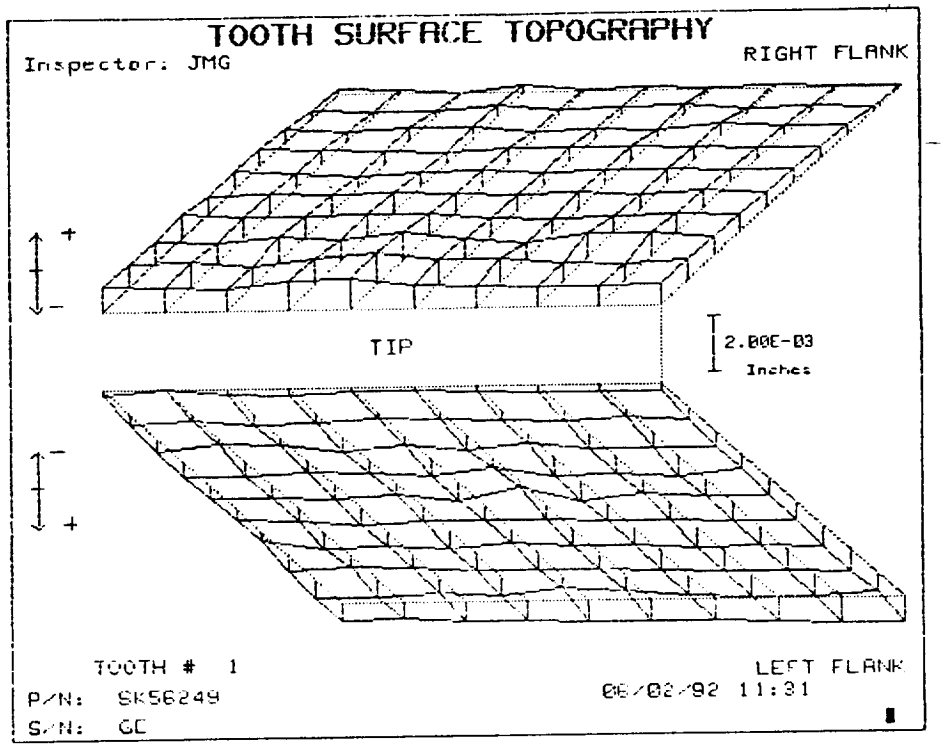

Figure B.9 Surface Topography of a 9310 Test Gear

Appendix C

Root Surface Finish Measurements

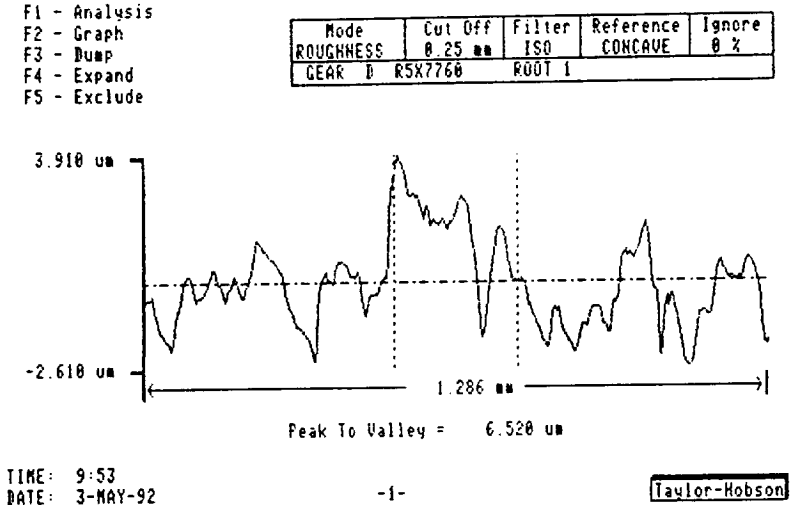

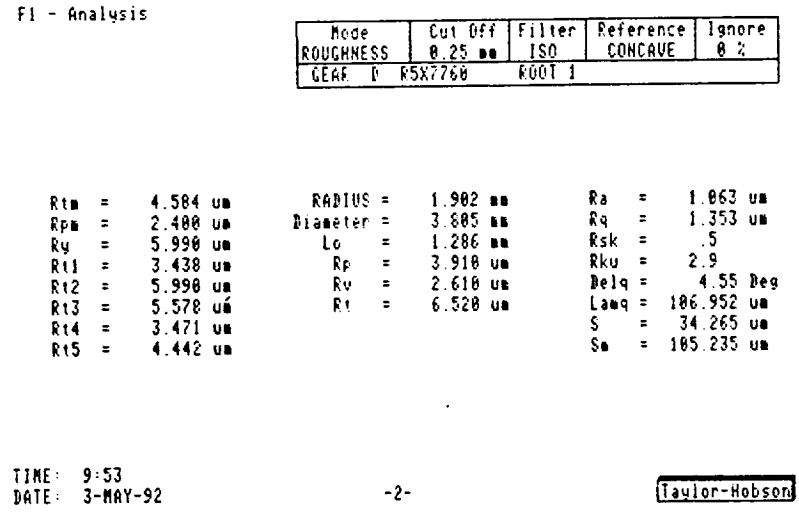

Figure C.1 Root Surface Finish Measurement for a 4118 Gear

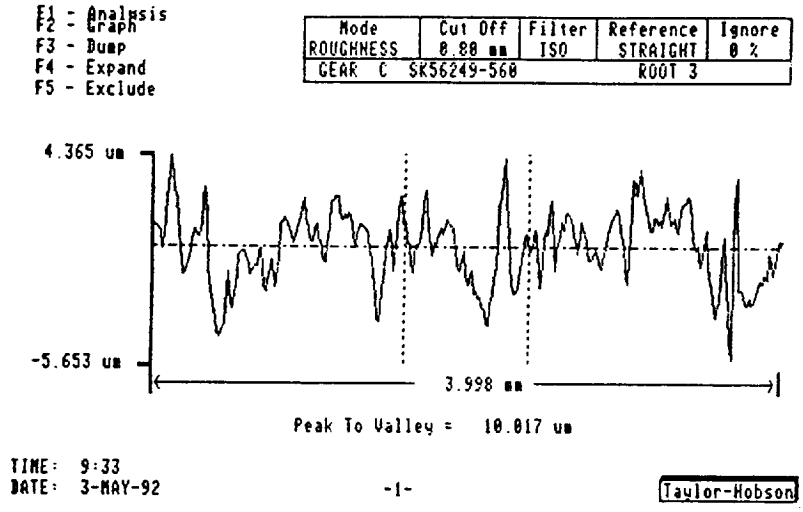

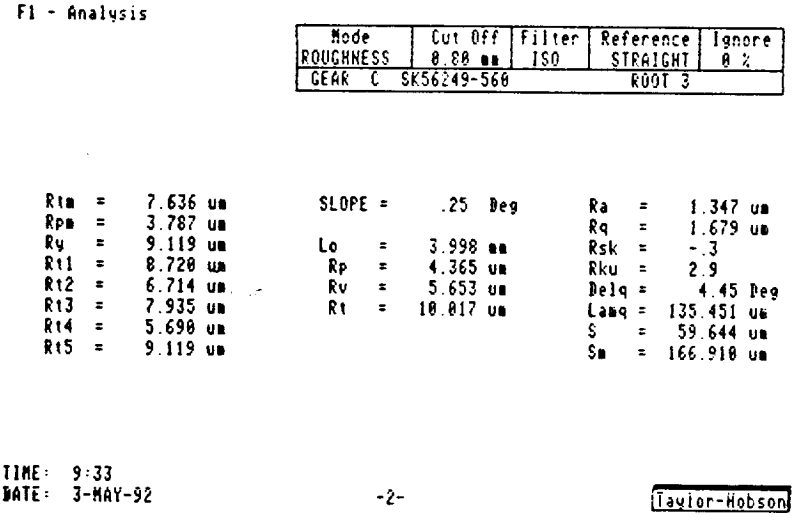

Figure C.2 Root Surface Finish Measurement for an 8620 Gear

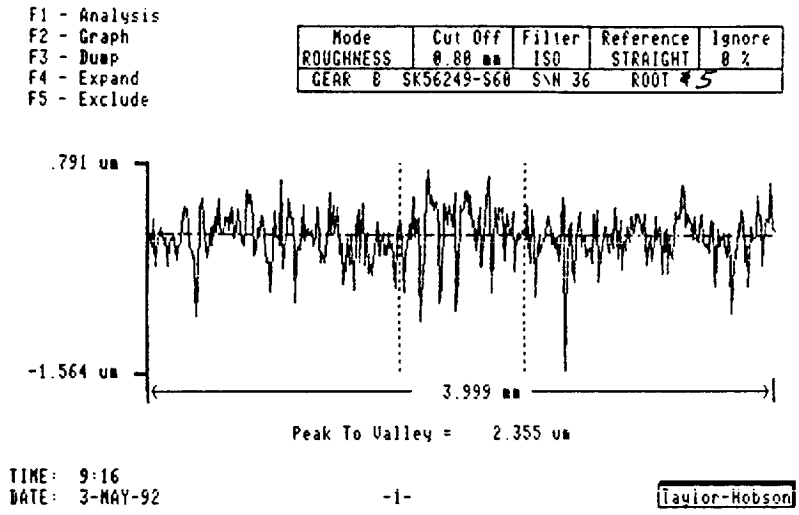

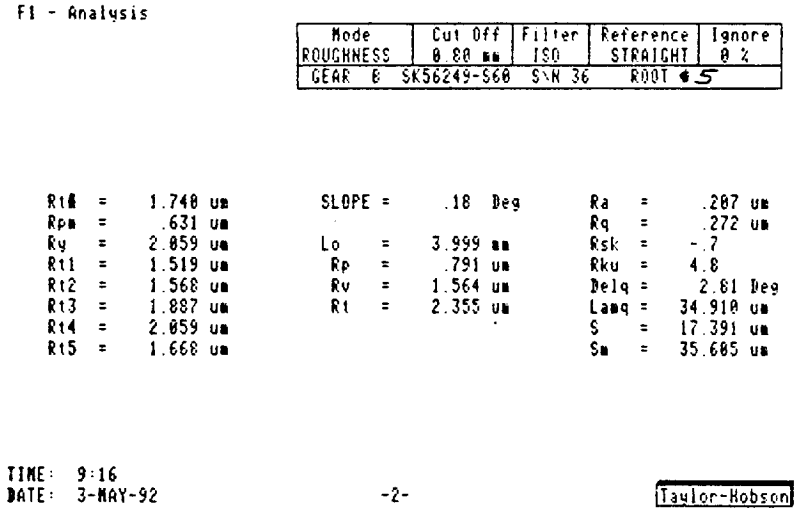

Figure C.3 Root Surface Finish Measurement for a 9310 Gear

Appendix D

Accelerometer Specifications

Calibration Certificate

Per ISA-RP37.2

Model No. 302B03

Serial No. 18775

PO No. _____ Customer _____

Calibration traceable to NIST (NBS) thru Project No. 732/245191-90

ICP™ ACCELEROMETER
with built-in electronics

Calibration procedure is in compliance with MIL-STD-45662 and traceable to NIST. (NBS)

CALIBRATION DATA

Voltage Sensitivity	299.9	mV/g
Transverse Sensitivity	4.9	%
Resonant Frequency	21	kHz
Time Constant	0.2	s
Output Bias Level	11.2	V

KEY SPECIFICATIONS

Range	16	± g
Resolution	0.0025	g
Temp. Range	-65/+175	°F

METRIC CONVERSIONS:
ms $^{-2}$ = 0.102 g
°C = 5/9 x (°F -32)

Reference Freq.

Frequency Hz	10	15	30	50	100	300	500	1000	3000	5000		
Amplitude Deviation %	-.6	-.3	-.3	-.6	0.0	.2	.5	.5	1.3	.9		

FREQUENCY RESPONSE

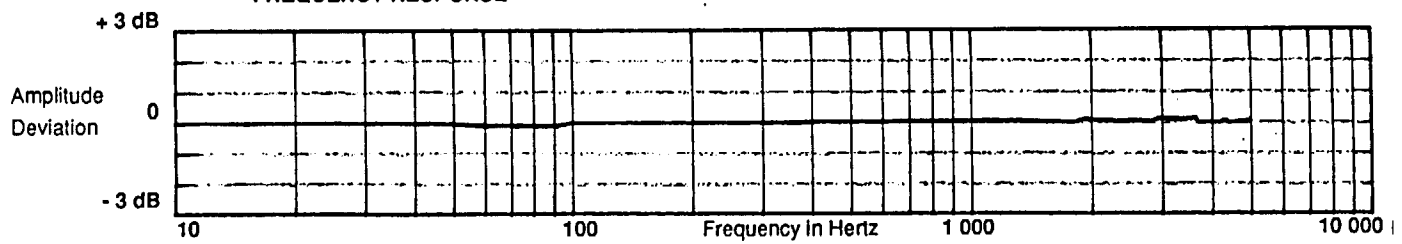

PCB Piezotronics, Inc. 3425 Walden Avenue Depew, NY 14043-2495 USA
716-684-0001

Date 3/15/91

Calibrated by J. Redmond

Appendix E

Computer Program for Remote Operation
of Wavetek 5820 Spectrum Analyzer

```
100 ! FATIGUE TESTING DATA PROGRAM FOR THE WAVETEK 5820
110 !
120 !            SPECTRUM ANALYZER.
130 !
140 !                   BY
150 !
160 !              JEFF WHEITNER
170 !
180 !
190 !  THIS PROGRAM USES A TIMER ROUTINE TO COLLECT FATIGUE TESTING DATA
200 !  FROM A WAVETEK 5820 SPECTRUM ANALYZER.  AN ACCELEROMETER IS MOUNTED
210 !  TO THE SOLENOID OF THE MTS 810 MATERIAL TEST SYSTEM AND ITS
220 !  SIGNAL IS INPUT TO CHANNEL A OF THE 5820.  THE MTS LOAD SIGNAL
230 !  IS CONNECTED TO CHANNEL B.  THE PROGRAM WILL SET UP THE 5820
240 !  VIA THE GPIB (IEEE 488) INTERFACE.  THE PROGRAM WILL DISPLAY
250 !  AND READ THE TRANSFER FUNCTION  F/A(iw) DURING THE TEST.  THE
260 !  DATA WILL THEN BE STORED ON THE HARD DISK (C:).
270 !
280 !
290 X = 1
300 A$ = CHR$(3)
310 DIM G$[10](50)
320 DIM Amp[5000]
330 DIM Cyc[5000]
340 CLEAR
350 PRINT "5820 DATA ACQUITION ROUTINE"
360 PRINT ""
370 PRINT "     BY JEFF WHEITNER"
380 FOR J = 1 TO 6
390   PRINT ""
400 NEXT J
410 INPUT PROMPT "INPUT GEAR NUMBER: ":G$[1]
420 INPUT PROMPT "INPUT MAX TESTING LOAD (lb): ":G$[2]
430 INPUT PROMPT "INPUT TESTING FREQUENCY (Hz): ":G$[3]
440 INPUT PROMPT "INPUT ANY OTHER PARAMETERS: ":G$[4]
450 INPUT PROMPT "INPUT DATA FILENAME WITHOUT EXTENSION (.DAT USED): ":G$[5]
460 SET DIALOG
470 CLEAR
480 PRINT "SETTING UP 5820 SPECTRUM ANALYZER ..."
490 PRINT @3:"SET FRONT PANEL REMOTE"
500 PRINT @3:"SET READOUT REMOTE"
510 PRINT @3:"TEXT"
520 PRINT @3:"5820 DATA ACQUISITION ROUTINE"
530 PRINT @3:" "
540 SLEEP 1
550 PRINT @3:"      JEFF WHEITNER"
560 SLEEP 1
570 FOR I = 1 TO 8
580   SLEEP 0.25
590   PRINT @3:" "
600 NEXT I
610 SLEEP 10
620 PRINT @3:A$ ! ----TERMINATE TEXT MODE----
630 PRINT @3:"SET READOUT LOCAL"
640 PRINT @3:"VIEW TRANSFER FUNCTION MAGNITUDE"
650 PRINT @3:"VIEW TRANSFER FUNCTION PHASE"
660 PRINT @3:"SET AVERAGER MODE SPECTRUM"
670 PRINT @3:"SET AMPLITUDE READOUT POWER"
680 PRINT @3:"SET N 2"
690 PRINT @3:"CURSOR 10"
```

```
 700 PRINT @3:"SET VERTICAL SCALE LINEAR"
 705 PRINT @3:"SET REFERENCE A 8.2E-01"
 710 PRINT @3:"AUTORANGE"
 720 SLEEP 30
 730 SET GPIB END 1024+44
 735 PRINT @3:"SET FRONT PANEL LOCAL"
 740 CLEAR
 750 INPUT PROMPT "PRESS RETURN TO START TEST":Dummy$
 755 PRINT @3:"SET FRONT PANEL REMOTE"
 760 CLEAR
 770 PRINT ""
 780 PRINT ""
 790 PRINT "PRESS ANY KEY TO STOP TEST"
 810 Tini$ = TIME
 820 Ts$ = SEG$(Tini$,7,2)
 830 Ts = VAL(Ts$)
 840 Tm$ = SEG$(Tini$,4,2)
 850 Tm = VAL(Tm$)
 860 Th$ = SEG$(Tini$,1,2)
 870 Th = VAL(Th$)
 880 Tini = Ts+Tm*60+Th*3600
 890 PRINT @3:"READ CURSOR BOTTOM"
 900 INPUT @3:Ao$
 910 Ao = VAL(Ao$)
 920 Cyc[1] = 1
 930 Amp[1] = Ao
 940 !
 950 ON KEY GOTO 1480
 960 !  ------- AVERAGE AMPLITUDE RATIO  SUBROUTINE -------
 970 PRINT "AVERAGING TRANSFER FUNCTION ..."
 980 Av = 1000
 990 DO WHILE Av>Ao-1.0
1000   Tot = 0
1010   FOR X = 1 TO 5
1020     PRINT @3:"READ CURSOR BOTTOM"
1030     INPUT @3:A1$
1040     A1 = VAL(A1$)
1050     PRINT "A1=";A1
1060     Tot = Tot+A1
1070     SLEEP 6
1080   NEXT X
1090   Av = Tot/5
1100   PRINT "AVERAGE=";Av
1110 LOOP
1120 X = X+1
1130 !  ------ READ N,A AFTER CRACK IS PRESENT -------
1140 PRINT "TRANSFER FUNCTION IS DROPPING"
1150 PRINT ""
1160 PRINT "DATA ACQUISITION STARTED ..."
1170 PRINT @3:"READ CURSOR BOTTOM"
1180 INPUT @3:A$
1190 Amp[X] = VAL(A$)
1200 E$ = TIME
1210 GOSUB 1360
1220 Cyc[X] = (Etime-Tini)*10
1230 PRINT Cyc[X],Amp[X]
1240 SLEEP 1
1250 IF Amp[X]>50 THEN
1260   SLEEP 3
1270   X = X+1
```

```
1280   GOTO 1170
1290 END IF
1300 PRINT @3:"SET FRONT PANEL LOCAL"
1310 OFF KEY
1320 GOSUB 1740
1330 END ! --- PROGRAM END ---
1340 !
1350 !
1360 ! ----   TIMER SUBROUTINE   --------
1370 !
1380 Es$ = SEG$(E$,7,2)
1390 Es = VAL(Es$)
1400 Em$ = SEG$(E$,4,2)
1410 Em = VAL(Em$)
1420 Eh$ = SEG$(E$,1,2)
1430 Eh = VAL(Eh$)
1440 Etime = Es+60*Em+3600*Eh
1450 RETURN
1460 !
1470 !
1480 !  ---- STOP SUBROUTINE -----
1490 PRINT @3:"READ CURSOR BOTTOM"
1500 INPUT @3:Finamp$
1510 E$ = TIME
1520 GOSUB 1380
1530 Tfin = Etime
1540 X = X+1
1550 Cyc[X] = (Tfin-Tini)*10
1560 INPUT PROMPT "PRESS RETURN TO RESTART TEST":Dummy$
1570 PRINT "PRESS ANY KEY TO STOP TEST"
1580 ON KEY GOTO 1480
1590 DO WHILE Av>Ao-0.5
1600   Tot = 0
1610   FOR X = 1 TO 3
1620     PRINT @3:"READ CURSOR BOTTOM"
1630     INPUT @3:A2$
1640     A2 = VAL(A2$)
1650     ! PRINT A2
1660     Tot = Tot+A2
1670     SLEEP 2
1680   NEXT X
1690   Av = Tot/3
1700   PRINT "AVERAGE=";Av
1710   GOTO 1130
1720   !
1730   !
1740   REM  ------ STORE DATA TO DISK -------
1750   PRINT "STORING DATA IN FILE: ";G$[5];".DAT   DRIVE C ..."
1760   Dsk$ = "C:" & G$[5] & ".dat"
1770   CLOSE
1780   OPEN #1:Dsk$,"U"
1790   PRINT #1:G$
1800   FOR K = 1 TO X
1810     PRINT #1:Cyc[K],",",Amp[K]
1820   NEXT K
1830   CLOSE
1840   RETURN
```

Appendix F

Acoustic Emission Transducer Sensitivity

PHYSICAL ACOUSTICS CORPORATION

CALIBRATION CERTIFICATE

''Sound Technology for Productivity and Safety''

DUNEGAN CORPORATION

MODEL NUMBER: NANO 30 DATE: 06/25/91

SERIAL NUMBER: 395 TESTED BY: C. H.

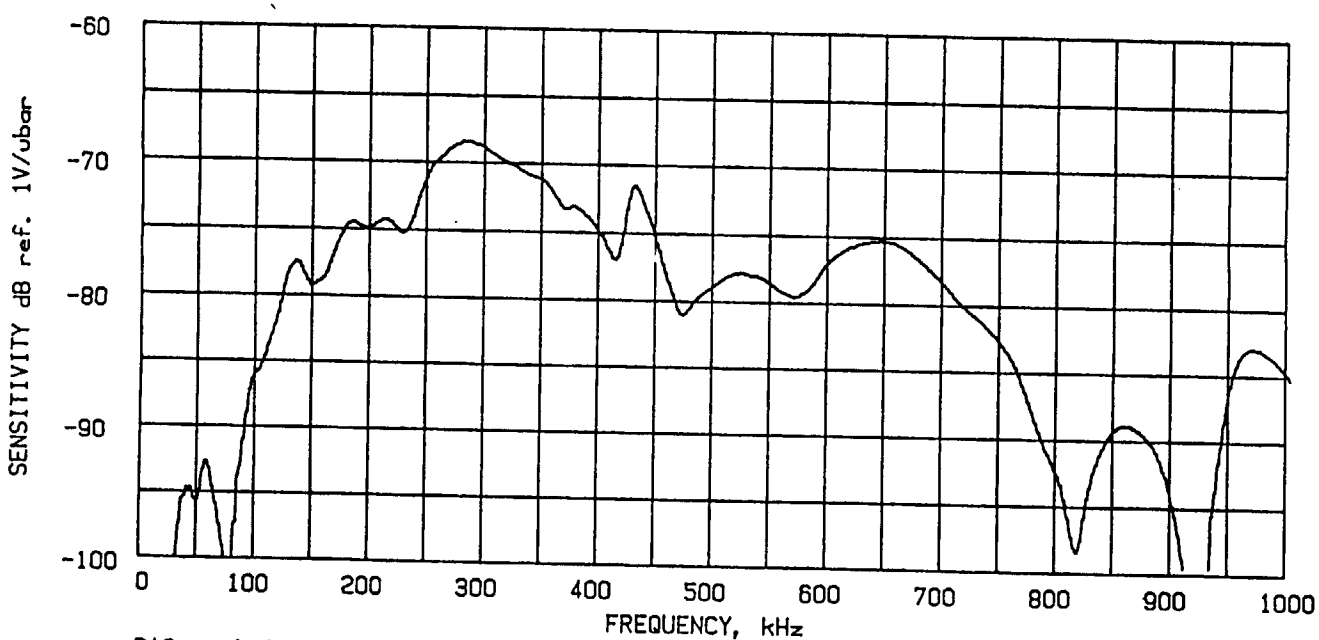

PAC certifies that this sensor meets all performance, environmental, and physical standards established in applicable PAC specifications. Calibration methodology based on ASTM standard E976- ''Standard Guide for Determining the Reproducibility of Acoustic Emission Sensor Response''.

Appendix G

Fatigue Life Data

Table G.1 Fatigue Life Data for 4118A

Stress	Ni	Cycles, Nf	Np	%Nf
224532.000	12800.000	14735.000	1935.000	0.131
187110.000	112200.000	125810.000	13610.000	0.108
187110.000	74500.000	97880.000	23380.000	0.239
187110.000	114200.000	123250.000	9050.000	0.073
177754.500	433000.000	476630.000	43630.000	0.092
187110.000	78600.000	97000.000	18400.000	0.190
205821.000	19200.000	27560.000	8360.000	0.303
205821.000	39400.000	48300.000	8900.000	0.184
224532.000	12750.000	16280.000	3530.000	0.217

Table G.2 Fatigue Life Data for 4118B

Stress	Ni	Cycles, Nf	Np	%Nf
205821.000	22500.000	29850.000	7350.000	0.246
187110.000	25750.000	37090.000	11340.000	0.306
187110.000	40700.000	52010.000	11310.000	0.217
177754.500	86800.000	95900.000	9100.000	0.095
168399.000	187000.000	202230.000	15230.000	0.075
177754.500	154300.000	173800.000	19500.000	0.112
224532.000	10400.000	14390.000	3990.000	0.277
224532.000	9000.000	12750.000	3750.000	0.294
205821.000	22100.000	31170.000	9070.000	0.291

Table G.3 Fatigue Life Data for 4118C

Stress	Ni	Cycles, Nf	Np	%Nf
187110.000	42500.000	56210.000	13710.000	0.244
187110.000		53090.000		
205821.000	18300.000	28490.000	10190.000	0.358
224532.000	6250.000	12010.000	5760.000	0.480
205821.000	29300.000	38150.000	8850.000	0.232
177754.500	64200.000	75900.000	11700.000	0.154
177754.500		55980.000		
168399.000	120100.000	142120.000	22020.000	0.155
168399.000	94300.000	107270.000	12970.000	0.121
224532.000	6200.000	10370.000	4170.000	0.402

Table G.4 Fatigue Life Data for 9310

Stress	Ni	Cycles, Nf	Np	%Nf
336798.000		20600.000		
336798.000		17200.000		
336798.000		10670.000		
336798.000	14300.000	14940.000	640.000	0.043
336798.000	21500.000	22320.000	820.000	0.037
336798.000		31000.000		
318087.000		87290.000		
318087.000	33400.000	34790.000	1390.000	0.040
318087.000	37400.000	38720.000	1320.000	0.034
318087.000		18740.000		
299376.000		580800.000		
299376.000		179000.000		
299376.000	516800.000	517980.000	1180.000	0.002
299376.000		115790.000		
280665.000		1000000.000		

Table G.5 Fatigue Life Data for 9310P

Stress	Ni	Cycles, Nf	Np	%Nf
336798.000		7620.000		
336798.000	7000.000	8010.000	1010.000	0.126
318087.000	9900.000	10930.000	1030.000	0.094
318087.000	13050.000	14610.000	1560.000	0.107
299376.000	17600.000	19090.000	1490.000	0.078
299376.000	15950.000	17480.000	1530.000	0.088
280665.000	27600.000	32120.000	4520.000	0.141
280665.000	27300.000	29480.000	2180.000	0.074
261954.000	69740.000	72720.000	2980.000	0.041
261954.000		61000.000		
261954.000		53710.000		
243243.000		1000000.000		

Table G.6 Fatigue Life Data for 8620

Stress	Ni	CYCLES, Nf	Np	%Nf
224532.000	5600.000	9940.000		
224532.000	5200.000	8370.000	3170.000	0.379
205821.000	14120.000	20060.000	5940.000	0.296
205821.000	14700.000	18390.000	3690.000	0.201
187110.000	57200.000	63770.000	6570.000	0.103
187110.000	35000.000	43740.000	8740.000	0.200
177754.500		88860.000		
177754.500	134200.000	145620.000	11420.000	0.078
168399.000		1000000.000		